


Fall 2010

# Surface morphology of platelet adhesion influenced by activators, inhibitors and shear stress

Melanie Groan Watson

Follow this and additional works at: <https://digitalcommons.latech.edu/dissertations>

 Part of the [Biomedical Engineering and Bioengineering Commons](#), and the [Nanoscience and Nanotechnology Commons](#)

---

**SURFACE MORPHOLOGY OF PLATELET ADHESION  
INFLUENCED BY ACTIVATORS, INHIBITORS  
AND SHEAR STRESS**

by

Melanie Groan Watson, B.S., M.S.E.

A Dissertation Presented in Partial Fulfillment  
Of the Requirements for the Degree  
Doctor of Philosophy

COLLEGE OF ENGINEERING AND SCIENCE  
LOUISIANA TECH UNIVERSITY

November 2010

UMI Number: 3438521

All rights reserved

**INFORMATION TO ALL USERS**

The quality of this reproduction is dependent upon the quality of the copy submitted.

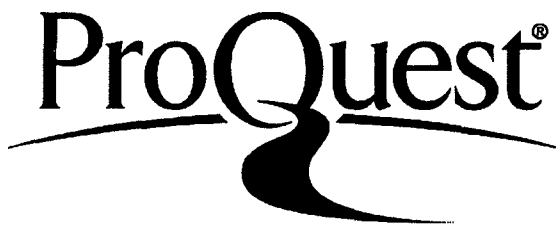
In the unlikely event that the author did not send a complete manuscript and there are missing pages, these will be noted. Also, if material had to be removed, a note will indicate the deletion.



UMI 3438521

Copyright 2011 by ProQuest LLC.

All rights reserved. This edition of the work is protected against unauthorized copying under Title 17, United States Code.



ProQuest LLC  
789 East Eisenhower Parkway  
P.O. Box 1346  
Ann Arbor, MI 48106-1346

LOUISIANA TECH UNIVERSITY

THE GRADUATE SCHOOL

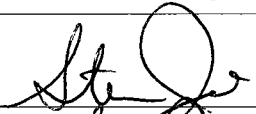

09/09/2010

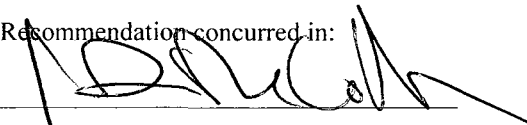

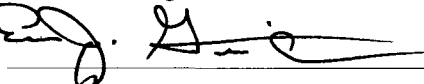

Date

We hereby recommend that the dissertation prepared under our supervision  
by Melanie Groan Watson


entitled Surface Morphology of Platelet Adhesion Influenced by Activators,  
Inhibitors and Shear Stress

be accepted in partial fulfillment of the requirements for the Degree of  
Doctor of Philosophy in Biomedical Engineering

  
\_\_\_\_\_  
Supervisor of Dissertation Research  
  
\_\_\_\_\_  
Head of Department  
Biomedical Engineering  
\_\_\_\_\_  
Department

Recommendation concurred in:  
  
\_\_\_\_\_  
  
\_\_\_\_\_  
  
\_\_\_\_\_  
  
\_\_\_\_\_

Advisory Committee

Approved:  
  
\_\_\_\_\_  
Director of Graduate Studies

Approved:  
  
\_\_\_\_\_  
Dean of the Graduate School

  
\_\_\_\_\_  
Dean of the College

## ABSTRACT

Platelet activation involves multiple events, one of which is the generation and release of nitric oxide (NO), a platelet aggregation inhibitor. Platelets simultaneously send and receive various agents that promote a positive and negative feedback control system during hemostasis. Although the purpose of platelet-derived NO is not fully understood, NO is known to inhibit platelet recruitment. NO's relatively large diffusion coefficient allows it to diffuse more rapidly than platelet agonists. It may thus be able to inhibit recruitment of platelets near the periphery of a growing thrombus before agonists have substantially accumulated in those regions.

Results from two studies in our laboratory differed in the extent to which platelet-derived NO decreased platelet adhesion. Frilot studied the effect of L-arginine (L-A) and N<sup>G</sup>-Methyl-L-arginine acetate salt (L-NMMA) on platelet adhesion to collagen under static conditions in a Petri dish. Eshaq examined the percent coverage on collagen-coated and fibrinogen-coated microchannels under shear conditions with different levels of L-A and Adenosine Diphosphate (ADP). Frilot's results showed no effect of either L-A or L-NMMA on surface coverage, thrombus size or serotonin release, while Eshaq's results showed a decrease in surface coverage with increased levels of L-A. A possible explanation for these contrasting results is that platelet-derived NO may be more important under flow conditions than under static conditions.

For this project, the effects of L-A, ADP and L-NMMA on platelet adhesion were studied at varying shear stresses on protein-coated glass slides. The surface exposed to platelet-rich-plasma in combination with each chemical solution was observed under AFM, FE-SEM and fluorescence microscopy. Quantitative and qualitative comparisons of images obtained with these techniques confirmed the presence of platelets on the protein coatings. AFM images of fibrinogen and collagen-coated slides presented characteristic differences. Adhered platelets were identified, particularly with the AFM. The effects of chemical additives were examined under the same microscopy techniques. The resulting fluorescent microscopy data suggests statistical differences between the percent surface coverage of different shear regions on the glass slides. No statistically significant change in surface coverage was found with the addition of ADP on fibrinogen-coated slides, but showed differences on collagen with all chemicals. However, in high shear regions, L-A produced a significant decrease in platelet adhesion and L-NMMA produced a statistically significant increase in platelet adhesion on fibrinogen and collagen-coated slides. The AFM images of the chemical additives provided no differences between one another except with ADP. The no shear and low shear conditions provided no variations between AFM images via visual confirmation and statistical significance. The only AFM image shear region differences were obtained from low to high shear regions and static to high shear regions comparisons.

The objective of this project was to determine whether the static conditions used by Frilot and the dynamic conditions used by Eshaq could explain the different effects of L-A observed in those studies. In addition, the ability of the fluorescent imaging technique to quantify platelet adhesion was examined by comparison of fluorescent

imaging to AFM and FE-SEM. The results of this study were consistent with both the lack of an effect of chemical additives under static conditions reported by Frilot and the reduction of platelet adhesion in response to L-A reported by Eshaq.

## APPROVAL FOR SCHOLARLY DISSEMINATION

The author grants to the Prescott Memorial Library of Louisiana Tech University the right to reproduce, by appropriate methods, upon request, any or all portions of this Dissertation. It is understood that "proper request" consists of the agreement, on the part of the requesting party, that said reproduction is for his personal use and that subsequent reproduction will not occur without written approval of the author of this Dissertation. Further, any portions of the Dissertation used in books, papers, and other works must be appropriately referenced to this Dissertation.

Finally, the author of this Dissertation reserves the right to publish freely, in the literature, at any time, any or all portions of this Dissertation.

Author Melanie G. Watson  
Date 9/9/10



## **DEDICATION**

This dissertation is dedicated to all of my family and friends for their many years of support. I specifically wish to recognize my amazing parents and brother: Mike, Leslie and Derrek for always believing in me. I wish to pay tribute to my wonderful husband, Ron, for being my rock. Lastly, I want to acknowledge my daughter, Chloe, for showing me a bright future.

## TABLE OF CONTENTS

ABSTRACT.....	iii
DEDICATION.....	vii
LIST OF FIGURES .....	xiv
LIST OF TABLES .....	xix
ACKNOWLEDGMENTS .....	xxi
CHAPTER 1 INTRODUCTION .....	1
1.1    Platelet Overview.....	1
1.1.1    Platelet Physiology.....	2
1.2    Experimental Processes .....	6
1.2.1    Layer-by-Layer .....	6
1.2.2    Biointerfaces .....	7
1.2.3    Chemical Additives.....	9
1.3    Current Work .....	10
1.3.1    Frilot’s Dissertation .....	10
1.3.2    Eshaq’s Thesis .....	10
1.3.3    Frilot vs. Eshaq .....	11
1.3.4    Vyavahare’s Thesis.....	12
1.3.5    Lopez’s Dissertation .....	12
1.4    Hypotheses.....	13
CHAPTER 2 METHODS.....	16
2.1    Overview.....	16

2.1.1	Hypothesis 1.....	16
2.1.2	Hypothesis 2.....	16
2.1.3	Hypothesis 3.....	17
2.1.4	Hypothesis 4.....	17
2.1.5	Hypothesis 5.....	17
2.2	Experimental Processes .....	18
2.2.1	Generation of sLbL and dLbL surfaces .....	18
2.2.2	Control Chamber Preparation .....	24
2.2.3	Petri Dish Preparation .....	25
2.2.4	Bovine Blood Collection.....	26
2.2.5	Centrifugation .....	27
2.2.6	PRP Collection Process.....	27
2.2.7	PRP Dilution.....	28
2.2.8	PRP Experimentation.....	28
2.2.9	Static Condition of PRP Experimentation .....	29
2.2.10	AO Staining .....	30
2.2.11	Sample Storage .....	31
2.2.12	Waste Disposal.....	31
2.2.13	Atomic Force Microscopy .....	31
2.2.14	Field Emission Scanning Electron Microscopy .....	33
2.2.15	Fluorescence Microscopy Imaging .....	34
2.2.16	Generation of dLbL surfaces .....	37
2.2.17	Dynamic Condition of PRP Experimentation.....	38
2.2.18	Particle Size Comparison.....	39
2.3	Temperature and Humidity Control Chamber .....	40

2.4	Mathematical Model .....	41
2.4.1	Model for Transport under Static Conditions .....	41
2.4.2	Model for Transport under Flow Conditions .....	42
2.5	Testing of Platelet Conditions.....	42
2.5.1	Bioanalyzer <sup>®</sup> Cytometry .....	42
2.5.2	Sodium Citrate Experimentation.....	44
2.5.3	Centrifuge Testing .....	45
2.6	Statistical Analysis.....	46
2.6.1	Analysis of Variance.....	46
2.6.2	t-Test .....	46
CHAPTER 3 RESULTS .....		48
3.1	Evaluation and Optimization of Experimental Conditions.....	48
3.1.1	Bioanalyzer <sup>®</sup> Cytometry for Platelet Counts .....	48
3.1.2	Sensitivity to Sodium Citrate Concentration .....	49
3.1.3	Optimization of PRP Extraction .....	52
3.2	PRP Experimentation Overview.....	53
3.3	Effect of Exposure to PRP.....	55
3.3.1	AFM.....	55
3.3.2	FE-SEM .....	59
3.4	Comparison of Surfaces after Static Exposure to PRP .....	63
3.4.1	Fluorescence Microscopy .....	63
3.4.2	AFM.....	64
3.4.3	FE-SEM .....	65
3.5	Comparison of Surfaces after Dynamic Exposure to PRP .....	67
3.5.1	Fluorescence Microscopy .....	67

3.5.2	AFM.....	68
3.5.3	FE-SEM.....	69
3.6	Comparison of Images after Exposure to PRP at Different Shears.....	70
3.6.1	Fluorescence Microscopy.....	71
3.6.2	AFM.....	73
3.7	Platelet Adhesion Sizes.....	75
3.7.1	Feature Sizes for dLbL-Fibrinogen Substrates.....	75
3.7.2	Feature Sizes for dLbL-Collagen Substrates.....	77
3.8	Effects of Additives on Surface Coverage.....	78
3.8.1	Fluorescence Microscopy.....	78
3.8.2	AFM.....	83
3.8.3	Feature Size Distributions.....	89
3.9	Statistical Comparisons.....	95
3.9.1	Statistical Comparison of Platelet Coverage Confirmation.....	95
3.9.2	Statistical Comparison of LbL Surfaces.....	97
3.9.3	Statistical Comparison of Biointerface Substrates.....	98
3.9.4	Statistical Comparison of Shear Stress.....	100
3.9.5	Statistical Comparison of Chemicals.....	103
CHAPTER 4 DISCUSSION.....		109
4.1	Evaluation and Optimization of Experimental Conditions.....	109
4.1.1	Overview.....	109
4.1.2	Limitations.....	110
4.1.3	New Questions.....	110
4.2	PRP Experimentation Overview.....	111
4.2.1	Limitations.....	112

4.2.2	New Questions .....	112
4.3	Platelet Coverage Confirmation.....	113
4.3.1	Overview.....	113
4.3.2	Limitations .....	113
4.3.3	New Questions .....	114
4.4	Layered Surfaces Exposed to PRP.....	114
4.4.1	LbL Surface Comparisons .....	114
4.4.2	Biointerface Substrate Comparisons.....	116
4.4.3	Dynamic vs. Static Conditions.....	117
4.4.4	Chemical Additive Comparisons .....	119
CHAPTER 5 CONCLUSIONS AND FUTURE WORK.....		122
5.1	Concluding Hypotheses Assessments.....	122
5.1.1	Hypothesis 1.....	122
5.1.2	Hypothesis 2.....	123
5.1.3	Hypothesis 3.....	123
5.1.4	Hypothesis 4.....	123
5.1.5	Hypothesis 5.....	124
5.2	Future Work.....	125
5.2.1	Testing the dLbL Technique using Flow Conditions .....	125
5.2.2	ADP Streaking Effect .....	126
5.2.3	Platelet Rolling Effect.....	126
5.2.4	dLbL-Collagen Surface.....	126
5.2.5	Imaging Improvement.....	127
5.2.6	PRP vs. PPP .....	127
5.2.7	Coagulation Control.....	128

5.2.8 Platelet Detection .....	128
APPENDIX A .....	130
APPENDIX B .....	137
APPENDIX C .....	143
APPENDIX D .....	146
APPENDIX E .....	148
REFERENCES .....	150

## LIST OF FIGURES

Figure 1	Platelet Mechanism for the Formation of a Thrombus [13] .....	3
Figure 2	Production of NO from L-arginine with the aid of NOs [24] .....	5
Figure 3	Mechanism for inhibition by NO .....	6
Figure 4	Crystal structure of fibrinogen [45]. .....	8
Figure 5	The structure of a collagen molecule .....	9
Figure 6	Static LbL Process: PDDA and PSS .....	22
Figure 7	Static LbL Process: PDDA and Fibrinogen .....	22
Figure 8	The Dynamic LbL process on the VWR shaker table .....	23
Figure 9	Petri Dish Marking.....	25
Figure 10	Whole Blood Samples mixed with Sodium Citrate .....	27
Figure 11	PRP collection process and PRP confirmation. (A) Collection from the centrifuged blood. (B) Separated PRP. ....	28
Figure 12	Exposure of glass slides to PRP under dynamic conditions .....	29
Figure 13	PRP Setup for a Static Experiment .....	30
Figure 14	Glass Slide Markings .....	35
Figure 15	Shear Region Gradient for Image Location Selection .....	36
Figure 16	PRP Setup for a Dynamic Experiment.....	39
Figure 17	Temperature and Humidity Control Chamber Design.....	41
Figure 18	Agilent Bioanalyzer <sup>®</sup> System .....	44
Figure 19	Bioanalyzer Histogram from 6/2/2010: Top: Samples 1-3; Bottom: Samples 4-6.....	49



Figure 20	Percent surface coverage of platelets on dLbL-fibrinogen surfaces after exposure to plain PRP, PRP+ADP, PRP+L-A and PRP+L-NMMA (L-N). Error bars indicate the standard deviation of surface coverage percentages from different slides on different days. ....	54
Figure 21	Percent surface coverage of platelets on dLbL-collagen surfaces after exposure to plain PRP, with no additive and with ADP and L-A. Error bars indicate the standard deviation of surface coverage percentages from different slides on different days. ....	55
Figure 22	AFM images of uncoated glass slides that were exposed to PRP under static conditions. Top: No AO stain. Bottom: AO stain. ....	56
Figure 23	AFM images of slides that were coated with sLbL-fibrinogen (top left), dLbL-fibrinogen (bottom left) and dLbL-collagen (bottom right), but not exposed to PRP and not stained. ....	57
Figure 24	AFM images of slides with sLbL-fibrinogen (top left), dLbL-fibrinogen (bottom left) and dLbL-collagen surfaces performed under static conditions while exposed to PRP and stained with AO. ....	58
Figure 25	FE-SEM images of plain glass slides exposed to PRP. Top: No AO stain. Bottom: AO stain. ....	60
Figure 26	FE-SEM images of slides with sLbL-fibrinogen (top left), dLbL-fibrinogen (bottom left) and dLbL-collagen surfaces without PRP exposure and AO stain. ....	61
Figure 27	FE-SEM images of slides with sLbL-fibrinogen (top left), dLbL-fibrinogen (bottom left) and dLbL-collagen (bottom right) surfaces exposed to PRP without flow and stained with AO. ....	62
Figure 28	Fluorescence microscopy images of slides with sLbL fibrinogen (top left), dLbL-fibrinogen (bottom left) and dLbL-collagen (bottom right) that were exposed to PRP under static conditions and stained with AO. ....	64
Figure 29	AFM images of slides with sLbL-fibrinogen (top left), dLbL-fibrinogen (bottom left), and dLbL-collagen (bottom right) slides that were exposed to PRP under static conditions, and stained with AO. ....	65
Figure 30	FE-SEM images of slides with sLbL-fibrinogen (top left), dLbL-fibrinogen (bottom left), dLbL-collagen (bottom right) exposed to PRP under static conditions and stained with AO. ....	66
Figure 31	Fluorescence microscopy images of slides with sLbL-fibrinogen, dLbL-fibrinogen, and dLbL-collagen surfaces exposed to PRP in the low shear region of the Petri dish and stained with AO. ....	68

Figure 32	AFM images of slides with sLbL-fibrinogen, dLbL-fibrinogen and dLbL-collagen surfaces exposed to PRP in the low shear region of the Petri dish and stained with AO.....	69
Figure 33	FE-SEM images of slides with sLbL-fibrinogen, dLbL-fibrinogen, dLbL-collagen substrates exposed to PRP in the low shear region of the Petri dish and stained with AO.....	70
Figure 34	Fluorescence microscopy images of slides with dLbL-fibrinogen under no shear (top left), low shear (bottom left), and high shear (bottom right) exposed to plain PRP and stained with AO. ....	71
Figure 35	Fluorescence microscopy images of slides with dLbL-collagen exposed to plain PRP under no shear (top left), low shear (bottom left) and high shear (bottom right) and stained with AO.....	73
Figure 36	AFM images of slides with dLbL-fibrinogen exposed to plain PRP under no shear (top left), low shear (bottom left) and high shear (bottom right) and stained with AO.....	74
Figure 37	AFM images of slides with dLbL-collagen under static conditions (top left), and dynamic conditions at low (bottom left) and high shear (bottom right) exposed to plain PRP and stained with AO .....	75
Figure 38	Feature size vs. number of features at that size for dLbL-fibrinogen surfaces exposed to plain PRP at low shear rate. Top: Curves for each image. Bottom: Mean for all images with standard deviation. ....	76
Figure 39	Feature size vs. number of features at that size for dLbL-collagen surfaces exposed to plain PRP at low shear rate. Top: Curves for each image. Bottom: Mean of all images with standard deviation. ....	77
Figure 40	Fluorescence microscopy images of AO-stained dLbL- fibrinogen slides that were exposed to PRP+L-A with no-shear (top left), low shear (bottom left) and high shear (bottom right) .....	79
Figure 41	Fluorescence microscopy images of AO-stained dLbL-collagen slides that were exposed to PRP+L-A with no-shear (top left), low shear (bottom left) and high shear (bottom right). ....	80
Figure 42	Fluorescence microscopy images of AO-stained dLbL-fibrinogen slides that were exposed to PRP+ADP with no-shear (top left), low shear (bottom left) and high shear (bottom right). ....	81
Figure 43	Fluorescence microscopy images of AO-stained dLbL-collagen slides that were exposed to PRP+ADP with no-shear (top left), low shear (bottom left) and high (bottom right).....	82

Figure 44	Fluorescence microscopy images of AO-stained dLbL-fibrinogen slides that were exposed to PRP+L-NMMA with no-shear (top left), low shear (bottom left) and high shear (bottom right). .....	83
Figure 45	AFM images of slides with dLbL-fibrinogen under static conditions (top left), and dynamic conditions at low (bottom left) and high shear (bottom right) exposed to PRP+L-A and stained with AO .....	84
Figure 46	AFM images of slides with dLbL-collagen under static conditions (top left), and dynamic conditions at low (bottom left) and high shear (bottom right) exposed to PRP+L-A and stained with AO .....	85
Figure 47	AFM images of slides with dLbL-fibrinogen under static conditions (top left), and dynamic conditions at low (bottom left) and high shear (bottom right) exposed to PRP+ADP and stained with AO .....	86
Figure 48	AFM images of slides with dLbL-collagen under static conditions (top left), and dynamic conditions at low (bottom left) and high shear (bottom right) exposed to PRP+ADP and stained with AO .....	87
Figure 49	AFM images of slides with dLbL-fibrinogen under static conditions (top left), and dynamic conditions at low (bottom left) and high shear (bottom right) exposed to PRP+L-NMMA and stained with AO .....	88
Figure 50	Feature size vs. number of features at that size for dLbL-fibrinogen surfaces exposed to PRP+L-A at low shear rate. Top: Curves for each image. Bottom: Mean of all images with standard deviation. ....	90
Figure 51	Feature size vs. number of features at that size for dLbL-fibrinogen surfaces exposed to PRP+ADP at low shear rate. Top: Curves for each image. Bottom: Mean of all images with standard deviation. ....	91
Figure 52	Feature size vs. number of features at that size for dLbL-fibrinogen surfaces exposed to PRP+L-NMMA at low shear rate. Top: Curves for each image. Bottom: Mean of all images with standard deviation. ....	92
Figure 53	Feature size vs. number of features at that size for dLbL-collagen surfaces exposed to PRP+L-A at low shear rate. Top: Curves for each image. Bottom: Mean of all images with standard deviation. ....	94
Figure 54	Feature size vs. number of features at that size for dLbL-collagen surfaces exposed to PRP+ADP at low shear rate. Top: Curves for each image. Bottom: Mean of all images with standard deviation. ....	95
Figure 55	Average peak heights and standard deviations from AFM scans of glass slides exposed to PRP and surfaces that were not exposed to PRP .....	96

Figure 56	Peak heights, with standard deviations, from AFM scans of LbL-generated surfaces, not exposed to PRP. ....	98
Figure 57	Average peak heights of biointerface interests with standard deviation error bars .....	100
Figure 58	AFM-derived peak heights for dLbL-fibrinogen and dLbL-collagen surfaces that have been exposed to plain PRP. Error bars represent standard deviation. ....	103
Figure 59	dLbL-fibrinogen and dLbL-collagen surfaces using AFM to obtain average peak heights of chemical additive interests with standard deviation error bars. ....	108

## LIST OF TABLES

Table 1	Configuration settings for AFM imaging .....	33
Table 2	Configuration settings for the Bioanalyzer .....	43
Table 3	Sodium citrate blood clot testing on 6/28/2010 – table excerpt.....	50
Table 4	Sodium citrate blood clot testing on 6/30/2010 – table excerpt.....	52
Table 5	AFM peak height t-Test p-values (2-tail) for statistical comparisons between a glass slide exposed to PRP and unexposed LbL surfaces.....	96
Table 6	Comparison of fluorescence-derived percent surface coverage between sLbL-fibrinogen and dLbL-fibrinogen surfaces .....	97
Table 7	t-Test two tail P-values using AFM to obtain peak heights of LbL technique interests.....	98
Table 8	Statistical tests to compared percent surface coverage between dLbL- fibrinogen and dLbL-collagen from fluorescent microscopy .....	99
Table 9	P-values using AFM to obtain peak heights of biointerface interests .....	100
Table 10	Fluorescence microscopy used to obtain statistical analysis of shear region interests from dLbL-fibrinogen .....	101
Table 11	Fluorescence microscopy used to obtain statistical analysis of shear region interests from dLbL-collagen .....	102
Table 12	P-values for comparisons of AFM-derived peak heights within different shear regions .....	103
Table 13	P-values from ANOVA analysis of surface coverage of dLbL-fibrinogen, as derived from fluorescence microscopy.....	105
Table 14	Comparison of percent surface coverage on dLbL-fibrinogen, as determined from fluorescence microscopy, for different chemical additives to coverage with plain PRP .....	106
Table 15	Fluorescence microscopy used to obtain statistical analysis of chemical additive interests for dLbL-collagen.....	107

Table 16	P-values using AFM to obtain peak heights of chemical additive interests using dLbL-fibrinogen and dLbL-collagen surfaces .....	108
Table D1	Bovine Blood Collection Journal.....	147

## **ACKNOWLEDGMENTS**

The author would like to express her gratitude to the following people for their work: Juan Lopez, my constant friend and colleague, Dr. Steven Jones, Dr. Alfred Gunasekaran, Dr. James Spaulding, Dr. Mark DeCoster, Dr. June Feng, Dr. Eric Guilbeau and Kinsey C. Kelly.

# CHAPTER 1

## INTRODUCTION

### 1.1 Platelet Overview

A thrombus is a blood clot located along the inside of a blood vessel. Thrombi damage the vasculature and organs by either obstructing blood flow at the site of formation or by dislodging fragments in the form of emboli [1] [2]. When atherosclerosis is present in an arterial blood vessel, plaque ruptures can lead to thrombi, which can lead to serious health conditions, including death [3]. Thrombi can further promote stenosis, and hence lead to a more rapid narrowing or occlusion of the vasculature [4]. Current studies of thrombosis use collagen and fibrinogen biointerfaces to localize and control platelet depositions to examine the effects of thrombi under shear rate, lumen narrowing and occlusion conditions [5] [6] [7]. Thrombi are composed of platelets proteins and other cells. Platelets play a key role in initiating thrombus formation and in stabilizing the clot by secreting platelet-activating factors and by adhering to one another and to other cells and proteins. Platelets also synthesize nitric oxide (NO), which is thus presumed to be important in the control of the thrombus formation. The conceptual model of current research is that NO is less important in the early formation of the clot, but that it becomes more important in controlling the size of the clot where platelet-derived NO is important in localizing the clot to the region around the damaged tissue. The mechanism being examined includes the following steps:



- a) A stimulus (such as tissue factor from a wound, or exposed collagen at the site of endothelial injury) initiates platelet activation.
- b) The platelets secrete activators which recruit more platelets to the region, which in turn recruit additional platelets in a positive feedback mechanism [8].
- c) After a delay of approximately 1 minute those platelets that were activated in the early stage of thrombosis begin to synthesize and secrete NO [9].
- d) NO's small size and consequent high diffusion coefficient cause it to be transported rapidly to the boundaries of the thrombus, where platelets are recruited. NO overtakes the agonists, shutting down recruitment and confining the thrombus [10] [11].

If this mechanism is valid, then the inhibition by NO near the periphery of the thrombus must overcome the effect of the activators. It will therefore be important to know how different concentrations of activators and inhibitors interact with one another to produce a composite effect. A better understanding of NO's regulation mechanism, through this research and others, may enable better prevention of coagulation in the previously mentioned diseases. One potential application is the modification of cardiovascular stents to control thrombus formation after angioplasty.

#### 1.1.1 Platelet Physiology

Platelets are the essential components of hemostasis. They are derived from shredded megakaryocyte cells found in bone marrow. The megakaryocytes measure 40 to 100  $\mu\text{m}$  across and contain polyploid nuclei. However, the platelets have no nucleus and range from 2 to 4  $\mu\text{m}$  in diameter [12]. Once produced, platelets circulate within the blood system awaiting activation. When they come into contact with exposed collagen,

they activate other platelets by discharging agonists, such as Adenosine Diphosphate (ADP), serotonin, thrombin, von Willebrand factor, and fibrin-stabilizing factors.

The steps in thrombus formation are diagrammed in Figure 1 [13]. Upon endothelial cell damage, platelets bind to the collagen and von Willebrand factor absorbed on the collagen [14]. von Willebrand factor attaches to platelets in a shear-dependent manner and is responsible for an increase in adhesion with increased shear stress [15] [16]. Platelet activation increases with increased shear and increased time of exposure to shear [17] [18]. Once adhered, platelets activate surrounding platelets. From this point, thrombin is produced, from prothrombin, which polymerizes fibrinogen to form fibrin. In the meantime, platelets bind to one another to form aggregates. The fibrin forms a mesh that encloses platelets, other cells and proteins to form the thrombus. Guyton describes two classical coagulation cascades the intrinsic and extrinsic pathways

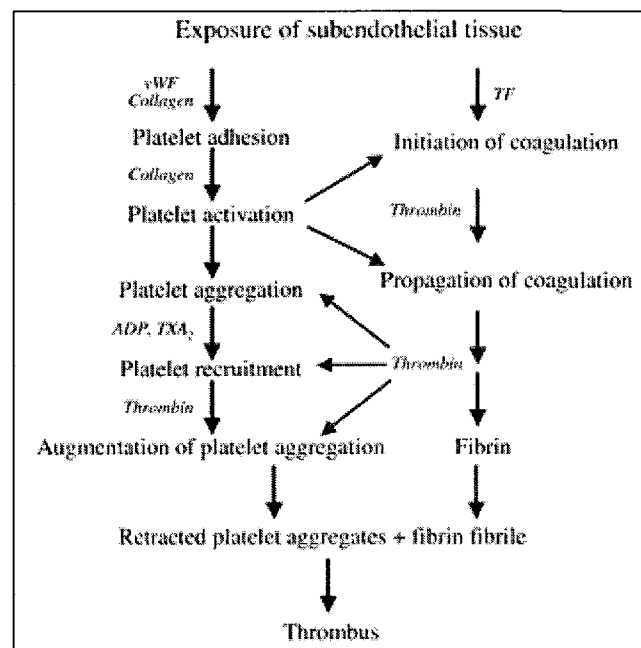


Figure 1 Platelet Mechanism for the Formation of a Thrombus [13]

which differ primarily in their trigger. However, much of the process occurs within a trigger-independent common pathway [19]. Within the cascade, platelets adhere not only to one another, but to traumatized endothelial cells with collagen fibers and the von Willebrand receptors [20] [21].

In addition to secreting platelet agonists, platelets produce NO, as do endothelial cells for vasodilation [22] [23]. NO is not stored in platelets, but the enzyme that produces NO, NO synthase (NOs), is present in them and becomes activated after platelet activation. Figure 2 displays the step-by-step process of NO synthesis. L-arginine, O<sub>2</sub>, and nicotinamide adenine dinucleotide phosphate (NADPH) are the reactions, and NO, L-citrulline and (NADP<sup>+</sup>) are the final products. The ion Ca<sup>2+</sup> serves as a catalyst for the mechanism [24] [25]. Once sufficient levels of NO are produced, they diffuse more quickly than the platelet agonists because their coefficient of 33 μm<sup>2</sup>/sec allowing NO to travel farther and faster through the body [26] [27].

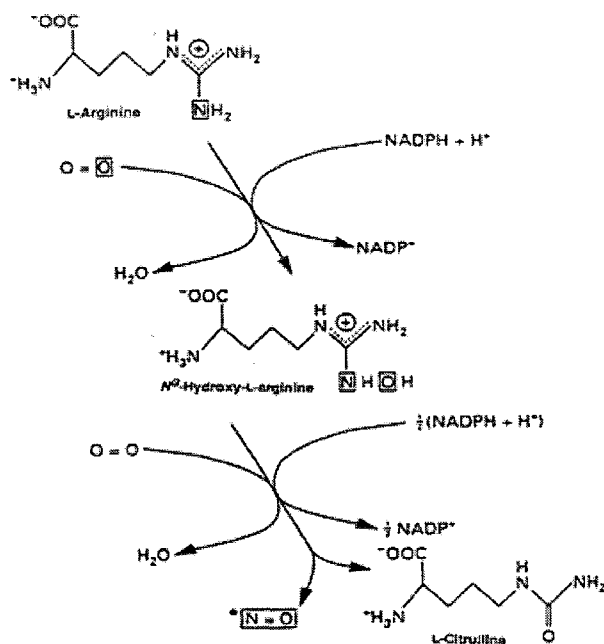


Figure 2 Production of NO from L-arginine with the aid of NOs [24]

The mechanism of action for NO is shown in Figure 3. NO causes generation of guanosine monophosphate (cGMP), which binds to phosphodiesterase III (PDE III). The PDE III decreases cyclic adenosine monophosphate (cAMP) metabolism [28]. Increased cGMP and cAMP levels increase protein kinase G (PKG) and protein kinase A (PKA) activities and inhibit protein C (PKC) activation and Ca<sup>2+</sup> mobilization [29] [30] [31] [32]. These last two agents inhibit platelet activation and promote vasodilation [33].

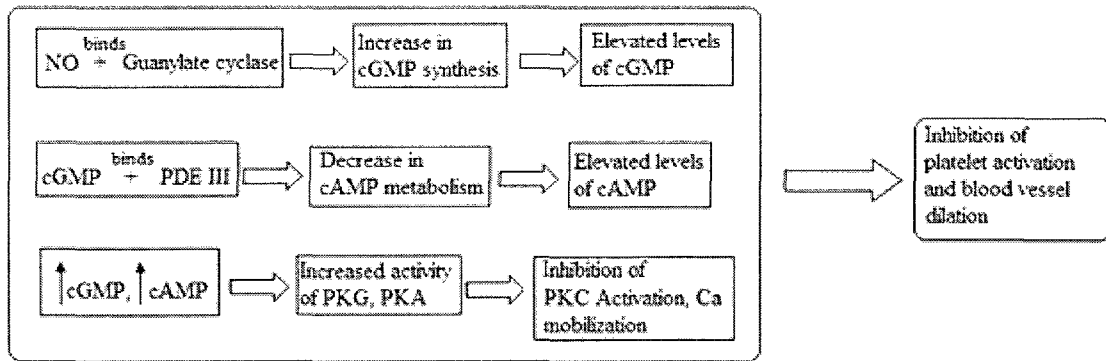


Figure 3 Mechanism for inhibition by NO

Because of NO's large diffusion coefficient, it is expected to diffuse from the thrombus core to places where other platelet-generated proteins, including activators, have not yet reached. This concept is the motivating hypothesis for this project in that this transport mechanism is important to the balance of positive and negative feedback in platelet function. Endothelial cells also produce NO through as the enzyme endothelial NO synthase (eNOs) [34]. Endothelial-derived NO relaxes smooth muscle cells, and therefore dilates the vasculature [35]. Endothelial cells produce several other hemostasis control factors that are produced by platelets, such as protein S and von Willebrand factor [36] [37].

## 1.2 Experimental Processes

### 1.2.1 Layer-by-Layer

The layer-by-layer (LbL) technique is a unique method for self-assembly nanomanufacturing. This technique is used for a variety of applications including some of the methods used in this project. Its versatility and simplicity allows the users to control the layering of materials and structures within a nanometer range [38]. A user is able to administer various chemicals, biointerfaces, mechanical, electrical, magnetic and thermal

properties. An object, such as a glass slide, silicon elastomer template and/or nanoshell, is layered with a series of alternatively charged polyionic solutions. The object structure is explicitly designed and layer thicknesses between 5 nm and 1000 nm can be controlled to within 1 nm [39] [40]. The objects to be coated are submerged into one polyionic solution at a time until a series of bi-layers are sufficiently structured. In turn, the last bi-layers may be used to affix a biointerface, such as fibrinogen or collagen, onto the object with the other polyionic solutions. These surfaces allow particulate and/or cellular membranes to adhere to the substrate for a strong coherence.

### 1.2.2 Biointerfaces

Fibrinogen is native to blood plasma and is produced in the liver [41] [42]. While its main role is to generate fibrin fibers in physiological conditions, it also functions as a bioactive surface for establishing platelet adhesions on LbL surfaces. Studies have demonstrated that platelets attach to this biointerface and have used this surface to investigate the effects of shear rate and perfusion time on platelet adhesion [43] [44]. Figure 4 displays a schematic of the fibrinogen molecule's crystal structure. Fibrinogen contains two sets of three chains labeled as  $\alpha$ ,  $\beta$  and  $\gamma$ . The chains are linked by disulfide bonds at the E and D terminals. Once fibrinogen is activated, fibrinogen is converted into fibrin through several steps to form a blood clot [45].

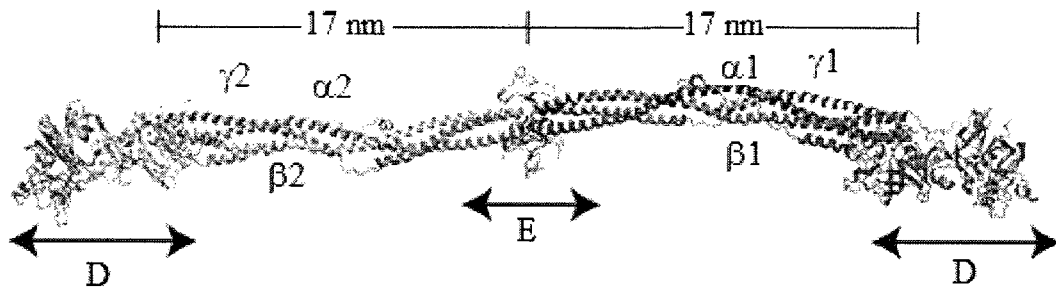


Figure 4 Crystal structure of fibrinogen [45].

Collagen is an alternative surface for platelet adhesion studies. Collagen bands are embedded into the tunica coats of the vasculature structures. When tissue damage exposes collagen to blood, factor XII and von Willebrand factor initiate the blood coagulation cascade [41] [46]. Studies have used collagen surfaces to examine the role of the NO inhibitor L-NAME and other chemical additives in platelet adhesion [47] [48]. Figure 5 displays a schematic of the inner structures of a collagen molecule and collagen fibrils. The figure illustrates a polypeptide chain contained in a triple-stranded collagen molecule. The collagen molecules form microfibril bundles which are then contained in a collagen fibril. A collection of fibrils make up a collagen fiber [49].

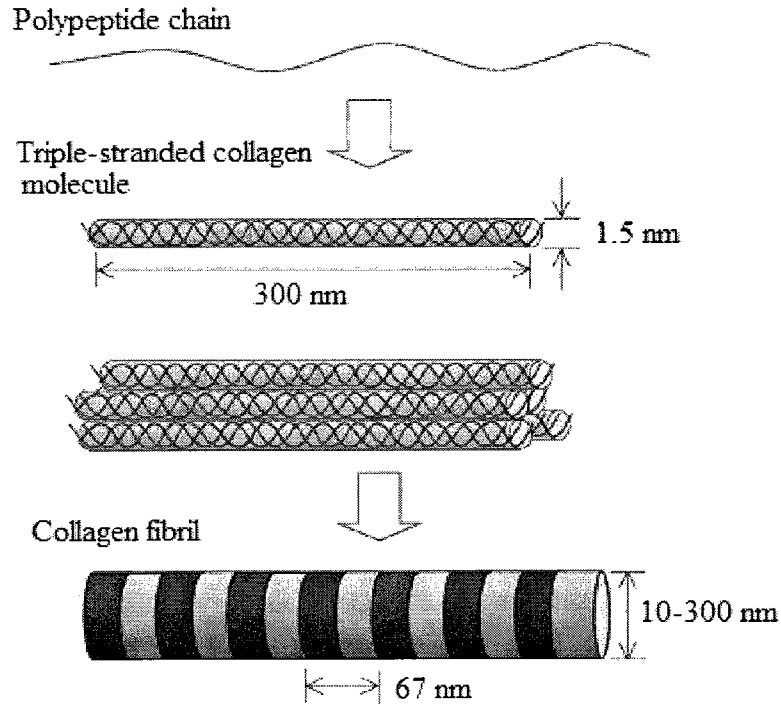


Figure 5 The structure of a collagen molecule

### 1.2.3 Chemical Additives

The additives of interest in this work are ADP, NO, L-A and N<sup>G</sup>-Methyl-L-arginine acetate salt (L-NMMA). Because ADP is a platelet activator, it can be used as a positive control for platelet activation, encouraging greater deposition along manipulative surfaces [50]. NO is the inhibitor interest [51] [27], and L-A is the known role of precursor to the NO synthesis. L-NMMA is a known inhibitor of NOs and can therefore be used to reduce production of NO [50] [52]. Thus, the biochemical additives, to be used in this study were selected to control, localize and/or increase the adherence of platelets along LbL generated biointerfaces.



### 1.3 Current Work

#### 1.3.1 Frilot's Dissertation

In examining the effect of NO on thrombus formation, two studies have produced seemingly conflicting results. Frilot studied the effect of L-A on the formation of thrombus on a collagen-coated Petri dish. He measured the production of serotonin, the size of the thrombi and the percentage of the dish that was coated with platelets. Because L-A is the precursor to NO, it was proposed increased levels of L-A would decrease all three measures of platelet activity. However, no statistically significant decrease was found in any of the measures of platelet activation and adhesion [53].

#### 1.3.2 Eshaq's Thesis

Eshaq examined the percent coverage of the bottoms of collagen and fibrinogen-coated microchannels under shear conditions with different levels of L-A, suggesting that platelet-derived NO can help to localize platelet adhesion. These studies demonstrated that percent coverage decreased with increasing levels of L-A in the microchannel system [13]. In addition, she measured the amount of thrombus formation in the microchannel system for different amounts of ADP and NO. The percent surface covered by platelets was relatively constant with ADP concentration in the absence of NO. The surface coverage decreased with increasing L-A, but as L-A concentration increased, the percent surface coverage depended more strongly on the ADP concentration. Thus, NO not only reduced platelet adhesion, but also increased the importance of ADP concentration in the positive feedback mechanism.

### 1.3.3 Frilot vs. Eshaq

The effect of L-A in Eshaq's work contrasts with the lack of effect in Frilot's work. The two studies differed in that Eshaq used dynamic flow conditions at a single shear rate, while Frilot used static conditions. They also differed in that Eshaq used fibrinogen as the substrate, while Frilot used collagen. To determine which, if either, of these two differences accounts for the differences in the results, it is necessary to use a system that allows one or both of the substrates to be used in both static and dynamic conditions.

In the current project, it was proposed that the effect of L-A depends on the shear rate along the biointerface. Several explanations can be proposed for the lack of effect in Frilot's studies, but the simplest is that the rate at which platelets came into contact with the surface was too slow, so that the NO produced by an adhered platelet was consumed before another platelet came into contact with the first platelet. This project therefore used a hybrid method that allowed one to control the shear rate and the NO/L-A concentration along with ADP and L-NMMA.

An understanding of the effect of shear on the action of NO would be useful in predicting the likelihood of a thrombosis in a patient's artery and could also be used in numerical simulations of thrombus formation (e.g. [54]). Moreover, it would provide insight into the interaction between the positive feedback mechanism inherent in platelet activation (e.g. activated platelets activating other platelets) and the negative feedback mechanisms that ultimately limit the extent of thrombus formation.

#### 1.3.4 Vyavahare's Thesis

Vyavahare numerically modeled the transport of NO near the wall in a microchannel with flow conditions. The geometry of his numerical model was a microchannel undergoing Couette flow with a constant-flux NO source at the wall. His study demonstrated that even with flow conditions in the microchannel, NO concentrations were still large enough to have an effect on the activation of platelet, according to previous studies on the effect of NO [55].

#### 1.3.5 Lopez's Dissertation

Lopez studied dynamically generated LbL (dLbL) surfaces as an alternative to statically generated LbL (sLbL) surfaces. The dLbL process is similar to the sLbL process, except that the fluid in contact with the surface during layering is in motion. The technique was introduced because results with sLbL suggested that the fluorescent label, Acridine Orange (AO) was trapped in pockets within the surface, so that the quantification of AO stain did not accurately provide the percent surface coverage of platelets. Lopez examined platelet adhesion to the dLbL-generated biointerface exposed to oscillatory flow of platelet-rich-plasma (PRP). He demonstrated that this surface provided more accurate fluorescence-based estimates of platelet surface coverage. He proposed that the sLbL surface included pockets that retained AO stain, even after rinsing.

Additionally, he designed a MATLAB particle tracking program to determine the shear stresses occurring over the LbL surfaces when oscillated on a shaker table. His particle tracking program discovered that the shear stresses for our laboratory's dynamically conditioned experiments were approximately  $0.003 \text{ dynes/cm}^2$  in the low

shear region of a glass slide,  $0.008 \text{ dynes/cm}^2$  in the medium shear region of a glass slide and  $0.01 \text{ dynes/cm}^2$  in the high shear region of a glass slide where human physiological shear stress conditions are approximately  $15 \text{ dynes/cm}^2$  [56].

#### 1.4 Hypotheses

To further examine the differences between the sLbL and dLbL topographies, and to understand the relationship between topography and platelet adhesion. The following hypotheses will be tested in this thesis:

- a) LbL surfaces that have been exposed to PRP will demonstrate features that are consistent with adhered platelet aggregates and that are not present on LbL surfaces that have not been exposed to PRP.
- b) Fluorescence Microscopy, Field Emission Scanning Electron Microscopy (FE-SEM) and Atomic Force Microscopy (AFM) images from surfaces generated by sLbL will indicate a rougher surface than those from surfaces generated by dLbL.
- c) Peak heights for AFM images taken from bioactive surfaces exposed to PRP will be greater when the surface is generated with dLbL instead of sLbL.
- d) Fluorescence Microscopy, FE-SEM and AFM images of dLbL-coated fibrinogen surfaces will indicate a rougher surface than those of dLbL-coated collagen surfaces.
- e) L-A, ADP and L-NMMA will have a stronger effect on platelet adhesion at higher shear rates than at lower shear rates. Specifically, increased L-A will decrease platelet adhesion to a greater extent at high shear rates than at low

shear rates, whereas ADP and L-NMMA will increase platelet adhesion at high shear rates than at low shear rates.

To test these hypotheses:

- a) Glass slides will be either sLbL coated with fibrinogen, dLbL coated with fibrinogen, dLbL coated with collagen or exposed to plain PRP will be imaged with AFM and FE-SEM. The sLbL and dLbL images will be compared to the plain PRP images to determine the peak height value differences and visual confirmations.
- b) sLbL-coated and dLbL-coated glass slides will be imaged using AFM, FE-SEM and Fluorescence Microscopy. Fluorescence Microscopy will supply surface coverage percentages based on platelet adhesion sizes for statistical analysis. The feature heights of the two surfaces will be compared from the maximum heights provided from AFM scans, while FE-SEM and Fluorescence Microscopy will provide a visual confirmation of surface topography differences. Fibrinogen and collagen dLbL slides will also be imaged with these modalities and compared.
- c) Glass slides with sLbL-fibrinogen, dLbL-fibrinogen and dLbL-collagen coatings will be scanned with the AFM to determine the peak height value variations for each of the four types of coatings.
- d) Fibrinogen-coated and collagen-coated dLbL surfaces will be imaged with Fluorescence Microscopy, AFM and FE-SEM to indicate the surface characteristics and roughness of fibrinogen and collagen via visual confirmation and peak heights comparisons.

- e) Predetermined amounts of L-arginine, ADP and L-NMMA will be added to PRP, which will be exposed to dLbL/fibrinogen-coated and dLbL/collagen-coated slides under static and dynamic conditions. The slides will then be imaged with AFM, FE-SEM and Fluorescence Microscopy, and the amount of platelet coverage will be compared qualitatively and quantitatively for the different shear rates.

## CHAPTER 2

### METHODS

#### 2.1 Overview

##### 2.1.1 Hypothesis 1

To determine whether platelet adhesion to sLbL and dLbL surfaces could be detected by AFM imaging and FE-SEM, sLbL and dLbL, surfaces with and without exposure to PRP were imaged. To produce sLbL and dLbL samples, glass slides were layered with polyionic solutions and a protein coating. Whole blood was then drawn from a bovine specimen and centrifuged to separate the PRP. Half of these samples were then exposed to PRP. After which, plain glass slides covered with PRP, prepared sLbL and dLbL samples exposed to PRP and prepared sLbL and dLbL samples without PRP were imaged. These images provided visual platelet confirmation and peak heights.

##### 2.1.2 Hypothesis 2

To determine whether the surface roughness of dLbL substrates differs from that of sLbL substrates, several glass slides were coated with fibrinogen or collagen both dynamically and statically. These slides were then layered with polyionic solutions and fibrinogen or collagen. Whole blood was then extracted from a bovine source and centrifuged for PRP collection. Subsequently, these slides were exposed to PRP and stained with AO. Following the experiment, all samples were imaged with the Olympus IX51 fluorescence microscopy, the Quesant Instrument Corp. atomic force microscopy

and the Hitachi S-4800 field emission scanning electron microscopy. The fluorescence microscopy images provided a visual reference for surface roughness as well as surface coverage percentages. The AFM images were analyzed by visual confirmation and for peak heights. The FE-SEM images supply visual supplements to support any surface roughness characteristics.

### 2.1.3 Hypothesis 3

To determine whether the peak heights for dLbL surfaces are greater than sLbL surfaces by detection of AFM, several glass slides were layered with polyionic solutions and a protein coating by a dynamic or static layering technique. Then, bovine whole blood was collected and centrifuged for PRP accumulation. Once PRP was collected, dLbL and sLbL surfaces were exposed to PRP and stained with AO. The samples were then scanned with the AFM to obtain peak heights.

### 2.1.4 Hypothesis 4

To determine whether the fibrinogen biointerface generated a rougher surface with the dLbL technique than a collagen coating, dLbL surfaces were layered with fibrinogen or collagen as the final coatings. The dLbL surfaces were prepared with polyionic solutions. Bovine whole blood samples were collected and centrifuged to obtain PRP. Next, the PRP was poured over the dLbL-fibrinogen or collagen substrates and stained with AO. These samples were imaged with fluorescence microscopy, AFM and FE-SEM for visual confirmation, surface coverage percentages and peak heights.

### 2.1.5 Hypothesis 5

To determine whether L-A, ADP, L-NMMA and plain PRP have a stronger effect on platelet adhesion at higher shear rates than at lower shear rates, dLbL surfaces



were generated using polyionic solutions and a protein coating. These surfaces were exposed to centrifuged PRP collected for a bovine source. During experimentation, samples were tested under dynamic and static conditions. For dynamic conditions, the slides were PRP was oscillated over the surface of the slides using a VWR Advanced Digital shaker table. For static conditions, the slides were placed beside the shaker table while exposed to PRP. Following the experimentation, all slides were stained with AO and imaged with fluorescence microscopy and AFM. From these imaging techniques, surface coverage percentages, platelet adhesion sizes and peak heights were accumulated.

## **2.2 Experimental Processes**

### **2.2.1 Generation of sLbL and dLbL surfaces**

#### **2.2.1.1 Slide Preparation**

Premiere<sup>®</sup> 75 mm x 25 mm plain glass microscope slides were cleaned with 91 % isopropyl alcohol and de-ionized (DI) water. Each slide was first inserted into a 50 mL polypropylene conical tube filled with isopropyl alcohol and swirled on a VWR Advanced Digital shaker table at 120 rotations per minute for 7 min. After which, the slides were inserted into 50 mL tubes containing DI water and swirled on the shaker table for 7 min at a rate of 120 rotations per minute. Immediately following this procedure, the slides were then dried and stored until needed for a PRP experiment.

Immediately before a PRP experiment, a strip of silicon elastomer was cut and adhered to the back side of each slide to protect it from contamination by particulate matter accumulation on the back side of the slide. The strips were removed directly before each slide was imaged under fluorescence microscopy. This technique was incorporated into the slide preparation to elimination any addition surface features. Tests

were performed with slides with and without the addition of silicon elastomer to prove the necessity of its use to the backside of the slides and were determined as essential.

#### 2.2.1.2 Chemical Preparation

Poly (diallyldimethylammonium chloride) (PDDA), Poly (sodium 4-styrene-sulfonate) (PSS), Sodium phosphate monobasic (PBS), AO hemi (zinc chloride) salt, Tris buffer saline tablet, Fibrinogen fraction 1 type 1-S, collagen from calf skin, Hydrochloric Acid (HCl), and Sodium citrate were purchased for Sigma Aldrich (St. Louis, MO). Sodium Hydroxide (NaOH) pellets were purchased from Fluka, a subsidiary of Sigma Aldrich (St. Louis, MO). The chemical solutions were prepared under the following specifications:

- a) HCl – The solution was laboratory stock as prepared by Eshaq at 2 M HCl. The pH was measured at 2.0. The solution was stored at room temperature in the laboratory Supreme Air<sup>®</sup> chemical hood.
- b) NaOH – Four NaOH pellets were added to 400 mL of DI water in a 500 mL flask. The solution was thoroughly mixed. The pH was measured at 12.0 and the solution was stored at room temperature.
- c) PDDA – A total of 94.6 mL of the reagent were thoroughly mixed with 905.4 mL of DI water in a 1 L flask. The pH was measured with a Mettler Toledo Seven Easy pH meter and adjusted to 7.5 if necessary with HCl and/or NaOH. The solution was stored at room temperature.
- d) PSS – A total of 3 g of powder was measured with the Acculab scale and added to 1 L DI water in a 1 L flask. The solution was thoroughly mixed. The

pH was measured, and, if necessary, HCl and/or NaOH were added to adjust it to 7.5. The solution was stored at room temperature.

- e) PBS – For every 12 mg of PBS, 1 mL of deionized water was added to a 1 L flask. Thus, 10.8 g was measured out on the Acculab Vicon<sup>®</sup> scale and added to the flask along with 900 mL of DI water. The pH did not need to be measured. The solution was stored in the refrigerator at 4 °C.
- f) Tris Buffer Saline – To ensure tablet dissipation with the DI water, 1 tablet was added to 37.5 mL of DI water in a 50 mL conical tube and vortexed with the Bio-Rad<sup>®</sup> vortexer. This process was repeated 12 times to produce 450 mL Tris Buffer Saline solution in a 500 mL flask. The pH level did not need to be measured. The solution was stored in the refrigerator at 4 °C.
- g) Fibrinogen – For every 1 mg of Fibrinogen, 1 mL of Tris Buffer was added to a 1 L flask. A total of 450 mg of fibrinogen powder was slowly mixed with 450 mL of Tris Buffer. According to the manufacturer's protocol, a 3M<sup>®</sup> Respirator was used during fibrinogen production. The pH was measured and adjusted to 7.5. The solution was stored in the refrigerator at 4 °C.
- h) AO – The solution was prepared entirely in a darkened room. For every 1 mg of AO powder, 1 mL of DI water was added and thoroughly mixed. A total of 500 mg of AO was added to 500 mL of DI water in a 500 mL beaker. In turn, the suspension was filtered using a 0.2 µm syringe filter into a 500 mL flask covered with aluminum foil. The pH was not adjusted. The solution was stored at room temperature.

- i) Collagen – A 0.1M solution of acetic acid was prepared from 5.75 mL of glacial acetic acid in 994.25 mL of DI water in a 1 L flask. Fifty mg of collagen powder was mixed in 50 mL of the 0.1 M acetic acid solution and was stored at in the refrigerator overnight. The following day, the collagen solution was placed on the shaker table and oscillated for 2 hrs to dissolve any remaining fibrils. The 50 mL solution was then added to 375 mL of DI water in a 500 mL flask to produce a 0.133 mg/mL collagen solution. The original 0.1 M acetic acid and/or NaOH were then added to adjust the solution's pH to approximately 7.5. The solution was stored in a refrigerator at 4 °C.
- j) Sodium Citrate – Sodium citrate was pre-prepared by Sigma Aldrich with a catalog number of S5770. The solutions were stored in a refrigerator at 4 °C.

### 2.2.1.3 Static LbL (sLbL)

#### 2.2.1.3.1 PDDA and PSS Precursor Layers

Several slides were prepared for sLbL self-assembly by placing four 750 mL rectangular Pyrex<sup>®</sup> dishes in the pattern illustrated in Figure 6. We dipped clean glass slides into a Pyrex<sup>®</sup> dish containing the cationic polyelectrolyte PDDA. We then removed the slides after 10 min and inserted them into another Pyrex<sup>®</sup> containing DI water which was used as a rinse. After a 1 min rinse, we dried the slides and placed in a controlled chamber with a temperature of 35 °C and a humidity of 20 % until completely dry. Following drying, we inserted the slides into another Pyrex<sup>®</sup> dish containing PSS. The slides were removed after 10 min. Finally, we rinsed the slides by inserting them into a another Pyrex<sup>®</sup> containing DI water, then dried and placed them in the controlled chamber. This process was repeated four more times for a total of five bilayers.

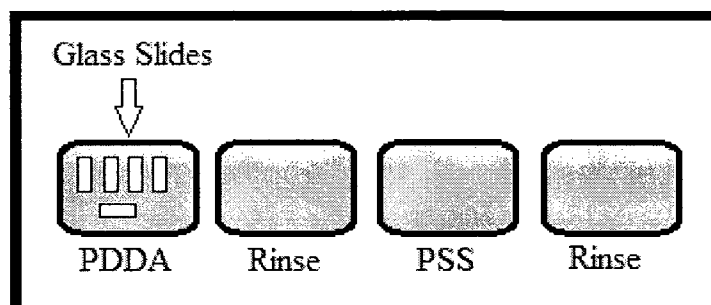


Figure 6 Static LbL Process: PDDA and PSS

#### 2.2.1.3.2 PDDA and Fibrinogen Biinterface Layer

The layout for the static layering of fibrinogen is shown in Figure 7. We poured PDDA into the first dish, DI water in the second dish, fibrinogen solution in the third dish, and DI water rinse in the fourth dish. We inserted the previously LbL'd slides into the PDDA for 10 min, rinsed for 4 min, dried and placed them in the controlled chamber. We then dipped the slides into the fibrinogen for 20 min, rinsed for 4 min, dried and placed them in the controlled chamber. This process was repeated two more times for three bilayers, so that each slide had eight bilayers total.

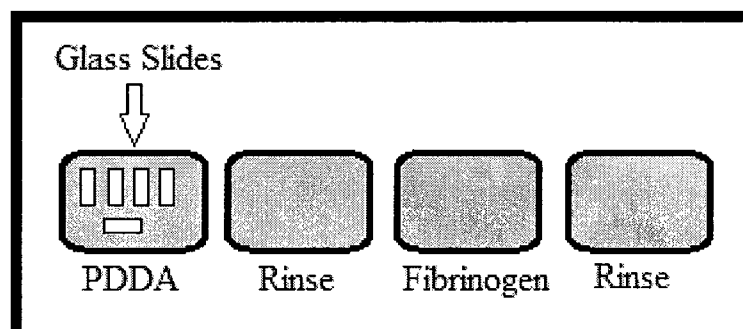


Figure 7 Static LbL Process: PDDA and Fibrinogen

#### 2.2.1.4 Dynamic LbL Technique (dLbL)

##### 2.2.1.4.1 PDDA and PSS Precursor Layer

For all of the biointerfaces, it was necessary to first coat the slides with a precursor layer that improved the ability of the biointerface layers to cover the surface. Each clean glass slide was dipped into a 50 mL tube containing 35 mL of cationic polyelectrolyte PDDA. The slides were removed after 10 min and inserted into another set of 50 mL tubes containing 45 mL of DI water, which was used as a rinse. After a 1 min rinse, the slides were dried and placed into the temperature and humidity-controlled chamber. Each slide was then inserted into a tube containing 35 mL of PSS for 10 min. The slides were then once again rinsed in a set of tubes containing 45 mL of DI water, dried and placed in the controlled chamber. This process was repeated four more times for a total of five bilayers. Figure 8 shows three tubes with slides inserted while oscillating on the shaker table surface.

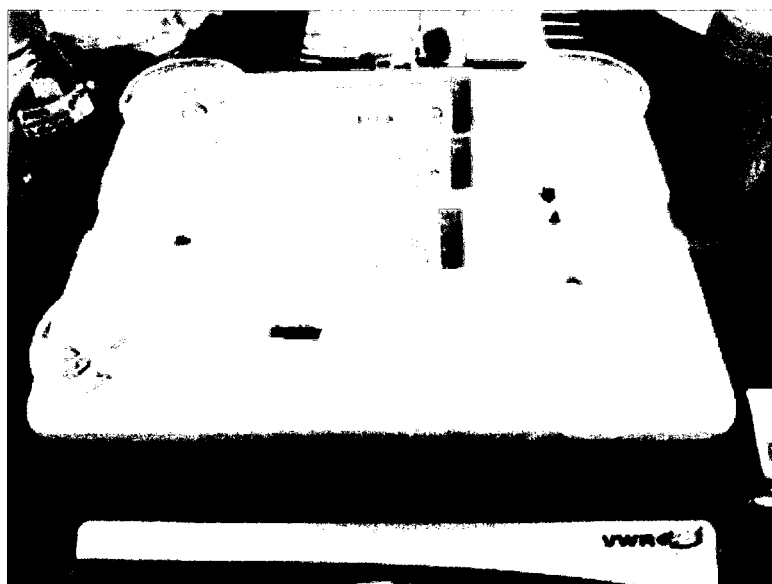


Figure 8 The Dynamic LbL process on the VWR shaker table

#### 2.2.1.4.2 PDDA and Fibrinogen Biointerface Layer

To prepare the PDDA/fibrinogen biointerface, 15 slides that were prepared with the PDDA/PSS precursor layer were first dipped into 50 mL tubes containing 35 mL of PDDA. The slides were then removed after 10 min and inserted into another set of 50 mL tubes containing 45 mL of DI water which was used as a rinse. After a 4 min rinse, we dried the slides and placed them in the controlled chamber. Following drying, we inserted the slides into tubes containing 35 mL of fibrinogen for 20 min. Finally, we rinsed the slides by inserting them into another set of tubes containing 45 mL of DI water, then dried and placed them in the controlled chamber. This process was repeated two more times for three bilayers. This second step brought the total count to eight bilayers.

#### 2.2.1.4.3 Collagen and PSS for dLbL-Collagen

To prepare slides with the collagen/PSS biointerface, 15 slides were prepared with the PDDA/PSS precursor layers and then alternatively layered with collagen and PSS, following the same dip/rinse/dry sequence as for the PDDA/fibrinogen biointerface. In each case, the slide was exposed to the collagen solution for 20 min and to the PSS solution for 10 min. The final surface had five PDDA/PSS bilayers and three collagen/PSS bilayers, for a total of eight bilayers.

#### 2.2.2 Control Chamber Preparation

Prior to dynamic and static PRP experiments, the control temperature and humidity devices were switched on and allowed to adjust to the desired parameters of 35 °C with 20% humidity. These parameters were determined by ambient temperatures and humidity thus maintaining Louisiana Tech dairy conditions. The chamber was cleaned with Clorox<sup>®</sup> wipes prior to each blood experiment to eliminate any particulate matter

along the interior of the box. Wax paper and paper towels were inserted on the floor of the box. The shaker table from the general laboratory was cleaned and placed into the box. A beaker for PRP and PBS waste along with pair of forceps for grasping the slides were put in the box.

### 2.2.3 Petri Dish Preparation

Twelve to fifteen 100 mm x 15 mm Petri dishes were prepared depending on the PRP experimentation requirements for that day's session. Each Petri dish was labeled according to the sample slide specifications on the lid and bottom dish. A permanent marker was used to indicate the sample specifications on each Petri dish. Figure 9 demonstrates a typical marked Petri dish. In this figure, "D" indicates a sample to be performed under dynamic conditions. The "20 L-A" marking denotes that this sample had PRP with L-A with a molarity of 20  $\mu$ M poured over the slide.

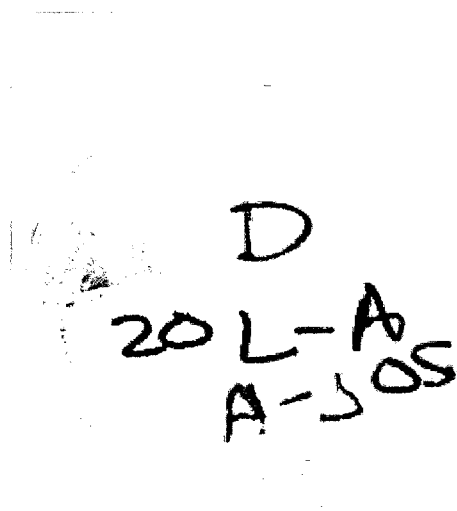


Figure 9 Petri Dish Marking



#### 2.2.4 Bovine Blood Collection

A total of 5 mL of sodium citrate were pipetted into a 50 mL conical tube for a 9:1 sodium citrate to whole blood ratio. Three tubes were then placed in an Igloo® ice chest along with a pair of medium size latex powdered gloves, paper towels, a bovine blood collection journal with pen and a 16-gauge needle. Bovine whole blood samples were collected from the Louisiana Tech University dairy located on Tech Farm Road in Ruston, Louisiana in accordance with the Louisiana Tech IACUC (Animal Care) Committee (Appendix E). On days of blood collection, my laboratory colleague, Juan M. Lopez, and I arrived at 1:30 pm and extracted blood samples from the same Jersey cow, #41. Blood samples were obtained from the milk vein located on the lower abdomen in front of the udder sack. A total of 45 mL of whole blood were collected in each 50 mL tube. After each accumulation, the 50 mL tubes were gently rocked back and forth to ensure sodium citrate/whole blood mixing. Afterwards, each tube was gently placed in the Igloo® ice chest for storage until arrival at the Louisiana Tech Biomedical Engineering Center. All blood samples were taken to the Biomedical Engineering Center directly after collection and centrifuged within 30 min. Figure 10 displays whole blood samples in 50 mL conical tubes being prepared for centrifugation.

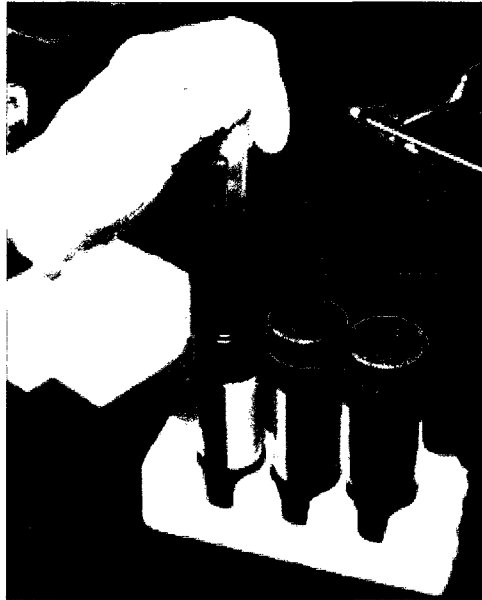


Figure 10 Whole Blood Samples mixed with Sodium Citrate

#### 2.2.5 Centrifugation

The blood from the 50 mL conical tube was divided into seven 15 mL centrifuge tubes, with 7 mL of blood in each tube. The blood was then centrifuged at 1000 rcf for 25 min at a temperature of 30 °C in the Eppendorf Centrifuge 5804R model. A brake setting of 6 up and down was applied. After each spin, the tubes were carefully removed from the centrifuge so as to not mix the supernatant with the red and white blood cells. The tubes were placed in a foam tube holder to allow for PRP extraction.

#### 2.2.6 PRP Collection Process

The PRP supernatant was removed from each 15 mL centrifuge tube and loaded back into a 50 mL conical tube by a plastic 3 mL capacity pipette extraction.

Approximately 30 mL of PRP was collected from a group of seven 15 mL tubes. Figure 11A shows the PRP collection process. Figure 11B shows the appearance of the collected PRP.



Figure 11 PRP collection process and PRP confirmation. (A) Collection from the centrifuged blood. (B) Separated PRP.

#### 2.2.7 PRP Dilution

From the estimated 30 mL of PRP collected in each 50 mL tube, approximately 20 mL of PBS were added to bring the total solution back to its original 50 mL of blood. After the PBS addition, the 50 mL tubes were gently rocked to mix the PBS and PRP.

#### 2.2.8 PRP Experimentation

For each PRP experiment, glass slides, previously layered with polyionic solutions and a protein substrate, were tested under dynamic and static conditions using bovine PRP and chemical additives. The coated slides were subjected to three LbL techniques including sLbL-fibrinogen substrate, dLbL-fibrinogen substrate and dLbL-collagen substrate. Once layered, the slides were grouped, according to whether they would be treated with ADP, L-NMMA, L-A, or plain PRP, and whether they would be subjected to dynamic or static conditions.

The PRP experiment began once centrifuged bovine PRP with and without chemical solutions was poured over each slide in a Petri dish. Figure 12 shows a dynamic and static condition PRP experiment with PRP being pipetted over the surface of the slides. After the exposure time, slides were rinsed, allowed to dry, stained with AO, rinsed and dried again.

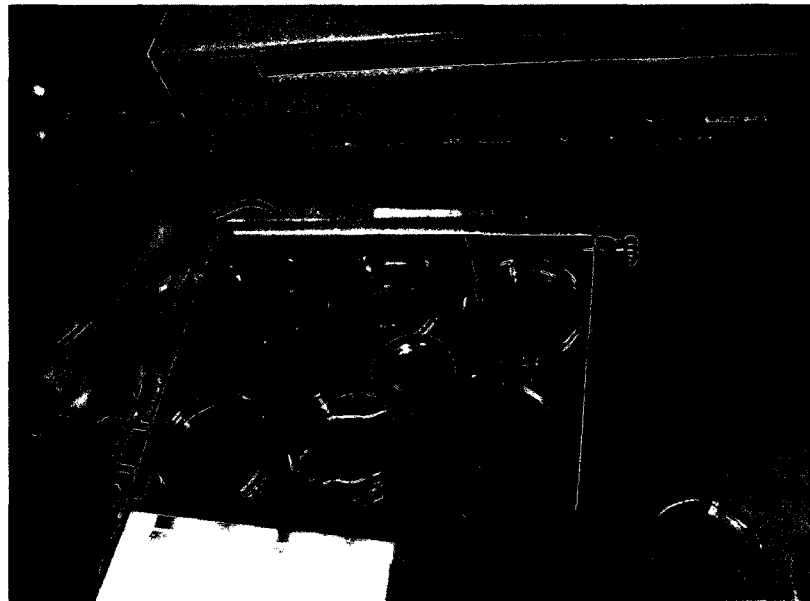


Figure 12 Exposure of glass slides to PRP under dynamic conditions

Data collected from each slide provided surface topography peak information, and both AFM and FE-SEM provided qualitative visual images, Microsoft Excel™ and MATLAB to analyze all of the collected data.

## 2.2.9 Static Condition of PRP Experimentation

### 2.2.9.1 Testing

For static conditions, the Petri dish/slide setups were placed directly in the temperature and humidity controlled chamber (Figure 13). The PRP+L-A, PRP+ADP, PRP+L-NMMA and plain PRP samples were poured over dLbL'd glass slides contained

in 100 mm x 15 mm Petri dishes. We exposed the samples to PRP for 30 min after which, the PRP solutions were disposed of in a waste container. We then rinsed the slides with PBS for 4 min and then dried them overnight in the controlled chamber.

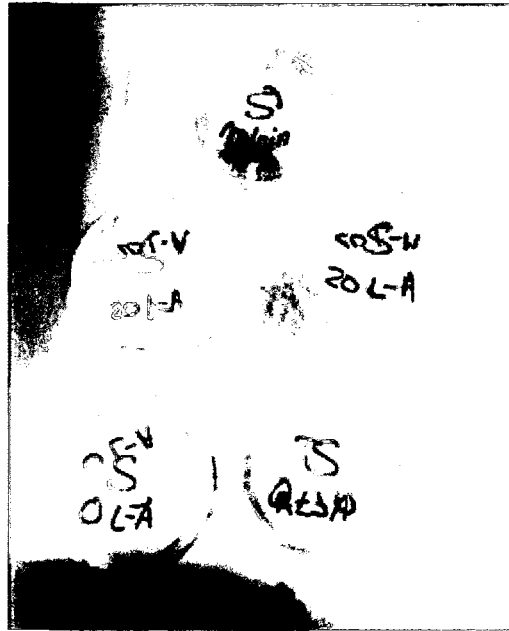


Figure 13 PRP Setup for a Static Experiment

### 2.2.10 AO Staining

AO stain was applied with the laboratory lights off under static conditions inside the temperature and humidity control chamber while using a General Electric® UV black light. A total of 7 mL of AO was distributed over each Petri dish/slide setup and allowed to rest over the slide for 20 min. The AO was then poured from the Petri dish into a waste container. The slides were rinsed and dried as described in Section 2.2.9.1. After which, we stored them in rectangular Pyrex® dishes covered with aluminum foil, and placed in the Roper Refrigerator at 4 °C until removed for imaging.

AO, a nucleic acid cell-permeant dye, stains platelets by binding electrostatically to platelet mRNA. When AO is bound to RNA, it fluoresces red at approximately  $\lambda \approx$

650 nm. AO also fluoresces green, as it is metachromatic, at approximately  $\lambda \approx 525$  nm when staining DNA. However, this green fluorescence is not a problem as platelets are known to contain mRNA only [57].

#### 2.2.11 Sample Storage

The stained slides were placed in rectangular Pyrex dishes that were lined with aluminum foil to block light and refrigerated at 4 °C.

#### 2.2.12 Waste Disposal

All liquid waste produced during the LbL processes and PRP experiments was transferred to a chemical waste container stationed in the chemical hood of Dr. Jones' laboratory. Dr. James Spaulding, Director of Biological Support Services, removed the liquid waste from the chemical hood at his discretion. All solid waste including: surplus whole blood in 50 mL tubes, used pipettes and latex gloves was disposed of in the laboratory biohazard waste container. Any broken glass and used needles were discarded in the laboratory sharps container.

#### 2.2.13 Atomic Force Microscopy

The Quesant Instrument Corporation atomic force microscope, located in the Institute for Micromanufacturing's Meterology laboratory, was used for scanning the topographical information on glass slides of interest. Dr. Alfred Gunasekaran assisted in my training on the AFM for the prolonged scanning studies and allowed me to work alone after several training exercises. Twenty-nine samples were AFM-imaged with approximately five scans per sample.

The slides were prepared for the AFM after fluorescence microscopy by spraying nitrogen gas over the samples to remove any particulate matter on the glass surface. The

slides were placed in a labeled Petri dish for proper storage in a refrigerator at 4 °C for later use. Once ready, samples were placed on the ministage platform of the AFM for analysis. The Stage Camera screen and Scan Head Control window were opened on the main screen by clicking the Scan Head Control button. The AFM laser was then switched on by clicking the Toggle Laser button on the menu bar. The cantilever was lowered close to the sample surface by clicking the Fast Up button on the Scan Head Control window. To acquire an image, a piezoelectric element drags the tip across the sample, and the tip moves up and down with the elevation of the sample. A laser beam is reflected from the cantilever and a multi-segment photodiode discerns the beam position, which in turn indicates the surface morphology of the sample [58].

Table 1 displays the configuration settings for AFM imaging. The Download button and then Set Cantilever Frequency buttons were clicked. This operation brought up the Wave Mode Signal menu. The lock button was clicked after the oscillator was set at around 1 to 2 for a frequency peak of approximately 150-180 Hz. Immediately following, the Engage button was clicked to bring up the Engage Response menu. In the Wavemode setting the signal damping was set at approximately 50%. In turn, the auto box was checked and the NSC16 cantilever was selected for the non-contact mode. Once in place, the Auto Engage was clicked. After signal feedback was achieved, the scan button was clicked in the Scanner Z-Voltage menu bar. Finally, the scan window was opened and the scan button was clicked to start the actual sample scan.

Table 1 Configuration settings for AFM imaging

AFM Settings	Values
Scan size	40 $\mu\text{m}$ x 40 $\mu\text{m}$
Scan rate	1 Hz
Integral gain	300
Proportional gain	250
Scan resolution	512
Bias voltage	-1.2 V to -0.06 V
X Center Dimension	0
Y Center Dimension	0
Z Center Dimension	0
XY Disabled	No
Scan Type	Wavemode
XY Signal Mode	Standard
Z Signal Mode	Standard

After each scan, tilt removal was selected to allow for a parabolic signal change. The scan was then viewed and transferred to the Microsoft Paint editing program for image manipulation. The images were then saved to a folder listed under Dr. Jones' name. All scans were rotated under the viewing program for different image angles. After viewing and imaging capturing was complete for a single scan, the Withdraw button was clicked and the scan window closed. The process was repeated numerous times according until a desired collection of samples were achieved. All images saved to the Dr. Jones folder were loaded onto a zip disk by the Dell computer's zip drive. An independent zip drive allocated for student use, was connected to my laptop to upload each bmp image.

#### 2.2.14 Field Emission Scanning Electron Microscopy

A Hitachi S-4800 Field Emission Scanning Electron Microscopy located in the Meterology laboratory of the Institute for Micromanufacturing was used for this project's qualitative platelet confirmation purposes. I/M regulations concerning FE-SEM student usage prevented me from operating the device. Thus, Dr. Gunasekaran took all of the FE-



SEM images for this project with my assistance in specifying the exact locus of research concern along each sample.

Before each FE-SEM session, the slides were cut into approximately 1 in squares so that they could fit on the 2 inch diameter scanning disk. The samples were then cleaned by spraying the slides with nitrogen gas. At this point, Dr. Gunasekaran loaded each sample into the FE-SEM and set the voltage at approximately 1 kV-2 kV. Once complete, all jpeg images were loaded onto a flash drive for analysis and storage transfer.

#### 2.2.15 Fluorescence Microscopy Imaging

##### 2.2.15.1 Slide Cleaning and Marking

Before each session, the backsides of each glass slide were cleaned with a Kim<sup>®</sup> wipe sprayed with 91% isopropyl alcohol once the McMaster<sup>®</sup> silicon elastomer backing was removed. The backsides were thoroughly wiped clean of any extra particulate matter so as to eliminate confusion from the platelet particles on the top side of the slide. To ensure particulate removal, slides were first observed on the backside before proceeding with top side imaging.

After each slide was imaged, they were marked with a permanent marker to indicate the day of the PRP experiment, the chemical solution or plain PRP, and the dynamic or static condition as illustrated in Figure 14 for a dynamic condition sample from session 2 with a 20  $\mu$ M L-A concentration added to the PRP.

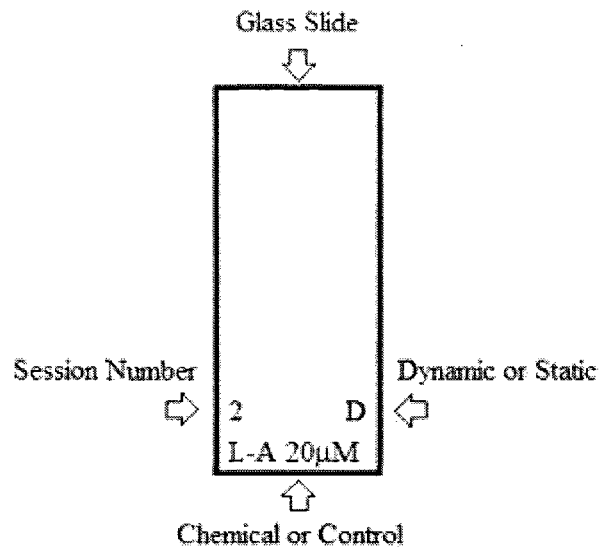


Figure 14 Glass Slide Markings

#### 2.2.15.2 Imaging

All slides were imaged using the Olympus IX51 fluorescence microscope with an Olympus DP71 camera in the microscopy laboratory of the Biomedical Engineering Center. The Olympus Corp. DP Controller and DP Manager software programs were opened on the Dell Precision 380 computer coupled with the microscope. Under the DP Controller program, Dr. Jones's laboratory settings were loaded from the user setting display. These settings generated an exposure time of 667 ms for a 10 x magnification. The DP Manager program allowed the pictures to be viewed and stored during captures. The TRITC filter was selected for proper imaging with AO. The 10 x magnification objective was selected. As a side note, the side microscope filter was inserted in all of the way to darken the image backgrounds of each slide. Before beginning each imaging session, the microscopy laboratory lights were switched off as to avoid slide bleaching.

Once slides were cleaned and ready for imaging, samples were placed top side down as the pictures from the camera will be taken from underneath the samples. The

fine and coarse focus controls were used to zoom in on the top surface of the slides. For static condition samples, a random location was selected somewhere along the left x-direction of the following slide figure. Images were taken along a column consecutively until reaching the right x-direction of the sample. From this right x-direction, the sample was then imaged until approximately 40 successive images were collected. For dynamic conditions samples, loci were selected based on the shear region of interest. Figure 15 shows approximate shear regions founded on concepts concerning a shear stress gradient discussed extensively in Lopez's dissertation concerning this matter for examining protein-coated slides under dynamic conditions [56]. Approximately 40 images were captured along columns in the y-direction of each shear region.

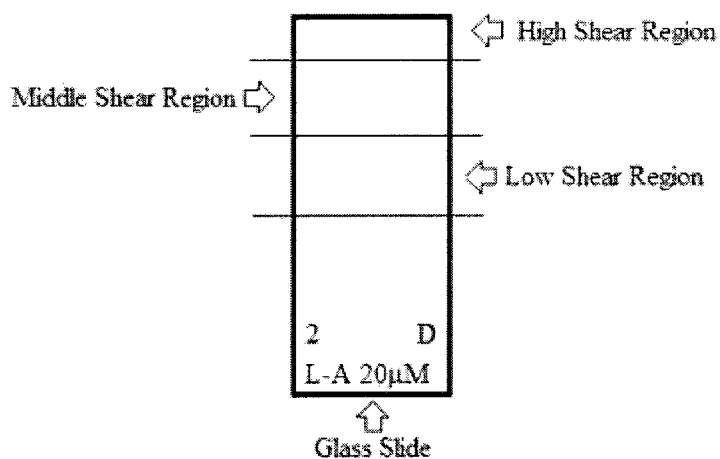


Figure 15 Shear Region Gradient for Image Location Selection

### 2.2.15.3 Data Processing

All images were downloaded from the Dell computer onto a flash drive and transferred to computer that had a MATLAB program installed. The image file conversion program with batch processing capabilities, InfranView, was used to convert all image

files from tiff to jpeg. The MATLAB m-file listed in Appendix A converted the images from color to black and white and calculated platelet percentage coverage as the ratio of white foreground areas to the black background area. The percent area coverage data were stored as Microsoft Excel™ files, and Excel™ statistical analysis tools were used to calculate averages, standard deviations, ANOVA information, and t-Tests results.

## 2.2.16 Generation of dLbL surfaces

### 2.2.16.1 Chemical Preparation

L-A, ADP, and N<sup>G</sup>-Methyl-L-arginine acetate salt (L-NMMA) were purchased from Sigma Aldrich (St. Louis, MO). The chemical solutions were prepared under the following specifications:

- a) L-A – 87 mg of L-A powder was added to 50 mL of DI water in a 50 mL conical tube to generate a 10 mM stock solution. To dilute the solution to 1 mM, 5 mL of the stock solution were thoroughly mixed with 45 mL of DI water in a 50 mL tube. The dilute aliquot was then filtered with a 0.2 μm syringe filter. The aliquot did not require a pH adjustment and was stored at room temperature.
- b) ADP – To generate a 1 mM ADP solution, 2.5 mg of ADP powder were added to 5 mL of PBS into a 15 mL tube. The solution's pH did not need to be measured or adjusted. The solution was stored in the freezer at -20 °C [50].
- c) L-NMMA – To prepare a 1 mM solution of L-NMMA, 25 mg L-NMMA powder were mixed with 5 mL DI water in the original L-NMMA bottle to remove all L-NMMA particles from the small container. The solution was added to 95 mL of DI water. The L-NMMA solution had a concentration of 1

mM. The solution's pH did not need to be measured. The solution was stored at room temperature [50].

#### 2.2.16.2 Addition of Chemicals

The PRP/PBS samples were divided into 15 mL tubes. For static condition, 7 mL of PRP were added to each tube with 140  $\mu$ L of L-A, 140  $\mu$ L of ADP and 140  $\mu$ L of L-NMMA for a 20  $\mu$ M solution. For dynamic conditions, 15mL of PRP was added to each tube with 300  $\mu$ L of L-A, 300  $\mu$ L of ADP and 300  $\mu$ L of L-NMMA for a 20  $\mu$ M. For the plain PRP, no chemicals were added. A Rainin P200 micropipette was used to transfer the  $\mu$ L quantities.

#### 2.2.17 Dynamic Condition of PRP Experimentation

##### 2.2.17.1 Testing

The setup for dynamic testing is shown in Figure 16. A VWR Advanced Digital shaker table was placed inside the temperature and humidity controlled chamber. The glass slides were placed in 100 mm x 15 mm Petri dishes on the shaker table, and PRP+L-A, PRP+ADP, PRP+L-NMMA and plain PRP samples were poured over the slides. The samples were then oscillated for 30 min at 60 rotations per minute. The PRP solutions were then poured from the Petri dishes and into a waste container.

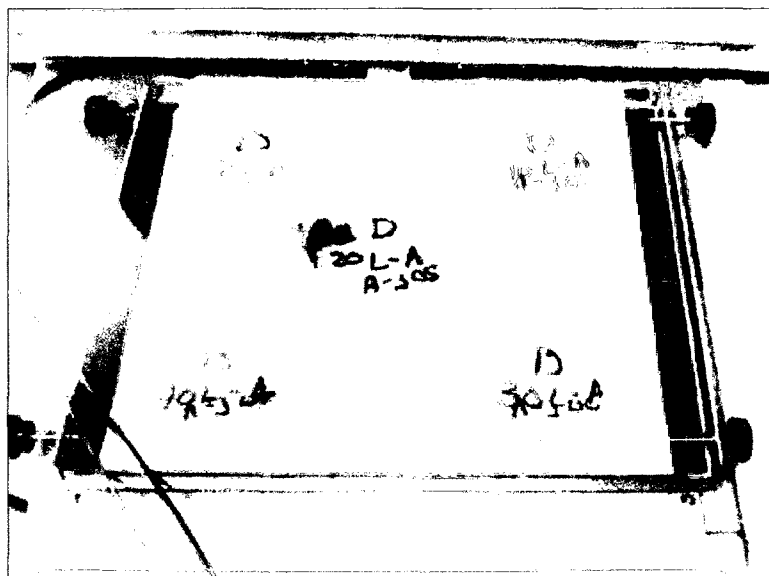


Figure 16 PRP Setup for a Dynamic Experiment

#### 2.2.17.2 Rinse

The slides were rinsed under static conditions with 7 mL of PBS for 4 min. The PBS was then poured from the Petri dishes into a waste container.

#### 2.2.17.3 Dry

The slides were allowed to dry in their respective Petri dishes overnight while still in the temperature and humidity controlled chamber. To eliminate drying rings on the slide surface, slides were placed at an angle with one side of the slide propped against the Petri dish lip and the other end placed in the middle of the slide. Therefore, the lower end of the slides that accumulated large amounts of PRP were not imaged.

#### 2.2.18 Particle Size Comparison

A MATLAB program, modified by Juan M. Lopez from a previous in-house code, was used to measure fluorescence microscopy image amalgamations for particle size comparisons based on each chemical's effect on the platelet adhesion size versus number of particles at that size. The complete program is listed in Appendix B. The program uses

fluorescence microscopy images that have been converted to black and white to calculate the size of each particle in each image. The program calculates the mean of a group of images taken from a given slide. The program provides one exponential curve with standard deviation error bars based on the given set of images. Each graph provides a plot of the mean with standard deviation versus the number of particles at that size.

### **2.3 Temperature and Humidity Control Chamber**

A temperature and humidity control chamber (Figure 17), originally constructed by Frilot, was used to eliminate temperature and humidity as variables for this project while performing a dynamic and static PRP experiment simultaneously. The box contains temperature and humidity probes, an aquarium pump for proper air ventilation, a small metal fan for convective purposes, a desiccant drying system for eliminating excessive humidity, a General Electric<sup>®</sup> heater, extended large arm gloves, foam sealants, clear plastic tubing and a surge protector outlet. The temperature and humidity control devices are stored on top of the box. Connected to these devices are the temperature and humidity probes. These control devices allow the user to adjust and maintain a desired temperature and humidity.

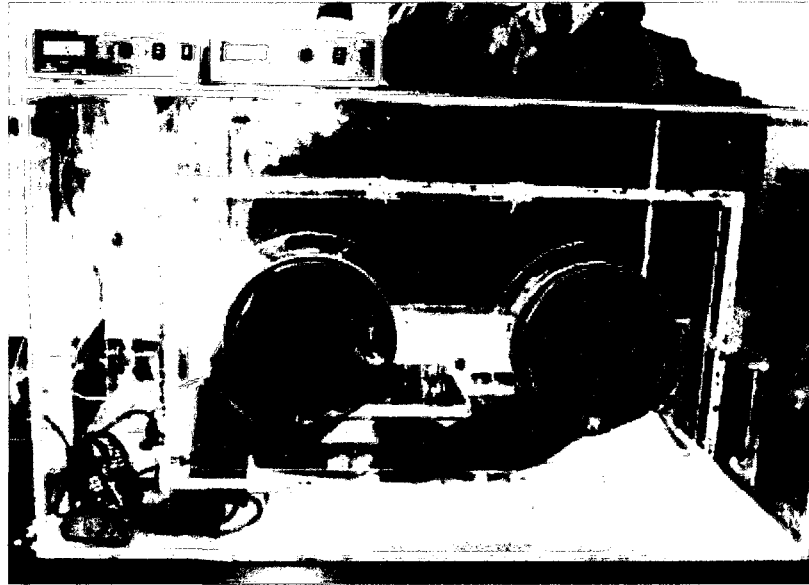


Figure 17 Temperature and Humidity Control Chamber Design

## 2.4 Mathematical Model

The concentrations of agents released by platelets are affected by diffusion and convection. To understand the interplay between these two effects, and to determine approximate values for concentrations of agents, separate transport models are considered for exposure of surfaces to plasma with and without flow.

### 2.4.1 Model for Transport under Static Conditions

Frilot presented two one-dimensional models for transport of platelet agonist into non-flowing plasma. The first model considered agents, such as NO and thromboxane  $A_2$  that are continually produced by the platelet and consumed within the plasma. The second model considered agents, such as ADP and serotonin that are secreted in a short period of time but are not consumed. The concentration of an agent described by the first model is described by Equation 1, where  $C_A$  is the species concentration,  $D_{AB}$  is the



constant diffusion coefficient of the species in PRP,  $K$  is the flux of the species from a layer of platelets at the biointerface,  $t$  is time, and  $z$  is the transport direction.

$$C_A(t, z) = \frac{K}{\sqrt{\pi D_{AB}}} \int_0^t \frac{e^{-\left(ku + \frac{z^2}{4D_{AB}u}\right)}}{\sqrt{u}} du \quad [\text{Eq. 1}]$$

Equation 2 is the activator release model. The variables are the same as in Equation 2, and the additional variables,  $m_0$ , is the mass of each agent released per unit area of the biointerface.

$$C_A(t, z) = \frac{m_0}{2\sqrt{\pi D_{AB}}} e^{-\frac{z^2}{4D_{AB}t}} \quad [\text{Eq. 2}]$$

#### 2.4.2 Model for Transport under Flow Conditions

The model for convective transport was based on flow over a flat plate. A local mass transfer coefficient,  $k_{f_{loc}}$ , is defined as  $q = k_{f_{loc}}(C_0 - C_\infty)$ , where  $q$  is the mass flux,  $C_0$  is the concentration at the biointerface, and  $C_\infty$  is the concentration within the plasma, far from the interface. The rate of transport under convective conditions can then be compared to the rate of transport under static conditions,  $q_{static} = D_{ij} \frac{\partial C}{\partial z}$ , as in Equation 3.

$$\frac{k_{f_{loc}} C_0}{D_{ij} \frac{dC_0}{dy}} = \frac{k_{f_{loc}} C_0}{D_{ij} \frac{C_0 - 0}{y(r) - 0}} = \frac{k_{f_{loc}} C_0}{D_{ij} \frac{C_0}{y(r)}} = \frac{k_{f_{loc}} y(r)}{D_{ij}} \quad [\text{Eq. 3}]$$

## 2.5 Testing of Platelet Conditions

Experiments were performed to examine platelet counts, sensitivity of coagulation to citrate concentration, and sensitivity of PRP separation to centrifugation conditions.

### 2.5.1 Bioanalyzer<sup>®</sup> Cytometry

The Agilent Bioanalyzer<sup>®</sup> device was used as a method for calculating platelet counts within PRP samples. Thus, platelet counts taken at each PRP experiment provided

a metric for determining whether or not samples were considered PRP or platelet-poor-plasma (PPP) based on published information for normal bovine and human conditions. The metric also supplied comparison values between testing sessions.

Our laboratory used the Agilent 2100 Bioanalyzer<sup>®</sup> located in the general laboratory of the Biomedical Engineering Center. The Agilent Cell Checkout kit and Cell Assay kit were purchased from Agilent Technologies.

Immediately after PRP extraction, a 10  $\mu$ L PRP sample was loaded into the lab-on-a-chip along with AO and a set of solutions provided in the cell assay kit. A 10  $\mu$ L of PRP sample, 10  $\mu$ L of AO, 10  $\mu$ L of Focusing Dye, 10 $\mu$ L of Priming Solution and 30  $\mu$ L of Cell Buffer were loaded into individual wells. A chip was then inserted into the Bioanalyzer<sup>®</sup> machine and the lid lower as pictured in Figure 18. Table 2 displays the Bioanalyzer<sup>®</sup> settings that were used to process the PRP sample for cytometry information. Once the software approves the setting profile with indicative green checks, the user could begin the run.

Table 2 Configuration settings for the Bioanalyzer

Bioanalyzer Settings	Selections
COM port	Select 2 for Bioanalyzer communication
Assay Selection	Generic Series II
Assay Details	Generic, Version 2.0
Destination	Custom (user specific)
File Prefix	(user specific depending on assay type)
Data Acquisition Parameters	Default



Figure 18 Agilent Bioanalyzer<sup>®</sup> System

### 2.5.2 Sodium Citrate Experimentation

Experiments were performed to determine the effect of variability in sodium citrate concentrations of the collected blood on coagulation. Two experiments were performed on separate days. The first observations tested the effect of errors in sodium citrate concentration. Blood was mixed at a 9:1 ratio and at concentrations of 10% higher and 10% lower than this standard ratio. To test the effect of mixing technique, the 15 mL collecting tubes were gently rocked multiple times for a well-mixed solution, only a few times for slightly-mixed solution or not-mixed after blood collection. Thus, nine samples were examined over a period of time starting from the point of blood collection. Samples were examined for clotting by slightly tilting the tubes to observe thrombus formations. These clotting observations were examined on a time interval of every 5 min for the first hour and a half, 10 min for the next two and a half hours, 20 min for the next four hours and once an hour for the next eight hours.

To further evaluate the effect of citrate concentration, the sodium citrate level was decreased by 33% and by 66%, and the samples were compared to another control at the 9:1 ratio. Mixing techniques were again varied as previously described, so that nine samples were compared. The observation time intervals were the same as those used in the first set of experiments, except the first time interval was increased to 10 min.

### 2.5.3 Centrifuge Testing

The Eppendorf centrifuge, located in the General Laboratory, was used to segregate platelets in plasma for white and red blood cells. Different centrifuge experiments on citrated whole blood were conducted to yield the “best” PRP results by reducing any plasma clouding for a transparent supernatant. Testing on PRP first included 50 mL tubes containing 12.5 mL of whole blood each placed in four centrifuge buckets. Three rotation rate/time/temperature/brake combinations were compared, 250 rcf for 20 min at 25 °C with a brake up and down of 9, as in Eshaq’s centrifuge protocol [13]. 800 rcf for 25 min at a temperature of 30 °C with a brake up and down of 6, and 1000 rcf for 25 min at 30 °C with a brake up and down of 6.

In the final protocols, the 50 mL tubes were replaced with 15 mL tubes containing 7 mL of citrated whole blood to increase the amount of whole blood centrifuged in one spinning session. The centrifuge is designed to spin either 4 50 mL tubes or 16 15 mL tubes. Thus, by changing to 15 mL tubes, our laboratory was able to increase the amount of whole blood centrifuged at a single time reducing the number of centrifuge spins.

## 2.6 Statistical Analysis

### 2.6.1 Analysis of Variance

The principal objective for analysis was to identify how the control factors affect platelet adhesion and accumulation. Analysis of variance, ANOVA, was performed to determine statistical significance of the relationships between control factors and platelet adhesion density and overall surface area [59]. The ANOVA can be performed using the Analysis Toolpak extension in Excel™, selecting Data Analysis → ANOVA, Single Factor. The ANOVA results are a simple hypothesis test, where the null hypothesis is that the populations have the same underlying statistical distribution and mean. Given significance,  $\alpha$ , the null hypothesis is rejected for  $p \leq \alpha$ . Therefore, for a significance of 0.05, as in this project, we would have a 95% statistical confidence that the source of variance exists in the differences between the rows, because the p-value was less than  $\alpha$ . Therefore, the null hypothesis would be rejected for the difference between columns. It is also possible for both the rows and columns to be significant, meaning that all combination changes have a statistically significant effect. In turn, it is possible that they are both insignificant, meaning that the result is independent of the control factors. Performing ANOVA in this project on the individual classes of results would indicate: accumulation and adhesion will provide a clear picture of how these results are affected by our control factors.

### 2.6.2 t-Test

The t-Test analysis was used to test the population mean equality for every sample under examination. For this project, the Two-Sample with Unequal Variances t-Test or heteroscedastic t-Test was used because the data collected from imaged suggested

sample population distributions that were not equal to one another. This test can resolve as to whether the two sample populations are generated from equivalent means [59]. The sample population is also considered unpaired or independent for this project and thus represent two samples from different populations being considered for mean equality. To produce t-Test calculations, a  $\alpha$  threshold was set at 0.05 for a favorable confidence interval. A computation table produced results based on the *t*-distribution for the null hypothesis providing a degrees of freedom value (number of final calculation values that are free to shift) and two-tail p-value (normal distribution – bell curve population where the null hypothesis is rejected if the value is found to be in either tail). Depending on the p-value, the null hypothesis can be rejected in approval of the alternative hypothesis or accepted. The t-Test can be implemented by applying the Analysis Toolpak extension in Excel™ by clicking Data Analysis → t-Test, Two-Sample Assuming Unequal Variances.

## CHAPTER 3

### RESULTS

#### 3.1 Evaluation and Optimization of Experimental Conditions

##### 3.1.1 Bioanalyzer<sup>®</sup> Cytometry for Platelet Counts

The Agilent Bioanalyzer<sup>®</sup> provided histogram cytometry results for analyzing PRP samples. Samples were extracted from the PRP used during PRP experiments to investigate platelet counts for individual sessions. The counts provided a metric for our laboratory's typical PRP range and allowed us to compare our count results to the normal bovine platelet range of  $1.0\text{-}8.0 \times 10^5/\mu\text{L}$  [60]. The histogram results revealed during the assay proved to be a factor of 10 offset from the normal bovine range. However, these results remained consistent between each sample scan in our laboratory. Thus, we used the results as a platelet count metric. A cytometry session was evaluated in Figure 19's top and bottom graphs. The top graph displays a histogram of sample wells 1-3. These wells were filled with high-concentrations of stained PRP. The bottom graph illustrates low-concentrations of stained PRP in wells 4-6. The top and bottom graphs show data for blue and red excitation fluorescence with higher event counts in the blue fluorescence windows than in the red. AO stain is capable of fluorescing in two separate emission wavelengths, as discussed in the Methods Section 2.2.10, as the red and blue excitation fluorescence represents AO's two fluorescence modes. The other sample session example is supplied in Appendix E (on Compact Disc).

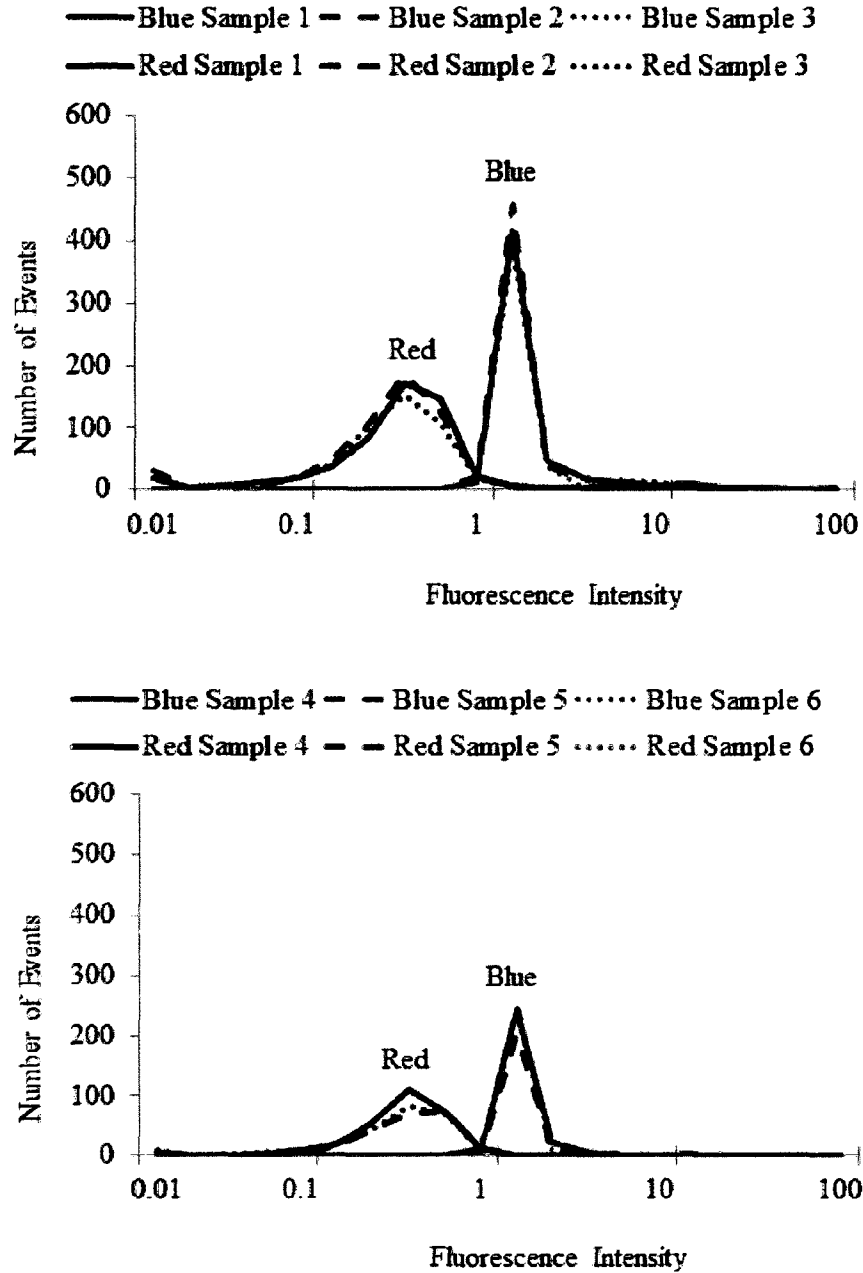


Figure 19 Bioanalyzer Histogram from 6/2/2010: Top: Samples 1-3; Bottom: Samples 4-6

### 3.1.2 Sensitivity to Sodium Citrate Concentration

Control tests were performed on whole blood samples mixed with sodium citrate.

The purpose was to evaluate sodium citrate's effect on whole blood at the time of blood



extraction thus eliminating sodium citrate and the method currently used for blood collection as a possible source for PPP. Sodium citrate experiments were performed on two days with full experimental results tables provided in Appendix E (on Compact Disc). Reference the files Blood Clotting 6/28/2010.xml and Blood Clotting 6/30/2010.xml on the compact disc for both tables. Table 3 is an excerpt of the blood clot test performed on 6/28/2010.

Table 3 Sodium citrate blood clot testing on 6/28/2010 – table excerpt.

Notes	Time	No S.C. No Mix	(+) 10% No Mix	(+) 10% N.M. L-A
5 min	2:30pm	slight clotting	No clotting	No clotting
started 20 $\mu$ L of chemicals	2:40pm	more clotting	No clotting	No clotting
	2:45pm	completely clotted	No clotting	No clotting
	2:50pm	completely clotted	No clotting	No clotting
	2:55pm	completely clotted	No clotting	No clotting
	3:00pm	completely clotted	No clotting	No clotting
	3:05pm	completely clotted	No clotting	No clotting
10 min	3:15pm	completely clotted	No clotting	No clotting
	3:25pm	completely clotted	No clotting	No clotting
	3:35pm	completely clotted	Borderline	No clotting
	3:45pm	completely clotted	Borderline	No clotting
Adding 80 $\mu$ L of chemicals	3:55pm	completely clotted	Borderline	Borderline

The comments listed in the cells to the right of the time column describe the blood clotting in each tube depending on the column category. These comments were subjective and intended to quickly describe any visual confirmations of clotting. The column

categories represent the amount of sodium citrate added or reduced plus all of chemical additives added at different concentrations as well the mixing method. After several hours of testing, minimal clotting was achieved with samples containing sodium citrate among all of the chemical additives. Sodium citrate sensitivity was then eliminated as a concern as (+) or (-) 10% sodium citrate did not present any addition clotting or reduction of clotting. The only full clotting discovered among the samples was visually confirmed in the tubes minus any added sodium citrate. These samples tended to fully clot even before we arrived at the Biomedical Engineering Center to examine each sample for clotting.

Subsequently, a second day of sodium citrate experiments was necessary to determine if extreme reductions in sodium citrate's 9:1 ratio presented any unknown issues. The ratio was reduced by a factor of by 33% and 66%. Table 4 evaluated sodium citrate with whole blood using different chemical additives along with varying mixing methods. As time progressed during the experiment, more chemical additives were pipetted into their relative tubes as indicated in the notes column of the table. This sodium citrate session produced more clotting than the previous session, but no tube was determined to have completely clotted. It is suspected that the DI water in the additional chemical additives eliminated any total clotting that would have occurred otherwise.

Table 4 Sodium citrate blood clot testing on 6/30/2010 – table excerpt

Notes	Time	Chemical	Normal -Well Mix	Normal - Well Mix-L-A
10 min	2:00 pm	0 $\mu$ M	No clotting	No chemicals added
	2:10 pm	0 $\mu$ M	No clotting	No chemicals added
chemicals added	2:20 pm	100 $\mu$ M	No clotting	No clotting
added 20 $\mu$ L	2:30 pm	100 $\mu$ M	No clotting	No clotting
	2:40 pm	100 $\mu$ M	No clotting	No clotting
added 20 $\mu$ L	2:50 pm	120 $\mu$ M	No clotting	No clotting
	3:00 pm	120 $\mu$ M	slightly viscous	No clotting
20 min - added 20 $\mu$ L	3:20 pm	140 $\mu$ M	slightly viscous	slightly viscous
added 20 $\mu$ L	3:40 pm	160 $\mu$ M	slightly viscous	slightly viscous
added 20 $\mu$ L	4:00 pm	180 $\mu$ M	slightly viscous	slightly viscous
added 20 $\mu$ L	4:20 pm	200 $\mu$ M	slightly viscous	viscous
added 100 $\mu$ L	5:00 pm	400 $\mu$ M	viscous	viscous

### 3.1.3 Optimization of PRP Extraction

Several testing methods were used to discover the “best” technique for producing consistently clear golden PRP results. Some of these methods involved using the same cow for each blood draw as referenced in the blood extraction journal provided in Appendix F, extracting blood at the same time each day and determining the best centrifuge technique. All centrifuge testing was based on a trial-and-error situation using the centrifuge’s reproducibility. My laboratory colleague, Juan M. Lopez and I adapted the centrifuge methods used by Eshaq as described in her thesis. We determined that spinning 12.5 mL of blood in 50 mL tubes at 250 rcf for 20 min proved insufficient for repeatability. Though several trials, we increased the amount of whole blood centrifuged at one time by using the 15 mL while still maintaining a low center of gravity by only pouring in 7 mL of blood in each tube. We also increased the centrifuge rotations to 1000 rcf for 25 min and increased the temperature to 30 °C. We increased the temperature from

Eshaq's 25 °C recommendation to 30 °C so that the levels remained closer to the bovine body temperature. Results produced repeatable PRP clarity with PRP supernatant extraction levels at approximately 30 mL per every 50 mL of blood drawn. Figure 11 from the Methods section furnishes an example of PRP extraction and preferred clarity.

### **3.2 PRP Experimentation Overview**

Platelet adhesions and aggregations were analyzed through fluorescence microscopy, AFM and FE-SEM to determine their two-dimensional platelet adhesion sizes, peak heights, surface area of coverage in each image and visual characteristics. The images illustrated the surface morphology of the biointerface substrates, the shapes of the superimposed features, the effects of dynamic and static conditions on platelet adhesions and the effect of chemical additives on platelet adhesions.

Figure 20 summarizes the percent surface coverage, as calculated from fluorescence imaging of AO stain, on dLbL-fibrinogen surfaces with and without PRP+ADP, PRP+L-A and PRP+L-NMMA. Under dynamic conditions, the surface coverage tended to increase with shear rate. The single exception to this trend was the case of high shear with L-A as an additive. At the higher shear rate, PRP+L-A reduced the surface coverage below the no additive case and PRP+L-NMMA increased the coverage, as expected. The decreased coverage with PRP+L-A agrees with Eshaq's results. However, PRP+ADP did not increase the percent surface coverage. This result is similar to that of Frilot for static conditions.

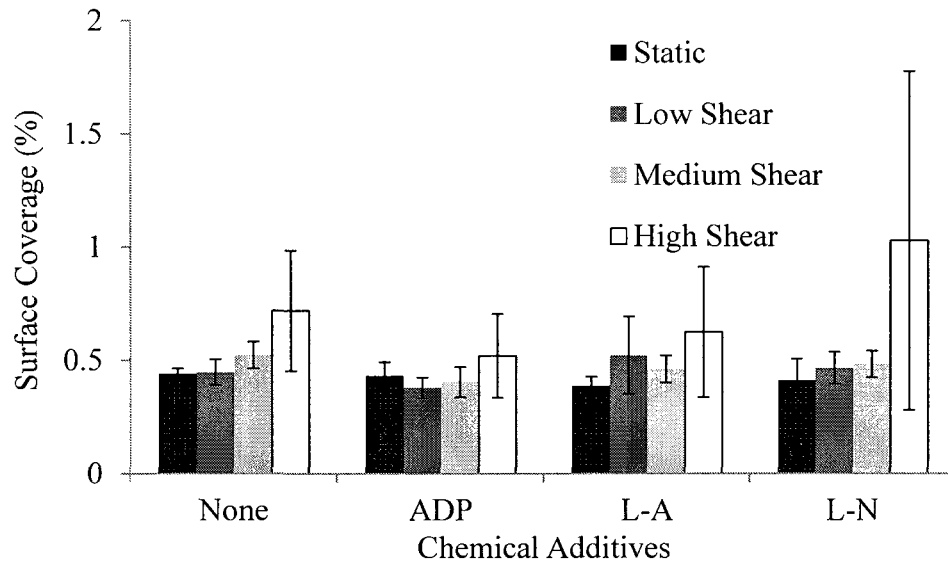


Figure 20 Percent surface coverage of platelets on dLbL-fibrinogen surfaces after exposure to plain PRP, PRP+ADP, PRP+L-A and PRP+L-NMMA (L-N). Error bars indicate the standard deviation of surface coverage percentages from different slides on different days.

Figure 21 summarizes the percent surface coverage, as calculated from fluorescence imaging of AO stain, on dLbL-collagen surfaces with and without added ADP, L-A and L-NMMA. The surface coverages under zero (static), low, and medium shear rate are similar for a given additive. However, at the high shear rate surface coverage was always highest. At each shear rate, L-A reduced the surface coverage below the no-additive case and both L-NMMA and ADP increased it, as expected from Eshaq's results. Under static conditions, the percent surface coverage increased with added ADP and added L-A. The increase in surface coverage with L-A was unexpected. However, because limited experiments were executed on the dLbL-collagen surfaces, it is difficult to assess the statistical significance of these results. These results illustrate the importance of verifying the ability of the AO staining technique to quantify platelet surface coverage.

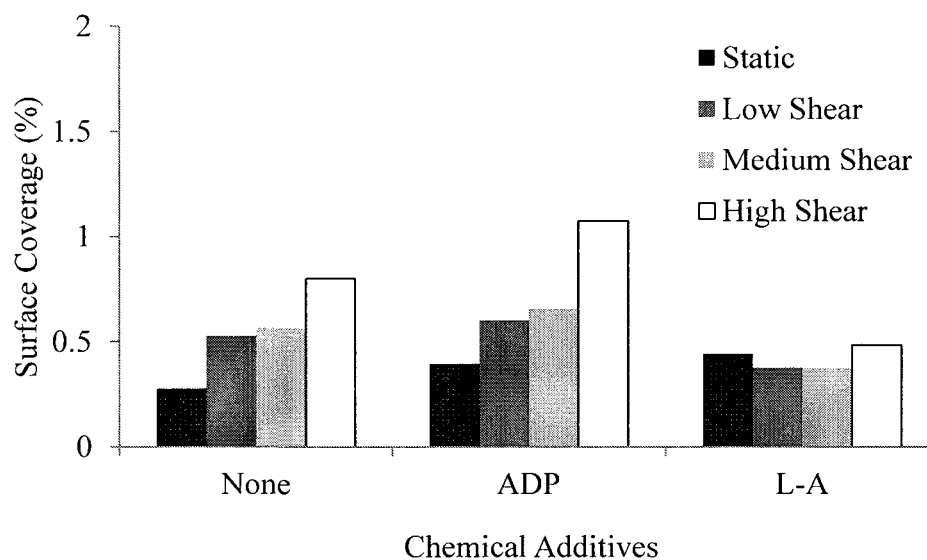


Figure 21 Percent surface coverage of platelets on dLbL-collagen surfaces after exposure to plain PRP, with no additive and with ADP and L-A. Error bars indicate the standard deviation of surface coverage percentages from different slides on different days.

### 3.3 Effect of Exposure to PRP

Initial experiments were performed to determine whether the presence of platelet aggregates could be identified with two imaging modalities, AFM and FE-SEM imaging. In the first set of experiments, glass slides were exposed to PRP. Because glass is a platelet activator, it was assumed that these slides would then contain platelet aggregates. Next, the three surfaces, sLbL-fibrinogen, dLbL-fibrinogen, and dLbL-collagen were imaged before and after exposure to PRP.

#### 3.3.1 AFM

##### 3.3.1.1 Plain Glass Slides Exposed to PRP

Figure 22 shows AFM scans of plain glass slides that were cleaned with isopropyl alcohol and then covered with PRP under static conditions. The slide in the top image was not stained, and the slide in the bottom image was stained with AO. In these figures

and all other AFM images to be shown in this dissertation, the surface dimensions are 40  $\mu\text{m}$  by 40  $\mu\text{m}$ , and the color intensity scale represents feature height from lowest (black) to highest (bright yellow). The color intensity scale is set by the software and varies from figure to figure, depending on the range of heights of the features that are scanned. The

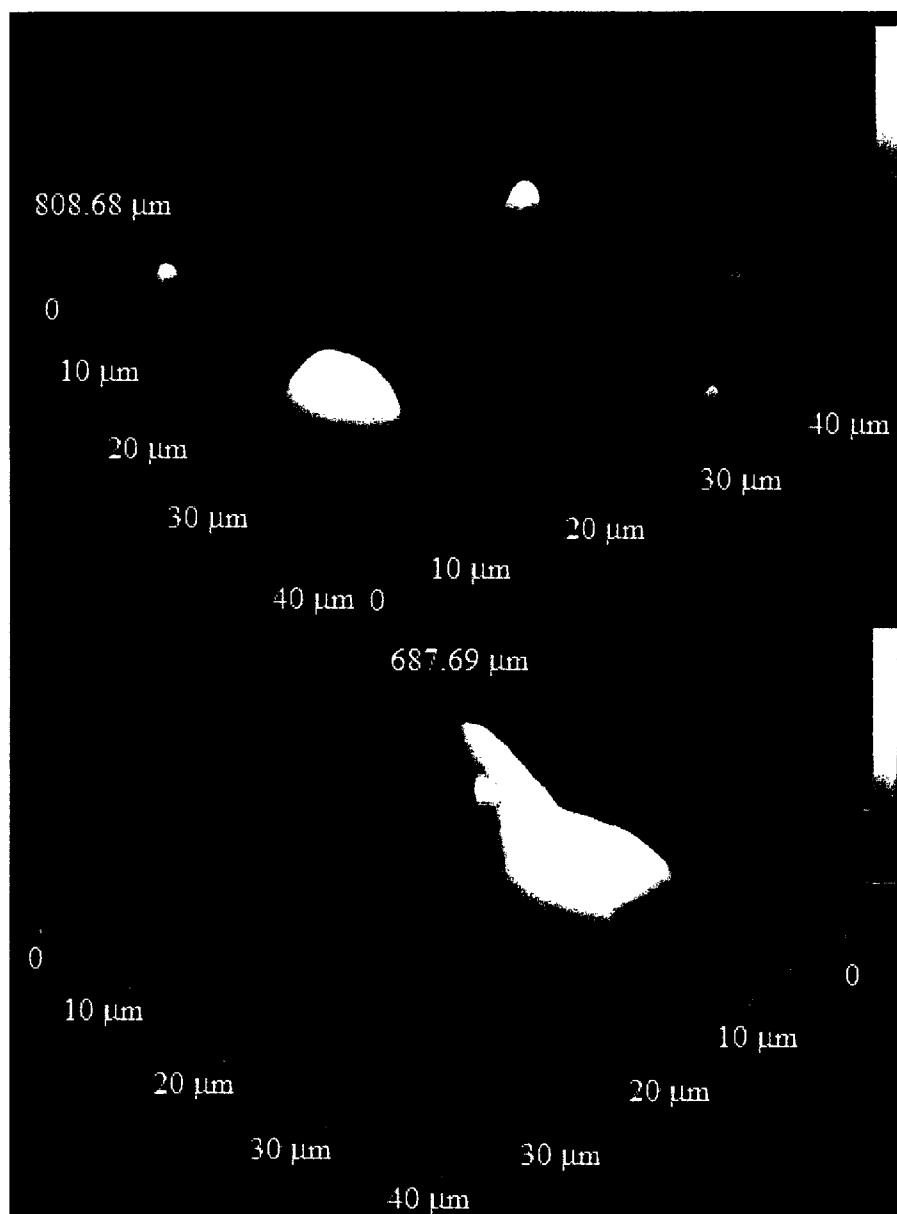


Figure 22 AFM images of uncoated glass slides that were exposed to PRP under static conditions. Top: No AO stain. Bottom: AO stain.

unstained figure displays what is understood to be a platelet or a platelet aggregation with a peak height of 808 nm and several smaller adhesions. In the peak height of the feature is 688 nm. The edges of the feature are less steep than those of the features in the unstained slide.

### 3.3.1.2 LbL-Coated Slides Not Exposed to PRP

Figure 23 shows AFM images of sLbL-fibrinogen (top left), dLbL-fibrinogen (bottom left) and dLbL-collagen (bottom right) substrate slides that were not exposed to PRP and were not stained with AO. The two fibrinogen-coated slides have similar textures with multiple peaks on the order of 2  $\mu\text{m}$  in diameter. A similar character can be



Figure 23 AFM images of slides that were coated with sLbL-fibrinogen (top left), dLbL-fibrinogen (bottom left) and dLbL-collagen (bottom right), but not exposed to PRP and not stained.



seen in all of the AFM sLbL-fibrinogen images seen in Appendix E (on Compact Disc), and it is consistent with AFM scans of fibrinogen presented by other researchers [61] [62]. The peak height for sLbL-fibrinogen (306 nm) is larger than that for dLbL-fibrinogen (135 nm). The dLbL-collagen image shows a feature, presumed to be a fiber that has a peak height of 226 nm. The surface is much smoother than the two fibrinogen surfaces.

### 3.3.1.3 LbL-Coated Slides Exposed to PRP and Stained with AO

Figure 24 displays AFM scans of sLbL-fibrinogen (top left), dLbL-fibrinogen (bottom left) and dLbL-collagen (bottom right) surfaces that were exposed to PRP,

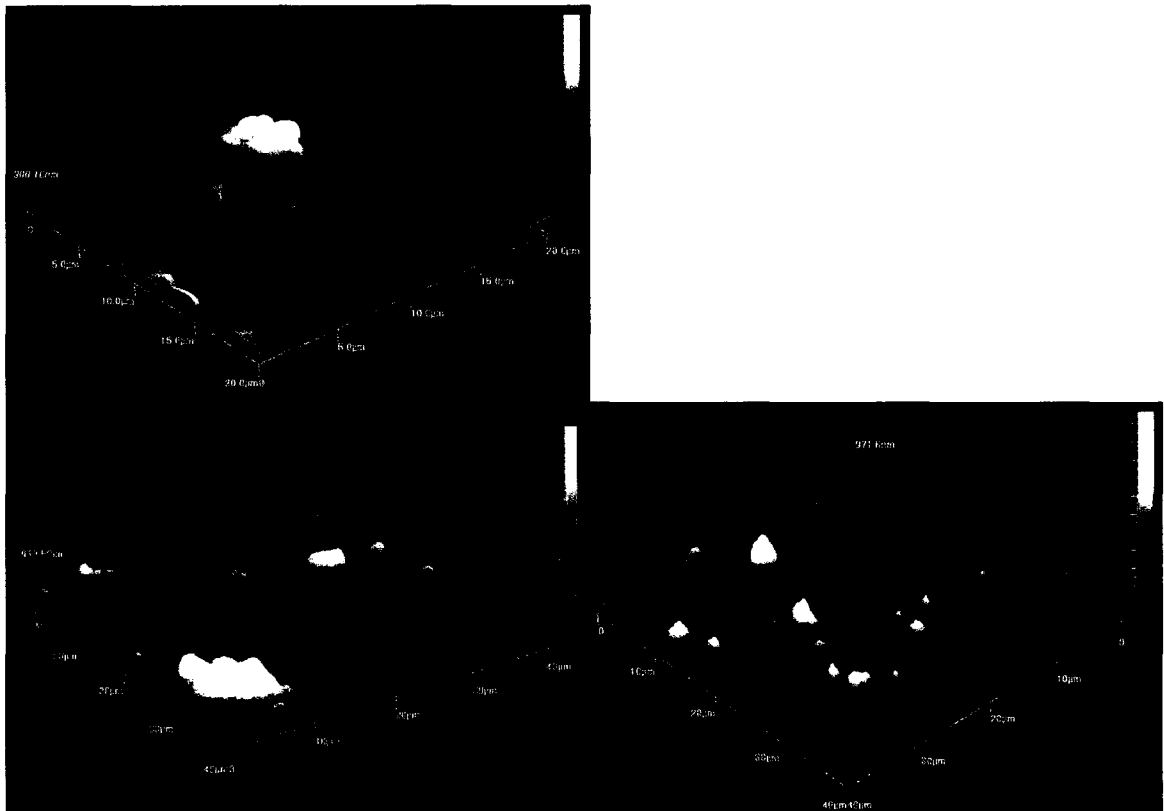


Figure 24 AFM images of slides with sLbL-fibrinogen (top left), dLbL-fibrinogen (bottom left) and dLbL-collagen surfaces performed under static conditions while exposed to PRP and stained with AO.

without chemical additives, under static conditions and stained with AO. For sLbL-fibrinogen, the most prominent feature, with peak height 900 nm, appears to be an activated platelet or multiple activated platelets with fibril extensions. The texture is smoother than those seen for surfaces without AO.

The dLbL-fibrinogen image has a peak height of 973 nm. The image's bottom corner suggests a large platelet attachment surrounded by a fibrinogen surface and is consistent with platelet AFM scans presented by other researchers [63]. Troughs on the surface appear that were not visible in the sLbL-fibrinogen image. The troughs may arise because sLbL surfaces tend to be overall thicker than dLbL surfaces. Thus, sLbL may be less vulnerable to rinsing with PBS during the rinse cycle. The dLbL-collagen image has a smooth surface, as was seen for dLbL-collagen that was not exposed to PRP. Several features are present that may be platelet adhesions. The peak heights of these features, approximately 971 nm, are similar to the features seen on the plain glass slide that was exposed to PRP (Figure 22). The widths of these features, on the order of 2  $\mu\text{m}$ , are consistent with typical platelet diameters.

### 3.3.2 FE-SEM

#### 3.3.2.1 Plain Glass Slides Exposed to PRP

Figure 25 displays FE-SEM images of plain glass slides that were exposed to PRP. The top slide was not stained, and the bottom slide was stained with AO. The top image shows the stria from the glass background and a circular object that may be a platelet undergoing activation. The bottom figure was originally intended to display PRP stained with AO, but AO concealed the platelets in all of the images from that sample set.

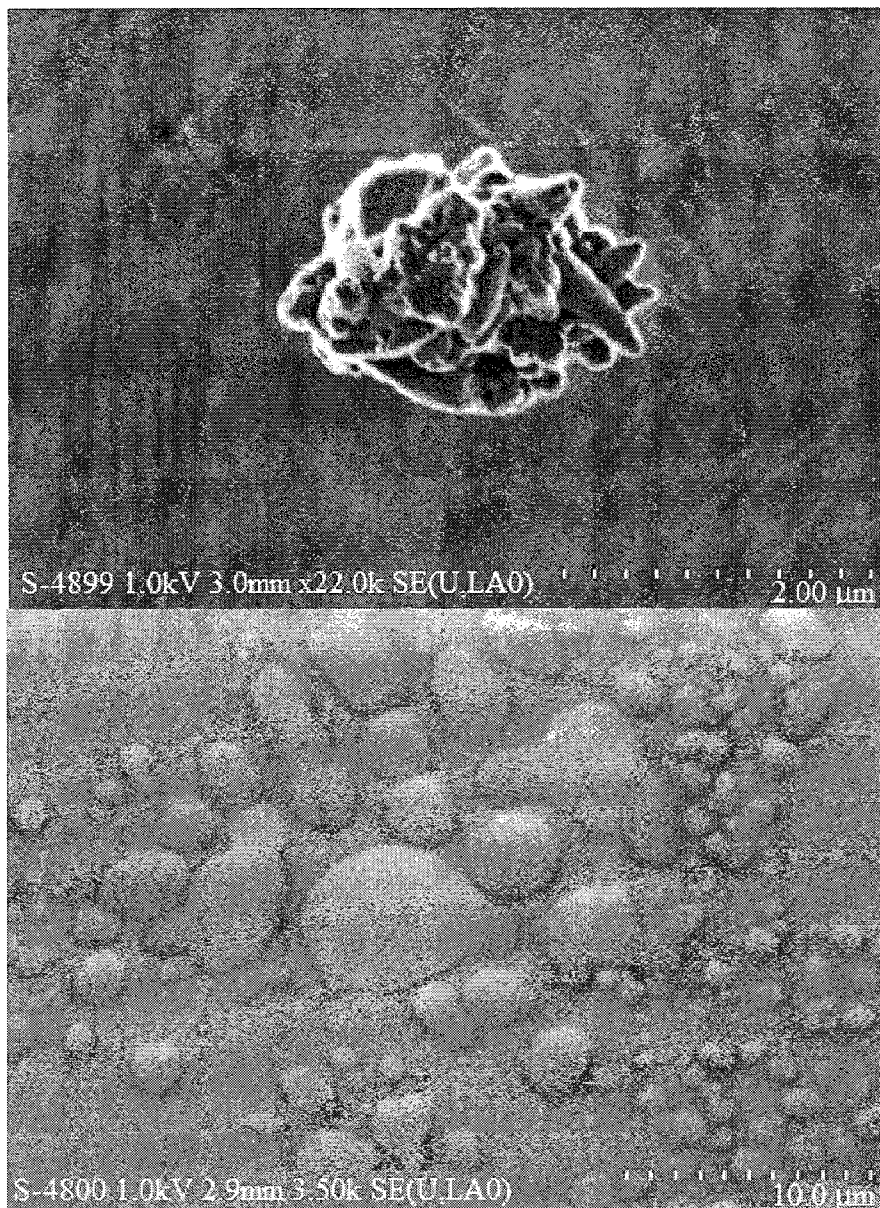


Figure 25 FE-SEM images of plain glass slides exposed to PRP. Top: No AO stain. Bottom: AO stain.

### 3.3.2.2 LbL-Coated Not Exposed to PRP

Figure 26 shows FE-SEM images of sLbL-fibrinogen (top left), dLbL-fibrinogen (bottom left) and dLbL-collagen (bottom right) surfaces that were not exposed to PRP or stained with AO. The sLbL-fibrinogen image displays a surface roughness that is consistent with the roughness of sLbL-fibrinogen surfaces imaged with AFM. In the

dLbL-fibrinogen image, a rough feature, qualitatively similar to the overall texture of the sLbL-fibrinogen surface, is present and is surrounded by a smooth field. The dLbL-collagen image illustrates collagen fibrils surrounded by a smooth surface.

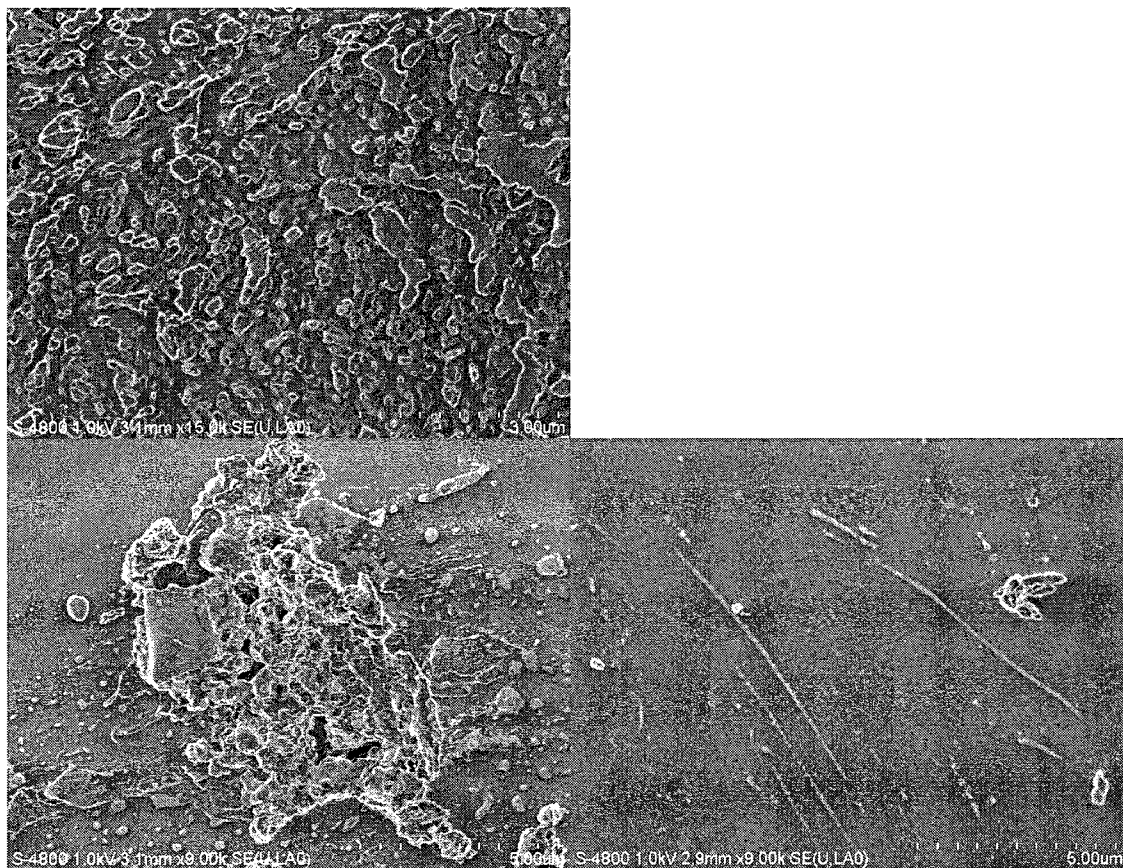


Figure 26 FE-SEM images of slides with sLbL-fibrinogen (top left), dLbL-fibrinogen (bottom left) and dLbL-collagen surfaces without PRP exposure and AO stain.

### 3.3.2.3 LbL-Coated Slides Exposed to PRP and Stained with AO

Figure 27 displays FE-SEM images of sLbL-fibrinogen (top left), dLbL-fibrinogen (bottom left) and dLbL-collagen (bottom right) surfaces that were exposed to PRP under static conditions and stained with AO. The sLbL-fibrinogen image shows two features of widths 10 to 15  $\mu\text{m}$  in diameter that appear to be adhered platelets with fibrils. The feature on the left side of the figure is similar FE-SEM images of platelets reported

by Zilla et al. [64], Minelli et al. [65] and Tsai et al. [66]. The irregular shapes of adhered platelets have been previously described by Fritz et al. [67], Gear et al. [68] and Minelli et al. [65]. The central feature of the dLbL-fibrinogen image, approximately 30  $\mu\text{m}$  across, may be an adhered platelet surrounded by AO. The dLbL-fibrinogen surface was less rough than the sLbL surface (Figure 26). The dLbL-collagen image exhibits three platelet-like features, approximately 15-20  $\mu\text{m}$  across, on an otherwise smooth surface. Although collagen fibers are not identifiable in this image, platelet aggregations are assumed to be adhered to underlying collagen fibers that are covered with AO.

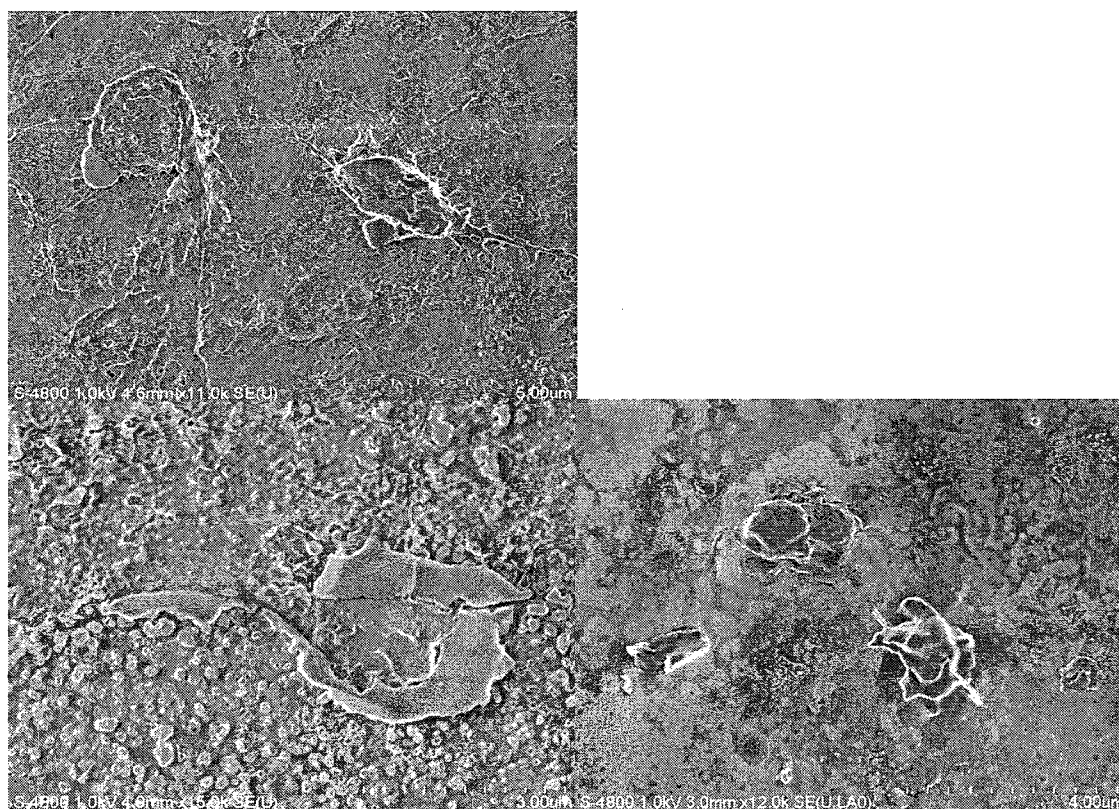


Figure 27 FE-SEM images of slides with sLbL-fibrinogen (top left), dLbL-fibrinogen (bottom left) and dLbL-collagen (bottom right) surfaces exposed to PRP without flow and stained with AO.

### **3.4 Comparison of Surfaces after Static Exposure to PRP**

The surface characteristics of sLbL-fibrinogen, dLbL-fibrinogen and dLbL-collagen were compared to determine which surface would provide the most consistent fluorescence-based measure of platelet adhesion.

#### **3.4.1 Fluorescence Microscopy**

Sample fluorescent images of sLbL-fibrinogen (top left), dLbL-fibrinogen (bottom left) and dLbL-collagen (bottom right) surfaces exposed to PRP under static conditions and stained with AO are shown in Figure 28. The image from sLbL-fibrinogen was taken with a 66.7 ms exposure time, and, in general, it was necessary to adjust exposure time manually for all images taken from sLbL surfaces. For all dLbL-fibrinogen and dLbL-collagen samples, the exposure time was set at 667 ms and did not require adjustment because all images presented similar contrast. The sLbL image demonstrates interconnected discrete patches of stained material. The greater brightness exhibited by the sLbL surface is not a consequence of exposure time, given that the shorter time would generally lead to a darker image for a given fluorescence intensity.



Figure 28 Fluorescence microscopy images of slides with sLbL fibrinogen (top left), dLbL-fibrinogen (bottom left) and dLbL-collagen (bottom right) that were exposed to PRP under static conditions and stained with AO.

### 3.4.2 AFM

Figure 29 shows AFM images of sLbL-fibrinogen (top left), dLbL-fibrinogen (bottom left) and dLbL-collagen (bottom right) surfaces that were exposed to PRP under static conditions and stained with AO. For the sLbL surface, the highest peak is 1135 nm and the surface roughness is qualitatively similar to that in other AFM scans of sLbL-fibrinogen surfaces. The feature in the bottom corner of the image is assumed to be a platelet adhesion. This figure demonstrates the typical surface roughness of sLbL substrates. The dLbL-fibrinogen scan shows a slightly smoother surface than sLbL scans

although the peak height, 1131 nm, was nearly identical to that for the sLbL scan. The dLbL-collagen scan has a qualitatively different texture, with collagen fiber features that appear as parallel channels. These features appear in other AFM scans of dLbL-collagen. The 661 nm peak height is approximately half of that for the two fibrinogen scans.



Figure 29 AFM images of slides with sLbL-fibrinogen (top left), dLbL-fibrinogen (bottom left), and dLbL-collagen (bottom right) slides that were exposed to PRP under static conditions, and stained with AO.

### 3.4.3 FE-SEM

Figure 30 shows FE-SEM images of sLbL-fibrinogen (top left), dLbL-fibrinogen (bottom left), and dLbL-collagen (bottom right) coated slides that were exposed to PRP under static conditions and stained with AO. Each slide has a feature that is assumed to be a platelet aggregate. The larger clumps, in the sLbL-fibrinogen image near the center



feature are assumed to be AO particles. The surface roughness is consistent with that of other sLbL images. The dLbL-fibrinogen image also suggests a platelet aggregate surrounded by AO. Again, the surface characteristics are similar to sLbL-fibrinogen, but regions are seen with lower roughness. The dLbL-collagen image exhibits collagen fibers and an overall smooth surface. Note the differences in scales among the images.

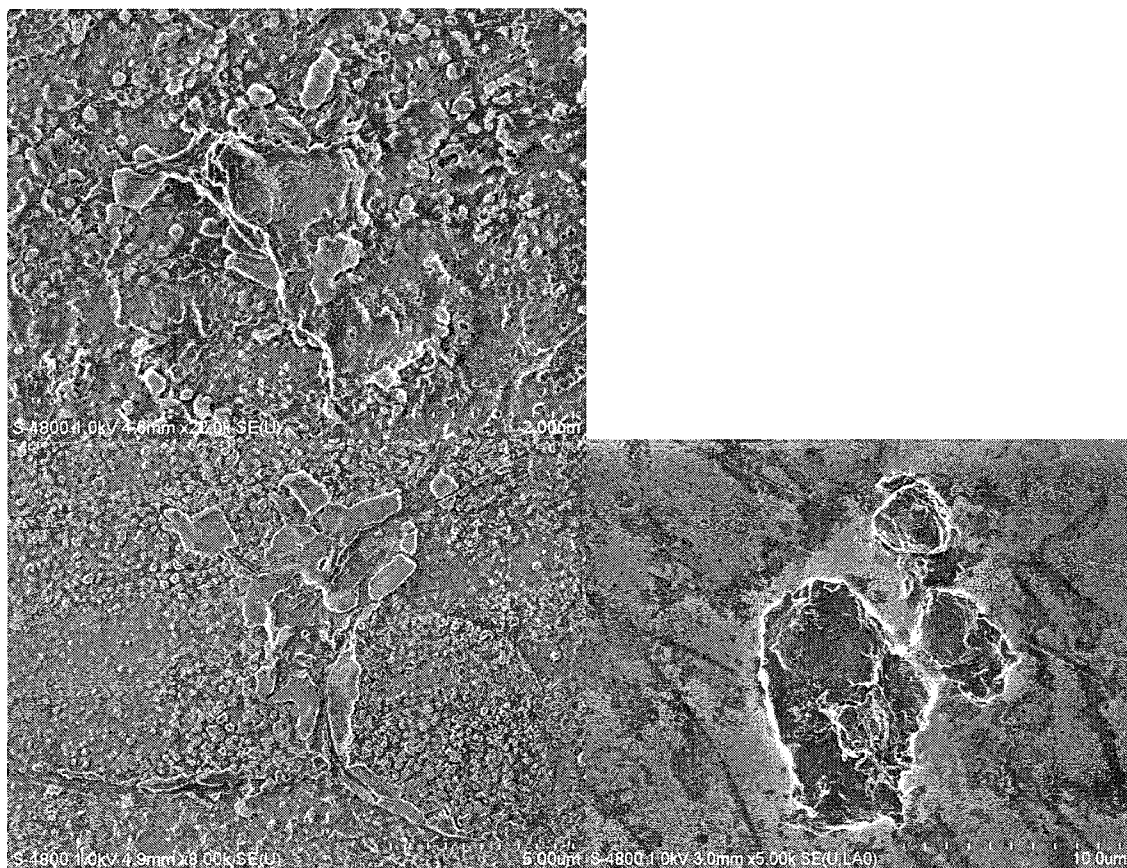


Figure 30 FE-SEM images of slides with sLbL-fibrinogen (top left), dLbL-fibrinogen (bottom left), dLbL-collagen (bottom right) exposed to PRP under static conditions and stained with AO

### **3.5 Comparison of Surfaces after Dynamic Exposure to PRP**

#### **3.5.1 Fluorescence Microscopy**

Figure 31 shows fluorescent images of sLbL-fibrinogen (top left), dLbL-fibrinogen (bottom left), and dLbL-collagen (bottom right) substrates that were exposed to PRP in the low shear region of the Petri dish. The sLbL-fibrinogen image is similar to that shown in Figure 28 for the no-shear case. Both were imaged at a short exposure time (66.7 ms), which highlights the large amount of staining. The reduced amount of staining for the dLbL-fibrinogen and dLbL-collagen surfaces allowed a longer exposure time (667 ms) and led to more discrete regions of staining.

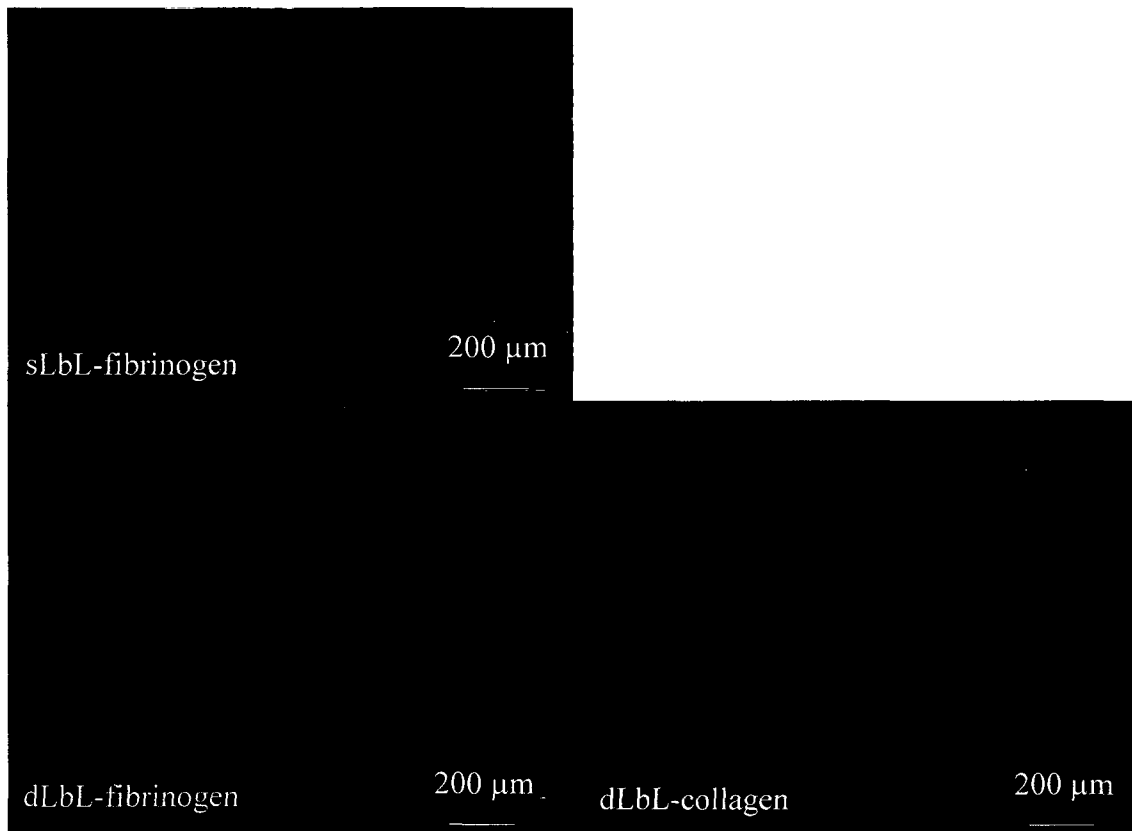


Figure 31 Fluorescence microscopy images of slides with sLbL-fibrinogen, dLbL-fibrinogen, and dLbL-collagen surfaces exposed to PRP in the low shear region of the Petri dish and stained with AO

### 3.5.2 AFM

Figure 32 shows AFM images of sLbL-fibrinogen (top left), and dLbL-fibrinogen (bottom left), and dLbL-collagen (bottom right) substrates that were exposed to PRP in the low shear region of the Petri dish. The characteristic rough surface for the sLbL-fibrinogen surface is seen, and the peak value is 883 nm. The yellow peaks may be platelet aggregations



Figure 32 AFM images of slides with sLbL-fibrinogen, dLbL-fibrinogen and dLbL-collagen surfaces exposed to PRP in the low shear region of the Petri dish and stained with AO

The dLbL-fibrinogen surface is less rough than the sLbL-fibrinogen surface, and the peak height is lower, at 663 nm. Troughs are again seen along the dLbL-fibrinogen surface, possibly caused during rinsing because of the thinner dLbL coating as compared to the sLbL coating. For the dLbL-collagen surface, the peak height was 721 nm. The feature in this image is interpreted as collagen fiber with platelet adhesion surrounded by a smooth collagen surface.

### 3.5.3 FE-SEM

Figure 33 shows FE-SEM images of sLbL-fibrinogen (top left), dLbL-fibrinogen (bottom left), and dLbL-collagen (bottom right) substrates that were exposed to PRP in the low shear region of the Petri dish. Once more, dLbL-fibrinogen appears almost

identical to sLbL-fibrinogen. The image of dLbL-collagen illustrates qualities similar to the dLbL-collagen FE-SEM image taken under static conditions.

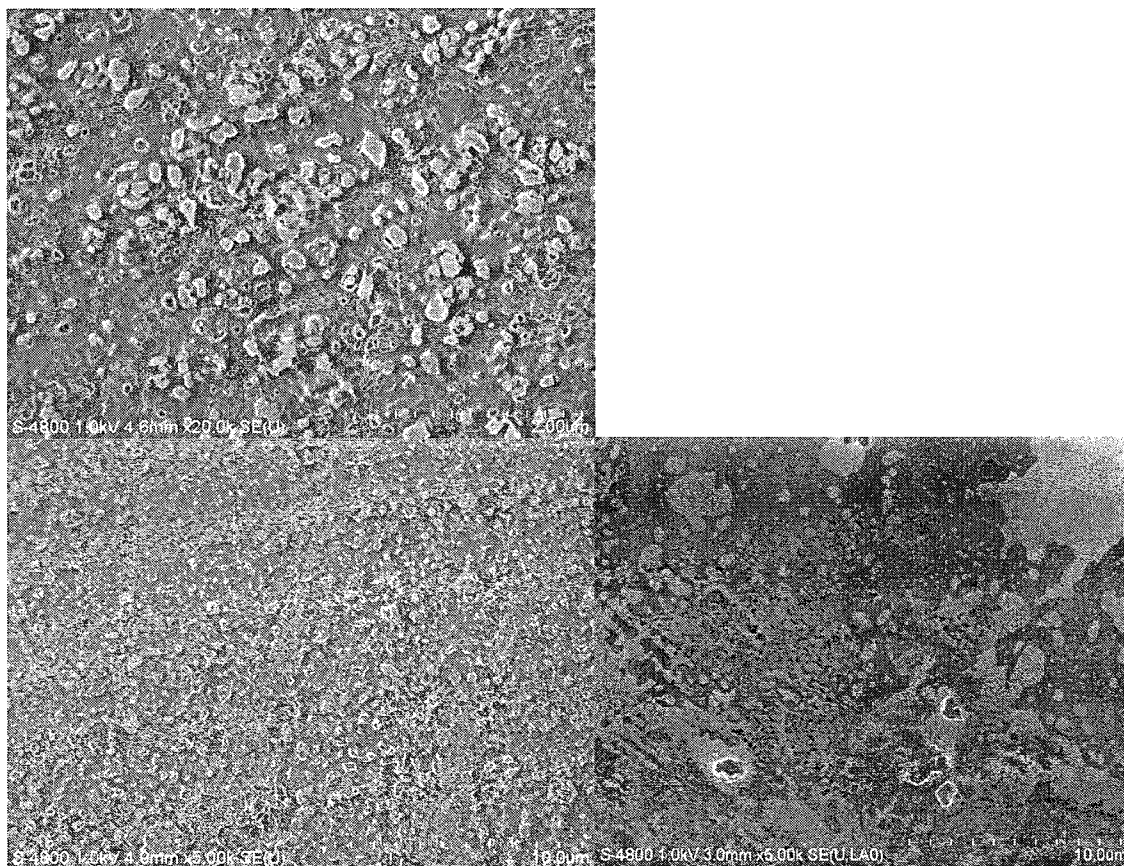


Figure 33 FE-SEM images of slides with sLbL-fibrinogen, dLbL-fibrinogen, dLbL-collagen substrates exposed to PRP in the low shear region of the Petri dish and stained with AO

### 3.6 Comparison of Images after Exposure to PRP at Different Shears

The comparison of different surfaces indicated that dLbL substrates provided fluorescent images that represented platelet adhesion more specifically than sLbL surfaces. Therefore, the dLbL surfaces were used to systematically compare platelet adhesion at different shear rates.

### 3.6.1 Fluorescence Microscopy

#### 3.6.1.1 dLbL-Fibrinogen

Figure 34 shows fluorescence microscopy images of dLbL-fibrinogen substrates exposed to PRP under no-shear (top left), low shear (bottom left) and high shear (bottom right) and stained with AO. The exposure time is 667 ms. The static exposure image displays a few platelet adhesions on a black background. The high shear image has more adhesions. The adhesion dimensions range approximately from 20  $\mu\text{m}$  to 150  $\mu\text{m}$ , as indicated by the 200  $\mu\text{m}$  scale, which is consistent with aggregates of platelets.

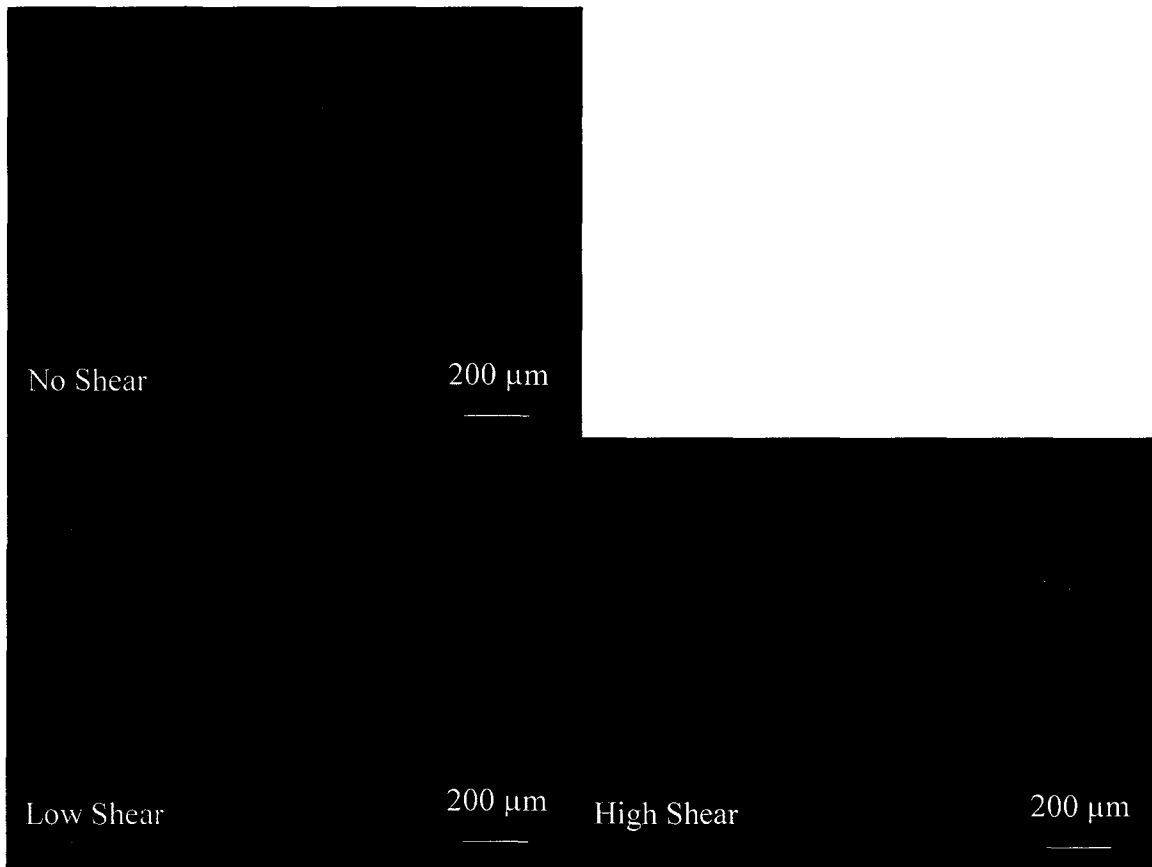


Figure 34 Fluorescence microscopy images of slides with dLbL-fibrinogen under no shear (top left), low shear (bottom left), and high shear (bottom right) exposed to plain PRP and stained with AO.

The high shear image illustrates a distinct pattern for platelet adhesion found only in the high shear regions. The adhesions are elongated, suggesting that platelet aggregations latched loosely to fibrinogen fibrils and rolled across the surface, creating a smearing, string impression. This pattern was also witnessed in all of the dLbL-fibrinogen slides that were exposed to PRP with chemical additives under high shear. This platelet aggregation elongation is also visible in AFM scan of dLbL-fibrinogen at high shear regions.

#### 3.6.1.2 dLbL-Collagen

Figure 35 shows fluorescence microscopy images of dLbL-collagen substrates exposed to PRP under no-shear (top left), low shear (bottom left) and high shear (bottom right) and stained with AO. In all three cases, the aggregates are similar in size and number to those observed in the no-shear and low shear cases for dLbL-fibrinogen that were shown in Figure 35.

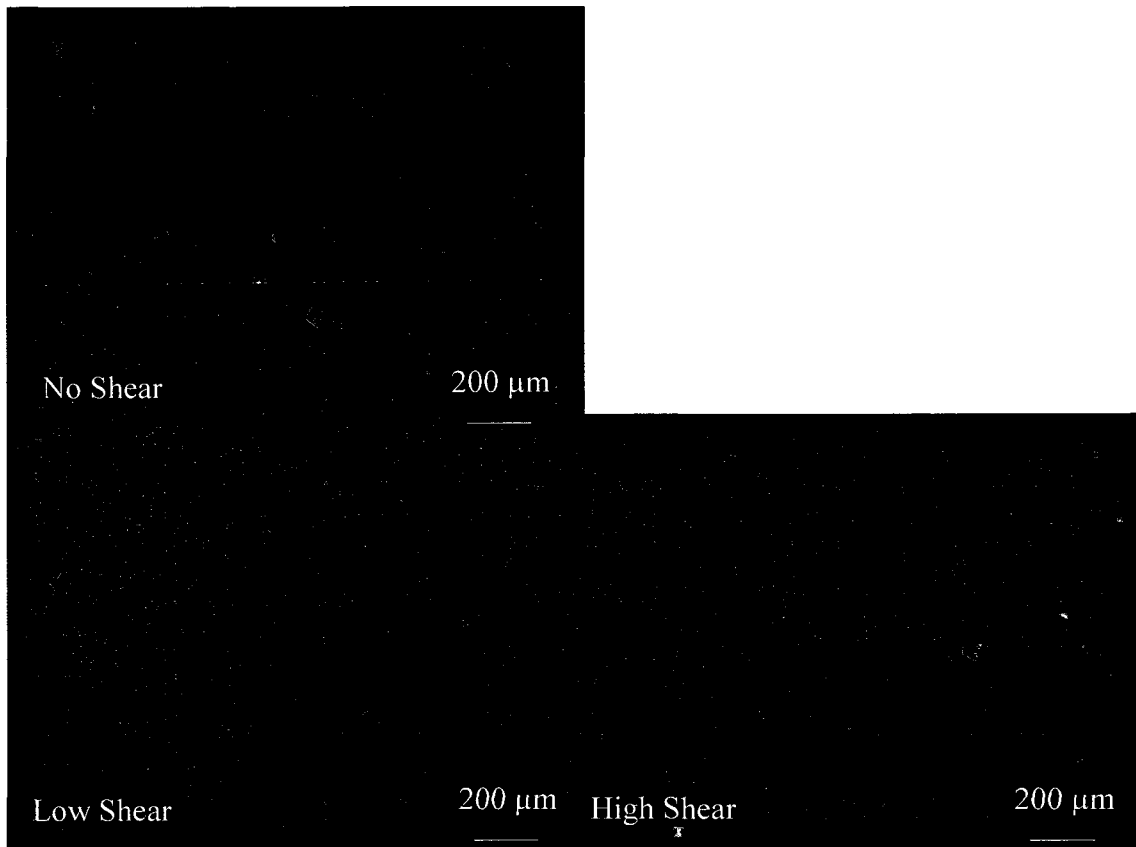


Figure 35 Fluorescence microscopy images of slides with dLbL-collagen exposed to plain PRP under no shear (top left), low shear (bottom left) and high shear (bottom right) and stained with AO.

### 3.6.2 AFM

#### 3.6.2.1 dLbL-Fibrinogen

Figure 36 shows AFM images of dLbL- fibrinogen substrates exposed to PRP under no-shear (top left), low-shear (bottom left) and high shear (bottom right) and stained with AO. The no-shear image displays a platelet adhesion with a peak height value of 1146 nm. The low-shear image illustrates one possible adhered platelet. The high-shear image shows a possible platelet adhesion with a peak height of 1954 nm. These images do not indicate visual difference between shear regions.





Figure 36 AFM images of slides with dLbL-fibrinogen exposed to plain PRP under no shear (top left), low shear (bottom left) and high shear (bottom right) and stained with AO

### 3.6.2.2 dLbL-Collagen

Figure 37 shows AFM images of dLbL-collagen substrates exposed to PRP under no-shear (top left), low shear (bottom left), and high shear (bottom right) and stained with AO. The no-shear image illustrates several peaks, approximately 2  $\mu\text{m}$  across, that are assumed to be platelets. The collagen surface is again smooth and the peak height is 987 nm. The low-shear image includes one central feature, approximately 10  $\mu\text{m}$  across that is interpreted as either a spread platelet or a platelet aggregate. No collagen fibers can be identified. The peak height for this image is 1109 nm. The high shear scan shows a presumed platelet adhesion adjacent to a collagen fiber. The presumed adhesion includes

a feature that is similar to that seen at low shear, but is nearly twice as high. The peak height for this image is 2015 nm.



Figure 37 AFM images of slides with dLbL-collagen under static conditions (top left), and dynamic conditions at low (bottom left) and high shear (bottom right) exposed to plain PRP and stained with AO

### 3.7 Platelet Adhesion Sizes

The fluorescent images of surfaces exposed to PRP, along with the MATLAB program listed in Appendix B, were used to obtain the areas of AO-stained features. These are examined individually for dLbL-fibrinogen and dLbL-collagen surfaces.

#### 3.7.1 Feature Sizes for dLbL-Fibrinogen Substrates

Figure 38 shows the distribution of feature sizes for dLbL-fibrinogen substrates that were exposed to PRP at the low shear region of the Petri dish. The upper graph

shows distributions for individual images, and the lower graph shows the means and standard deviations over several images. The number of features declines monotonically with feature size.

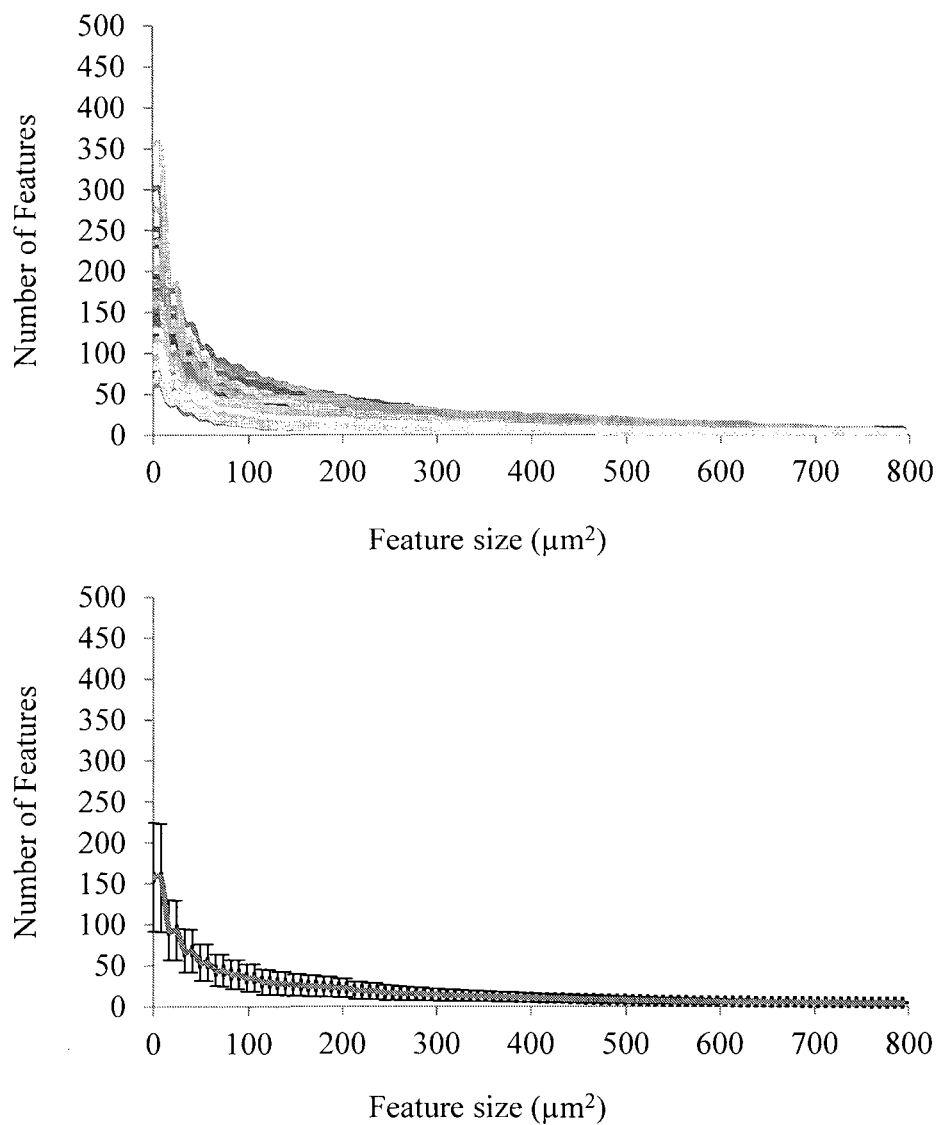


Figure 38 Feature size vs. number of features at that size for dLbL-fibrinogen surfaces exposed to plain PRP at low shear rate. Top: Curves for each image. Bottom: Mean for all images with standard deviation.

### 3.7.2 Feature Sizes for dLbL-Collagen Substrates

Figure 39 shows the distribution of features sizes from all fluorescent images obtained from dLbL-collagen surfaces that were exposed to plain PRP. The curves are generally similar to those obtained from dLbL-fibrinogen.

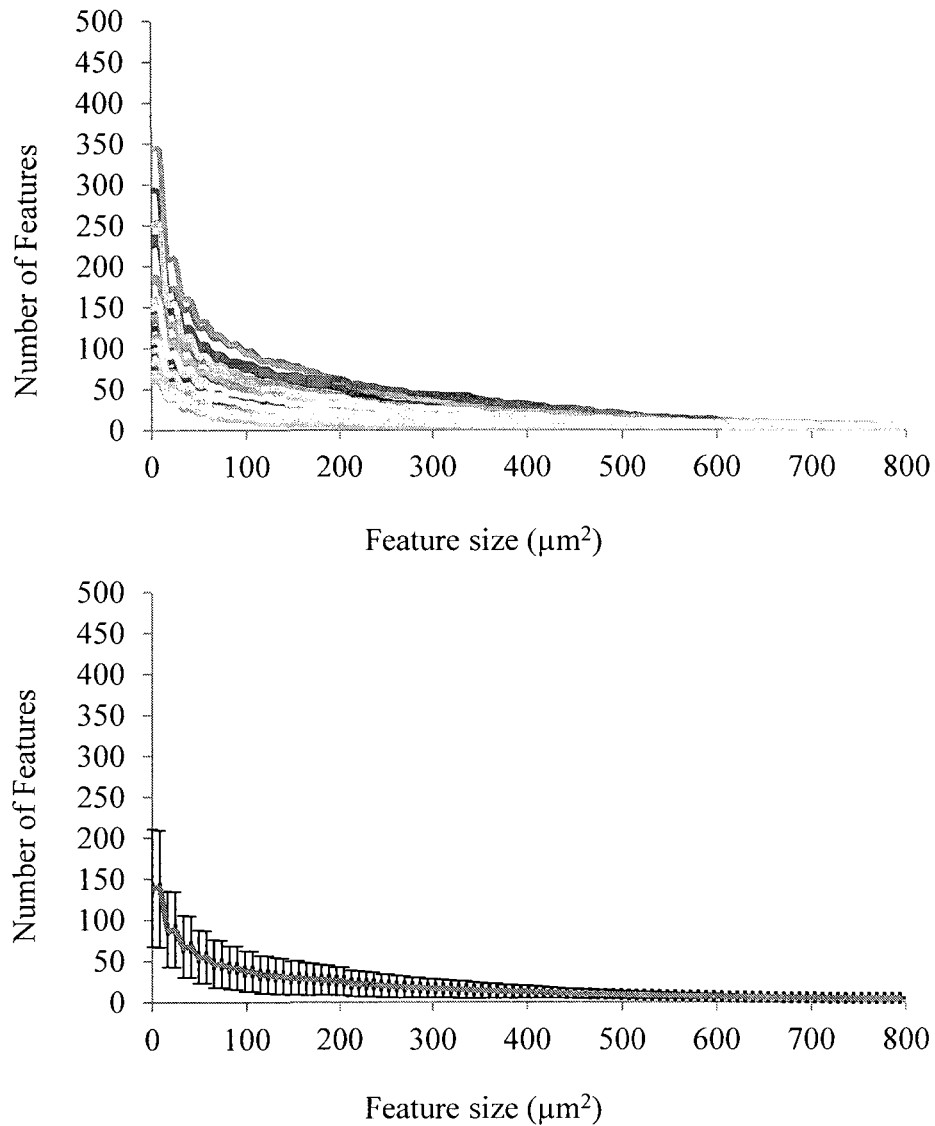


Figure 39 Feature size vs. number of features at that size for dLbL-collagen surfaces exposed to plain PRP at low shear rate. Top: Curves for each image. Bottom: Mean of all images with standard deviation.

### 3.8 Effects of Additives on Surface Coverage

Fluorescent microscopy and AFM were used to examine the effects of added L-A, ADP and L-NMMA on apparent platelet adhesion under different shear conditions. In this section, the images are compared for different shear rates and the feature size distributions are then examined.

#### 3.8.1 Fluorescence Microscopy

##### 3.8.1.1 dLbL-Fibrinogen with Added L-A

Figure 40 shows fluorescence microscopy images of dLbL-fibrinogen surfaces that were exposed to PRP and 20  $\mu\text{M}$  L-A with no-shear (top left), low shear (bottom left), and high shear (bottom right) and stained with AO. The patterns are similar to those observed under the same conditions but without L-A. The no-shear and low shear cases exhibit discrete features that are typically 20  $\mu\text{m}$  across, and the high shear case includes streaks that are roughly 20  $\mu\text{m}$  wide and 200  $\mu\text{m}$  long. These streaks are oriented in different directions, possibly because the flow the pattern varies strongly in the swirled dish.

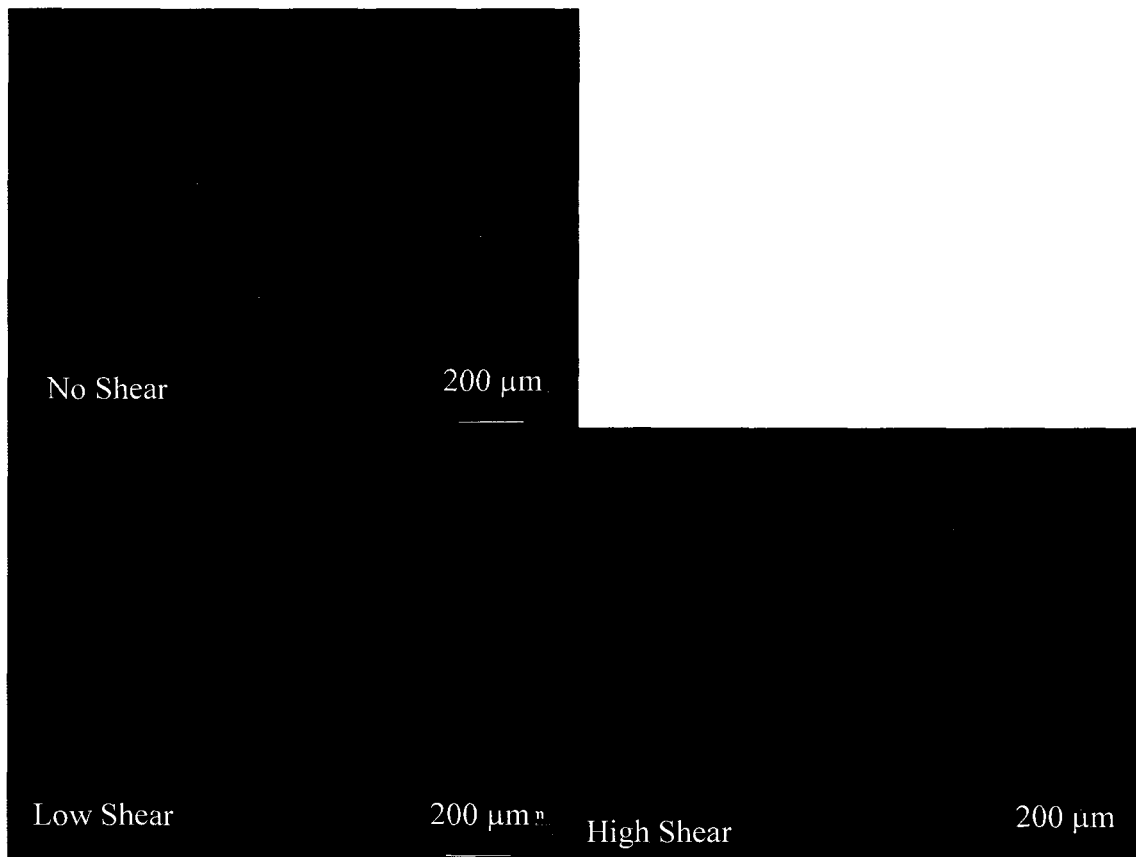


Figure 40 Fluorescence microscopy images of AO-stained dLbL-fibrinogen slides that were exposed to PRP+L-A with no-shear (top left), low shear (bottom left) and high shear (bottom right)

### 3.8.1.2 dLbL- Collagen with Added L-A

Figure 41 shows fluorescent images of dLbL-collagen surfaces that were exposed to PRP and 20  $\mu$ M L-A with no-shear (top left), low shear (bottom left) and high shear (bottom right) and stained with AO. The patterns are similar to those observed without L-A and with L-A on fibrinogen. Where the no-shear and low shear images show discrete features and the high shear image shows streaks. However, the no-shear and low shear images exhibit features, on the order of 50 to 100  $\mu$ m across, that are larger than those observed in Figure 41. For the collagen surface, the streaks observed at high shear rate could be interpreted as collagen fibers onto which platelets have attached. However, the

presence of similar streaks on the fibrinogen surface at high shear suggests a common mechanism for the two surfaces that is unrelated to the presence of collagen fibers.

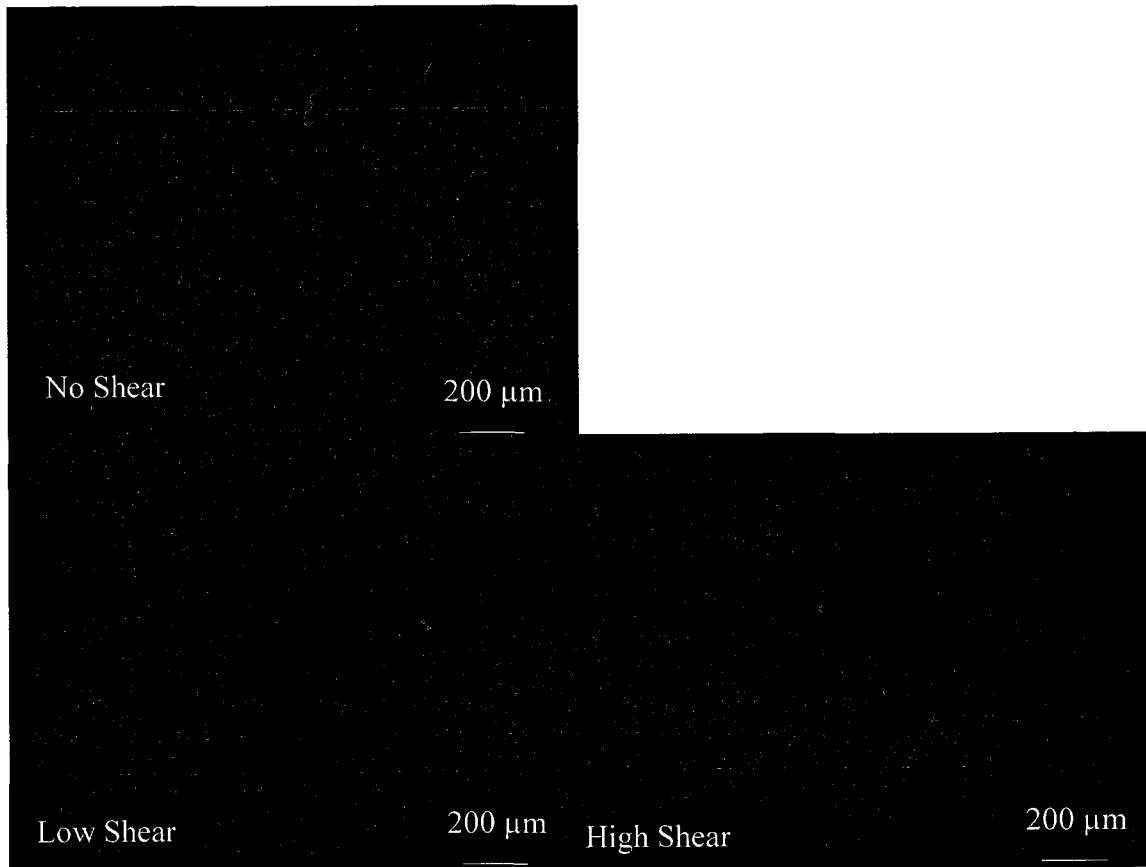


Figure 41 Fluorescence microscopy images of AO-stained dLbL-collagen slides that were exposed to PRP+L-A with no-shear (top left), low shear (bottom left) and high shear (bottom right).

### 3.8.1.3 dLbL-Fibrinogen with Added ADP

Figure 42 shows fluorescent images of dLbL-fibrinogen surfaces that were exposed to PRP and 20  $\mu$ M ADP with no-shear (top left), low shear (bottom left) and high shear (bottom right) and stained with AO. The no-shear and low shear cases exhibit the larger feature sizes (approximately 100  $\mu$ m) that were observed at these shear rates

for the images of dLbL-collagen with L-A. The high shear case exhibits multiple smaller features (approximately 20  $\mu\text{m}$ ) and shows slight evidence that these features are elongated.

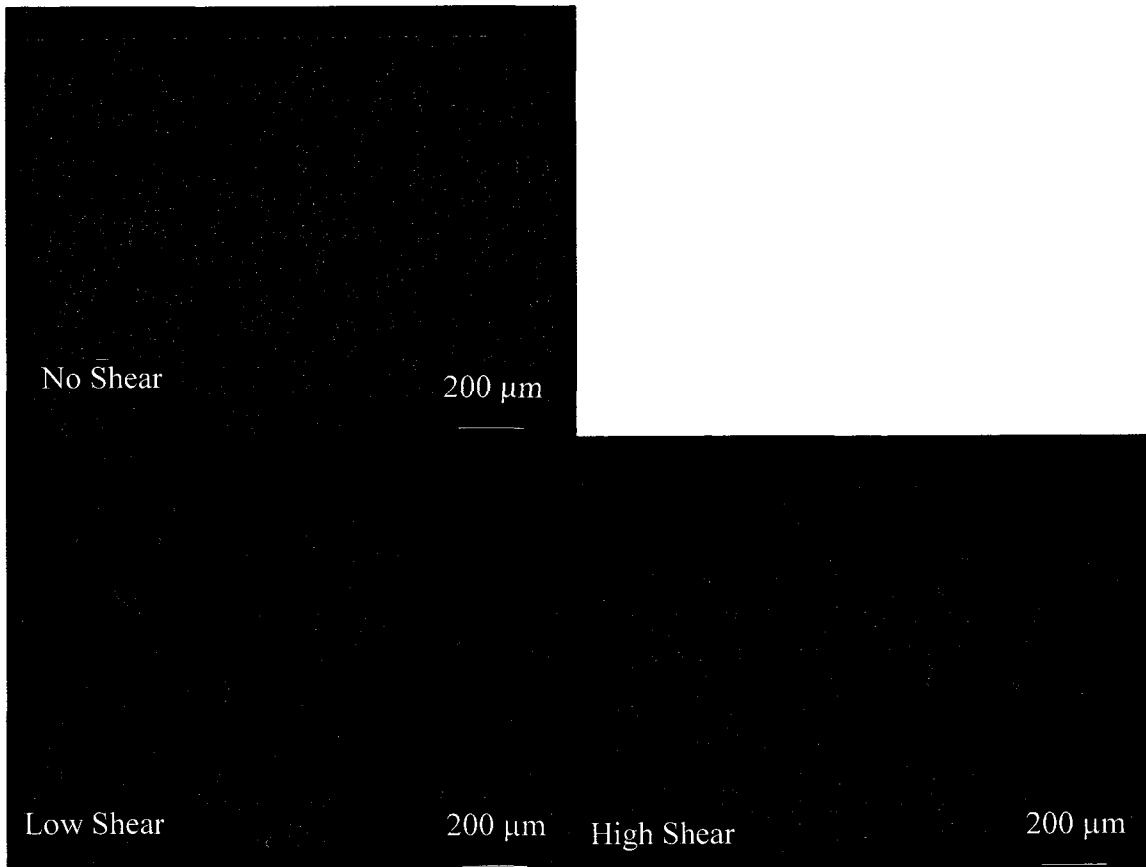


Figure 42 Fluorescence microscopy images of AO-stained dLbL-fibrinogen slides that were exposed to PRP+ADP with no-shear (top left), low shear (bottom left) and high shear (bottom right).

#### 3.8.1.4 dLbL-Collagen with Added ADP

Figure 43 shows fluorescent images of dLbL-collagen surfaces that were exposed to PRP and 20  $\mu\text{M}$  ADP with no-shear (top shear), low shear (bottom left) and high shear (bottom right) and stained with AO. The images are similar to the previous cases. The larger discrete features are approximately 80  $\mu\text{m}$  across for the no-shear case and 40  $\mu\text{m}$



across for the low shear case. The high shear case exhibits dashed streaks that are about 40  $\mu\text{m}$  wide and 500  $\mu\text{m}$  long.

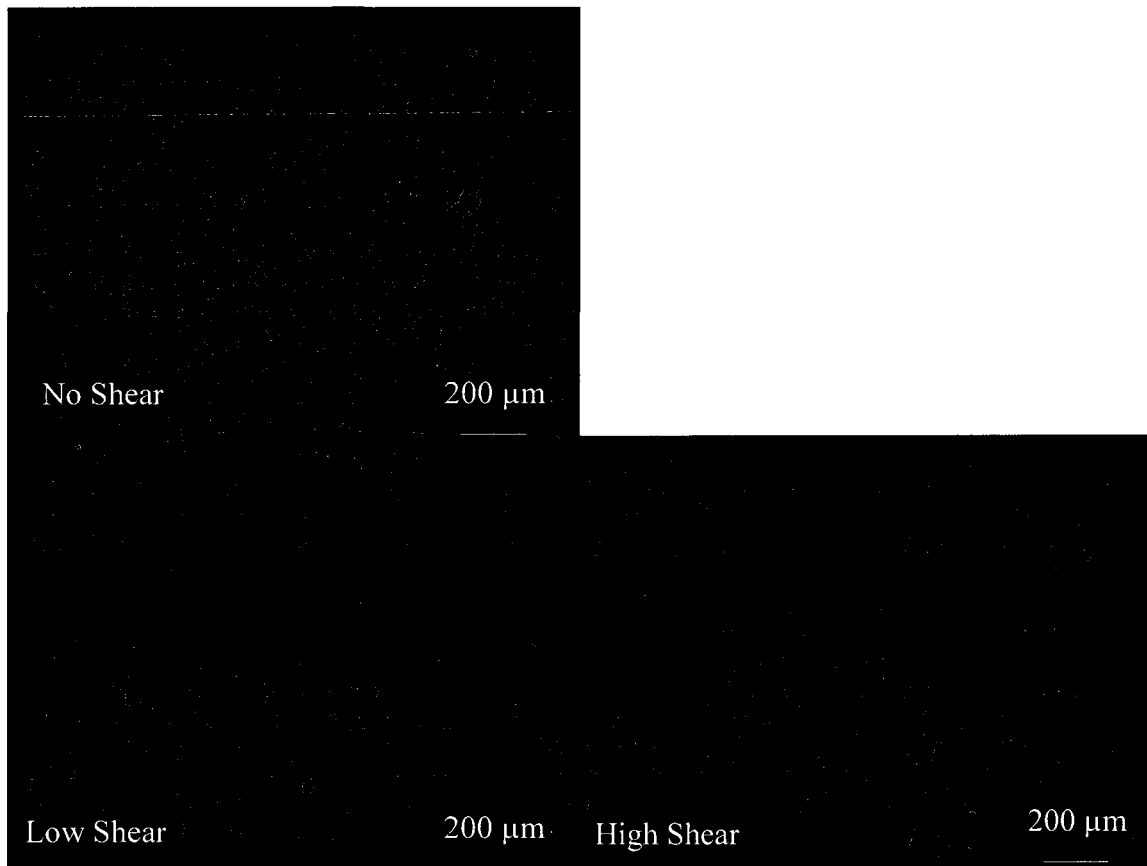


Figure 43 Fluorescence microscopy images of AO-stained dLbL-collagen slides that were exposed to PRP+ADP with no-shear (top left), low shear (bottom left) and high (bottom right).

#### 3.8.1.5 dLbL-Fibrinogen with L-NMMA

Figure 44 shows fluorescent images of dLbL-fibrinogen surfaces that were exposed to PRP and 20  $\mu\text{M}$  L-NMMA with no-shear (top left), low shear (bottom left) and high shear (bottom right) and stained with AO. The images for no-shear and low shear are similar and contain small features, on the order of 5  $\mu\text{m}$  across, along with a

few features that are closer to 100  $\mu\text{m}$  across. The high shear condition is dominated by the larger features.

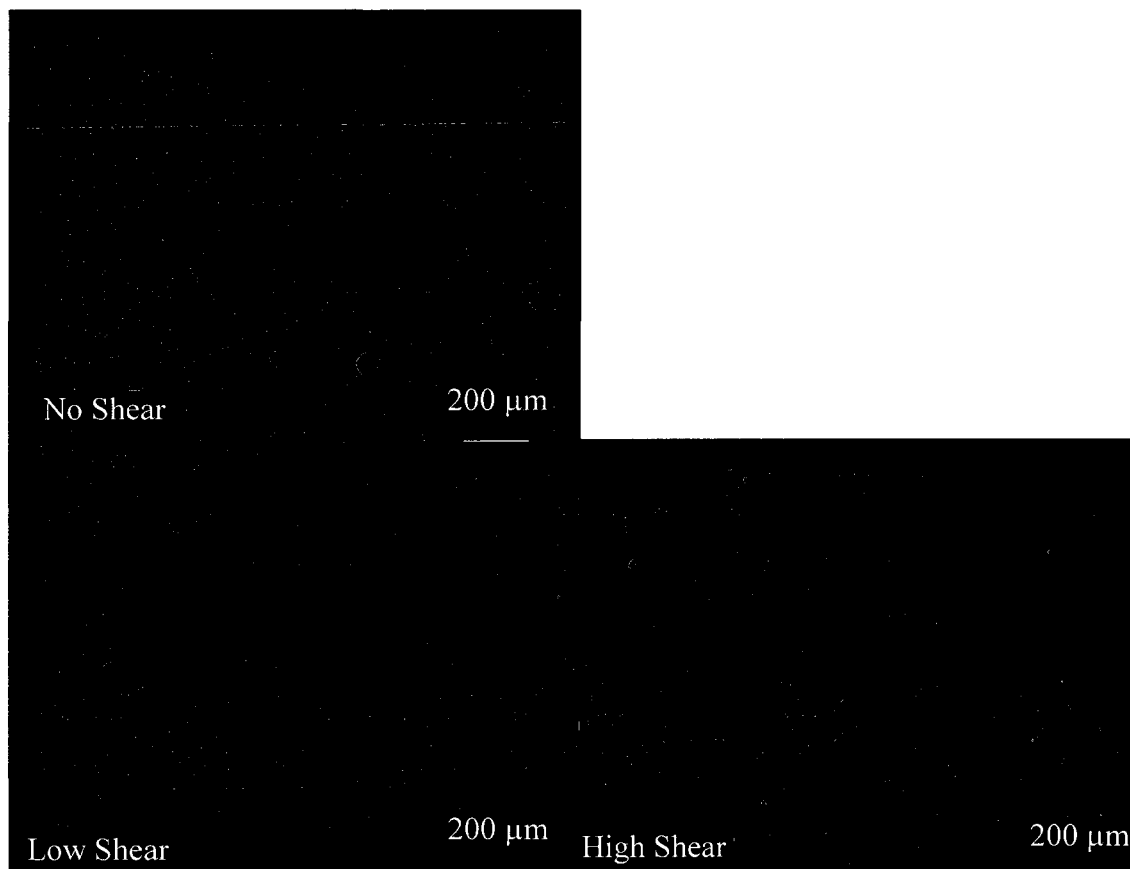


Figure 44 Fluorescence microscopy images of AO-stained dLbL-fibrinogen slides that were exposed to PRP+L-NMMA with no-shear (top left), low shear (bottom left) and high shear (bottom right).

### 3.8.2 AFM

#### 3.8.2.1 dLbL-Fibrinogen with Added L-A

Figure 45 shows AFM images of dLbL-fibrinogen substrates exposed to PRP+L-A under no-shear (top left), low shear (bottom left) and high shear (bottom right) and stained with AO. The no-shear image displays several small platelet aggregations with a peak height of 1220 nm. The low shear image illustrates prodigious platelet adhesions

with a peak height of 1626 nm. The high shear image shows activated platelets extending across the fibrinogen biointerface with a peak value of 1398 nm. The platelet extension is an example of platelet elongation or the rolling effect.

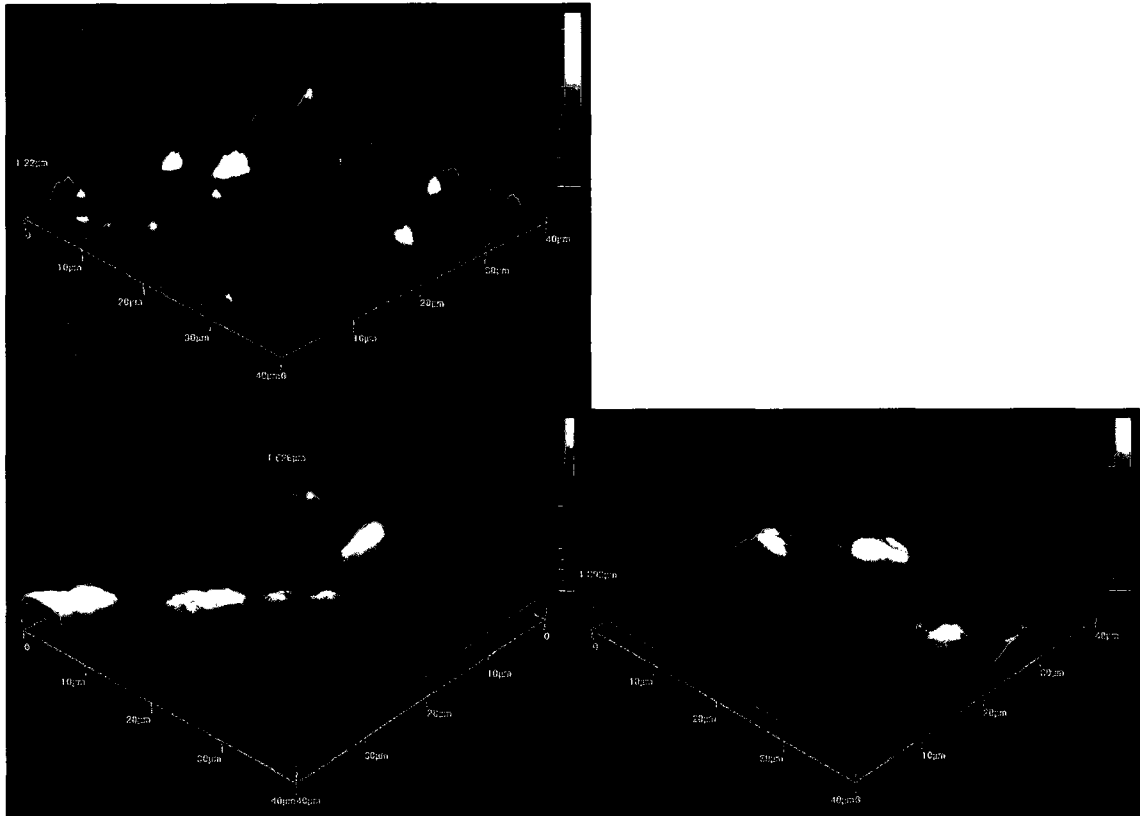


Figure 45 AFM images of slides with dLbL-fibrinogen under static conditions (top left), and dynamic conditions at low (bottom left) and high shear (bottom right) exposed to PRP+L-A and stained with AO

### 3.8.2.2 dLbL-Collagen with Added L-A

Figure 46 shows AFM images of dLbL-collagen substrates exposed to PRP+L-A under no-shear (top left), low shear (bottom left) and high shear (bottom right) and stained with AO. The no-shear image displays no obvious platelet aggregations with a peak height of 596 nm. The low shear image illustrates platelet adhesions along collagen

fibers with a peak height of 900 nm. The high shear image shows platelet adhesions extending across the collagen biointerface with a peak value of 816 nm.

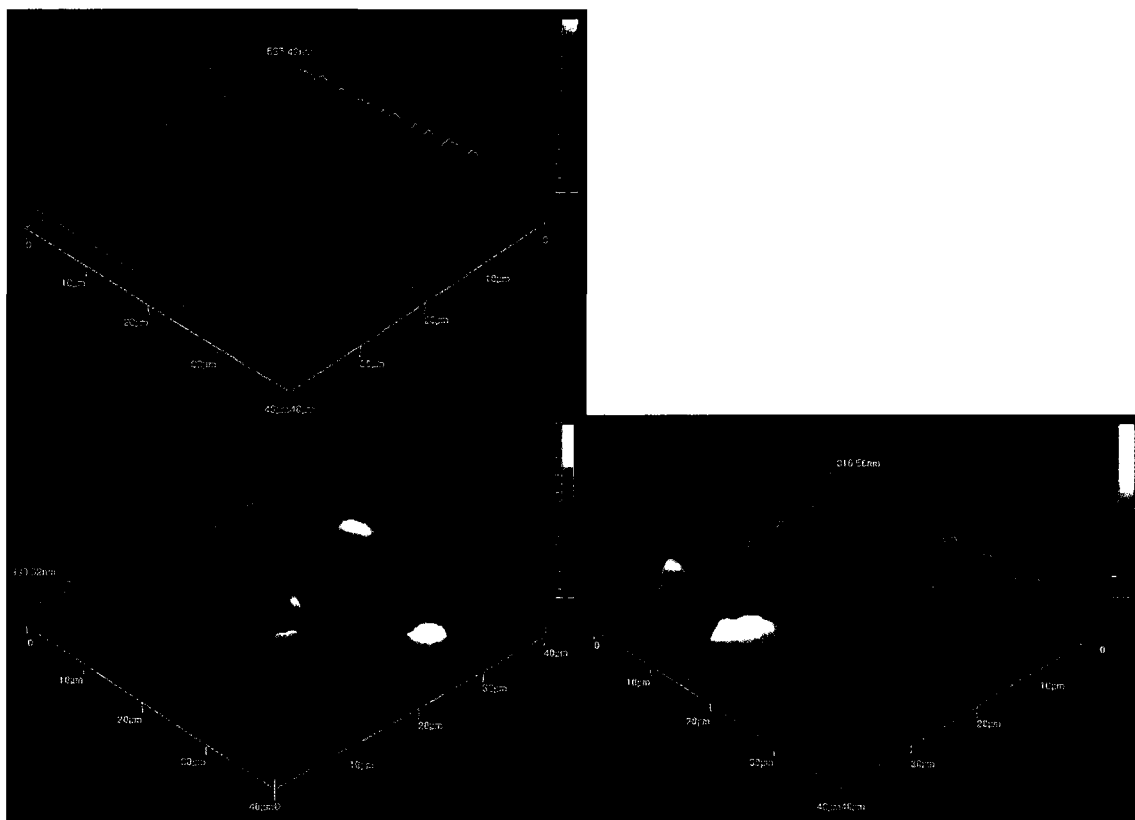


Figure 46 AFM images of slides with dLbL-collagen under static conditions (top left), and dynamic conditions at low (bottom left) and high shear (bottom right) exposed to PRP+L-A and stained with AO

### 3.8.2.3 dLbL-Fibrinogen with Added ADP

Figure 47 shows AFM images of dLbL-fibrinogen substrates exposed to PRP+ADP under no-shear (top left), low shear (bottom left) and high shear (bottom right) and stained with AO. The no-shear image displays ADP's streaking effect and has a peak height of 1045 nm. The low shear image also illustrates the streaking effect and has a peak height of 2124 nm. Although in the streaking effect appears different than the image in the top left image, a streaking pattern is evident along the surface. One possible

reason for the image difference could be that as shear stress is applied to the surface the dLbL-fibrinogen is shifted and/or washed away unlike the static condition with ADP. The high shear image shows activated platelets rolling across the fibrinogen biointerface and/or demonstrates ADP's streaking effect with a peak height of 1571 nm. The platelet extension is seen in the high shear regions only, and may be caused by platelet rolling, by a direct effect of ADP on surface streaking, as seen in other ADP images, or by a combination of both mechanisms.



Figure 47 AFM images of slides with dLbL-fibrinogen under static conditions (top left), and dynamic conditions at low (bottom left) and high shear (bottom right) exposed to PRP+ADP and stained with AO

### 3.8.2.4 dLbL-Collagen with Added ADP

Figure 48 shows AFM images of dLbL-collagen substrates exposed to PRP/ADP under no-shear (top left), low shear (bottom left) and high shear (bottom right) and stained with AO. The no-shear image displays large collagen fibers with a possible platelet aggregate attached to the fiber surface with a peak height of 596 nm. The low shear image illustrates the archetypal collagen biointerface surface minus platelet adhesions with a peak height of 638 nm. The high shear image shows platelet aggregations and adhesion along the collagen biointerface with a peak value of 1673 nm. The image also appears to include the ADP streaking effect and/or platelet rolling effect.



Figure 48 AFM images of slides with dLbL-collagen under static conditions (top left), and dynamic conditions at low (bottom left) and high shear (bottom right) exposed to PRP+ADP and stained with AO

### 3.8.2.5 dLbL-Fibrinogen with Added L-NMMA

Figure 49 shows AFM images of dLbL-fibrinogen substrates exposed to PRP+L-NMMA under no-shear (top left), low shear (bottom left) and high shear (bottom right) and stained with AO. The no-shear image displays several smaller platelet adhesions of no particular notable structures with a peak height of 1119 nm. The low shear image illustrates one large platelet adhesion seen in the edge of the scan and several smaller ones with a peak height of 1628 nm. The high shear image shows small platelet adhesions and one large activated platelet aggregate with a peak height of 1617 nm.

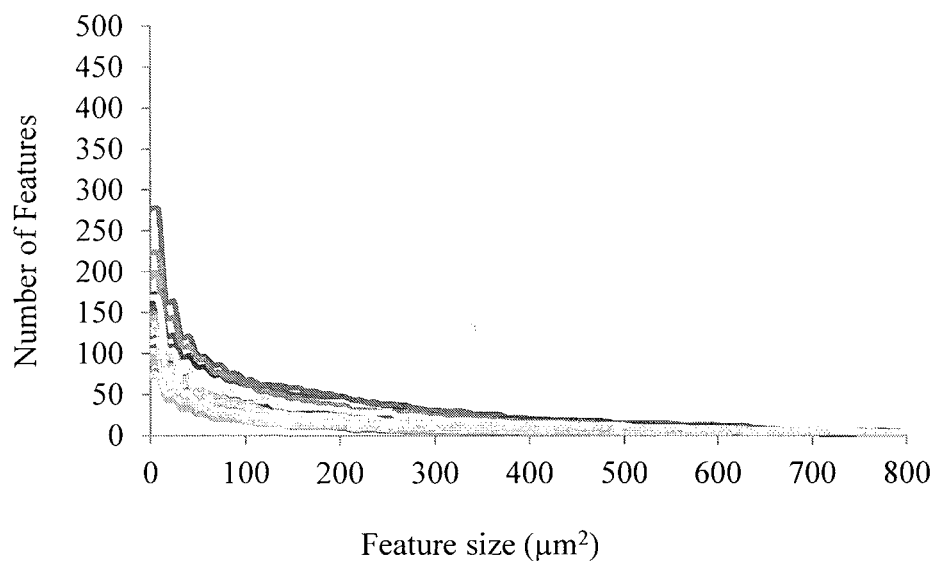


Figure 49 AFM images of slides with dLbL-fibrinogen under static conditions (top left), and dynamic conditions at low (bottom left) and high shear (bottom right) exposed to PRP+L-NMMA and stained with AO

### 3.8.3 Feature Size Distributions

#### 3.8.3.1 dLbL-Fibrinogen with Added L-A

Figure 50 shows the distribution of feature sizes for dLbL-fibrinogen substrates that were exposed to PRP+L-A. The upper graph shows distributions for individual images and the lower graph shows the means and standard deviations over several images. The number of features declines monotonically with feature size. The upper graph maintains a compact cluster of individual exponential curves as the number of features at a certain pixel size approaches the feature size threshold. The lower graph shows compact error bars as the curve approaches larger platelet adhesion sizes.





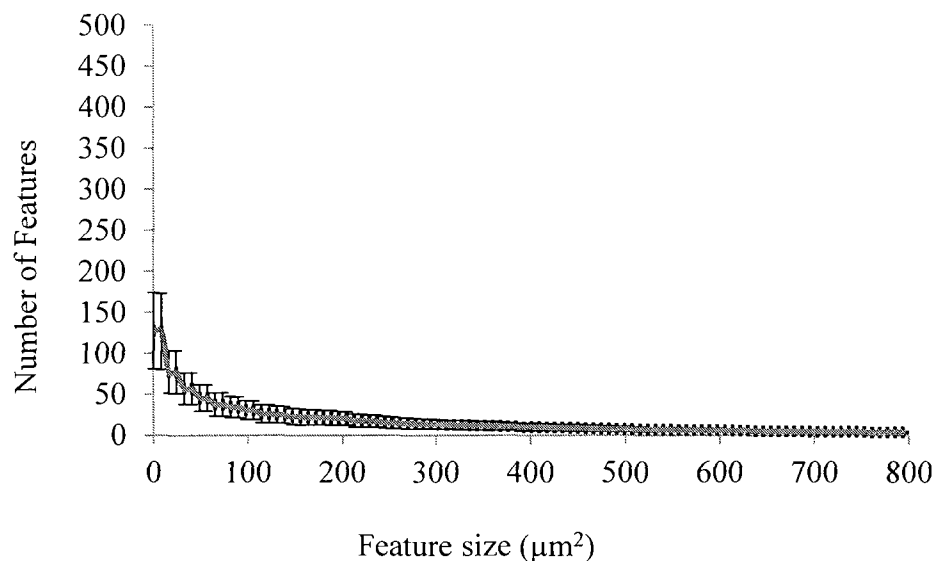


Figure 50 Feature size vs. number of features at that size for dLbL-fibrinogen surfaces exposed to PRP+L-A at low shear rate. Top: Curves for each image. Bottom: Mean of all images with standard deviation.

### 3.8.3.2 dLbL-Fibrinogen with Added ADP

Figure 51 shows the distribution of feature sizes for dLbL-fibrinogen substrates that were exposed to PRP+ADP. The upper graph show distributions for individual images and the lower graph show the means and standard deviations over several images. The number of features declines monotonically with feature size. The upper graph displays a feature curve cluster that is visibly spread. The lower graph shows larger standard deviations.

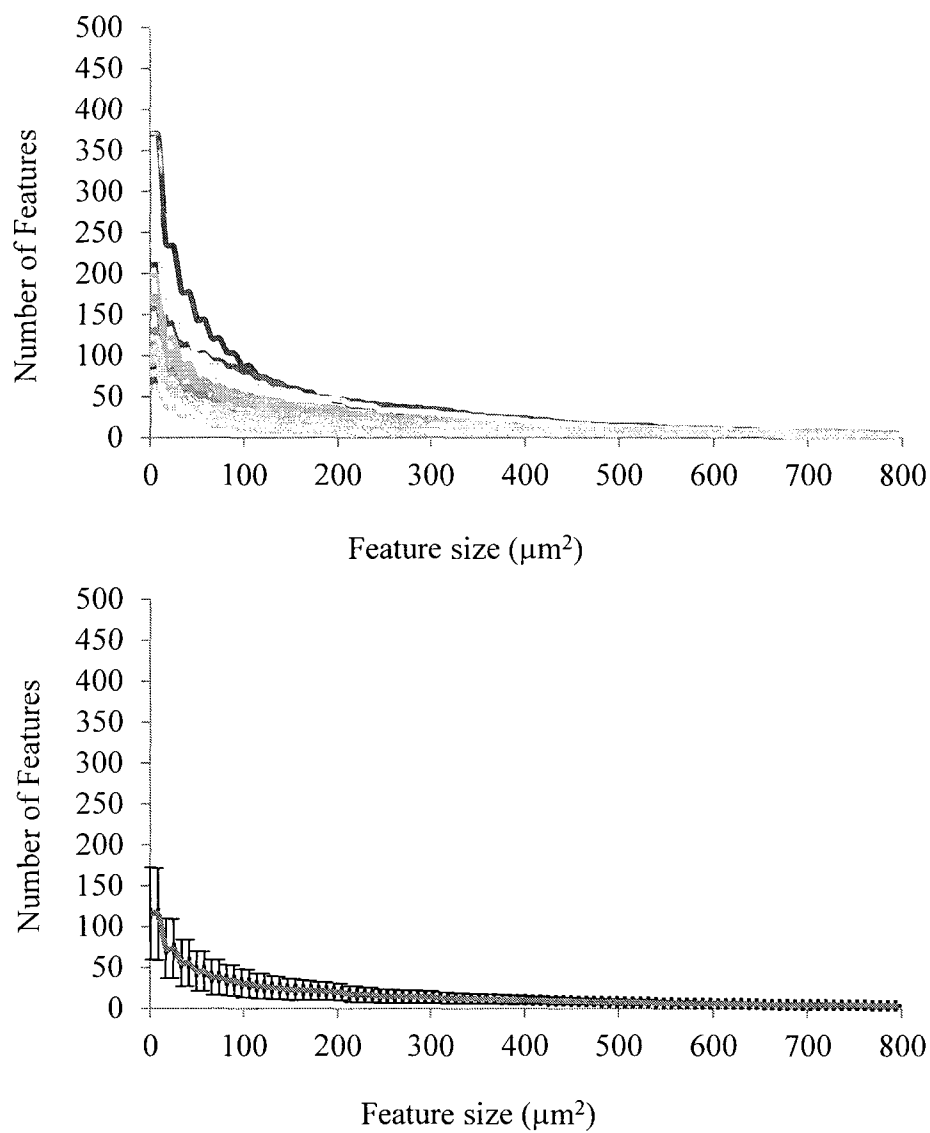


Figure 51 Feature size vs. number of features at that size for dLbL-fibrinogen surfaces exposed to PRP+ADP at low shear rate. Top: Curves for each image. Bottom: Mean of all images with standard deviation.

### 3.8.3.3 dLbL-Fibrinogen with Added L-NMMA

Figure 52 shows the distribution of feature sizes for dLbL-fibrinogen substrates that were exposed to PRP+L-NMMA. The upper graph show distributions for individual images and the lower graph show the means and standard deviations over several images.

The number of features declines monotonically with feature size. Platelet adhesion sizes are consistent from one experiment to another, and the standard deviations are smaller.

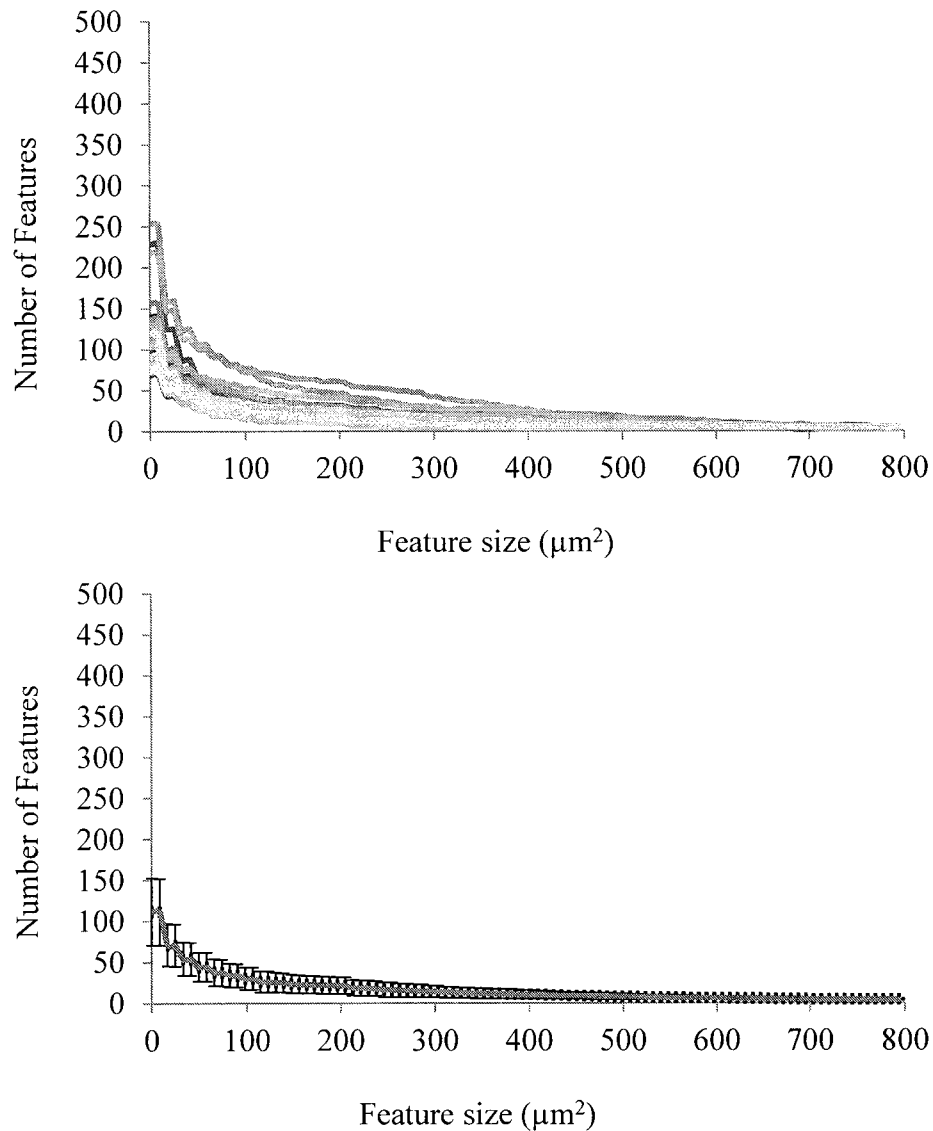
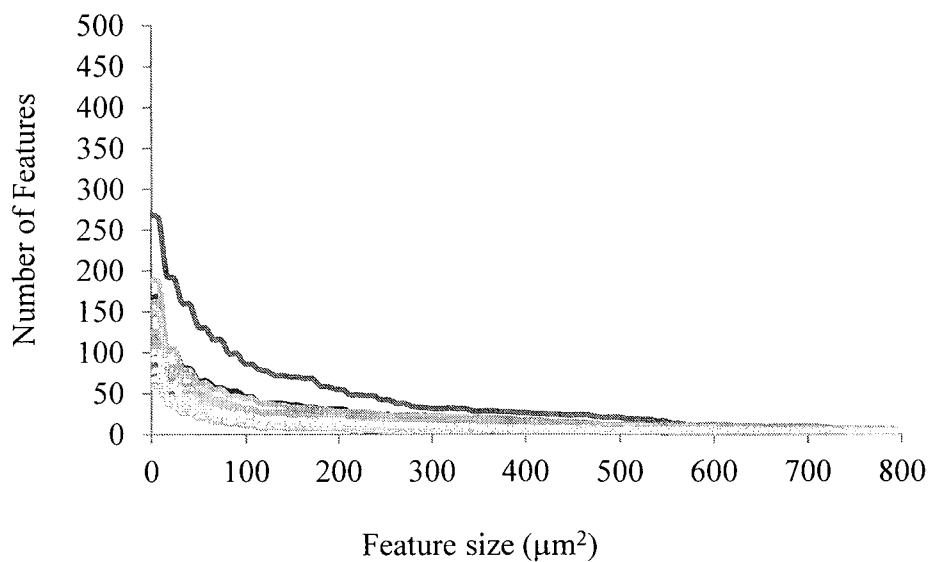


Figure 52 Feature size vs. number of features at that size for dLbL-fibrinogen surfaces exposed to PRP+L-NMMA at low shear rate. Top: Curves for each image. Bottom: Mean of all images with standard deviation.

### 3.8.3.4 dLbL-Collagen with Added L-A

Figure 53 shows the distribution of feature sizes from all fluorescent images obtained from dLbL-collagen surfaces that were exposed to PRP+L-A. The curves are generally similar to those obtained from dLbL-fibrinogen. The upper graph shows one displaced exponential curve in contrast to the other images. However, the outlying curve does not affect the standard deviation in the lower graph. The lower graph displays bars that appear small as the platelet adhesion sizes increase.



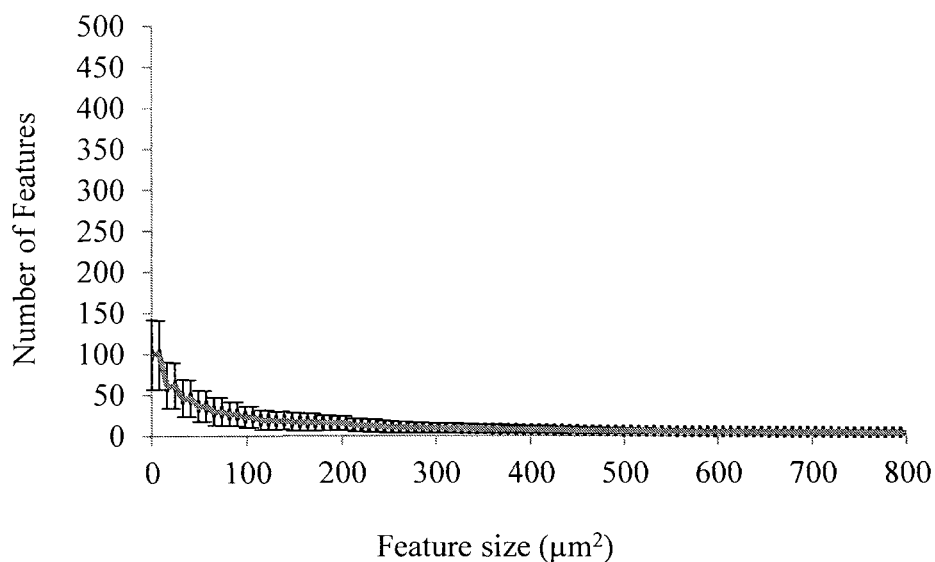


Figure 53 Feature size vs. number of features at that size for dLbL-collagen surfaces exposed to PRP+L-A at low shear rate. Top: Curves for each image. Bottom: Mean of all images with standard deviation.

#### 3.8.3.5 dLbL-Collagen with Added ADP

Figure 54 shows the distribution of feature sizes from all fluorescent images obtained from dLbL-collagen surfaces that were exposed to PRP+ADP. The curves are generally similar to those obtained from dLbL-fibrinogen. The upper graph displays a broad spectrum for feature curves. The lower graph shows larger standard deviations.

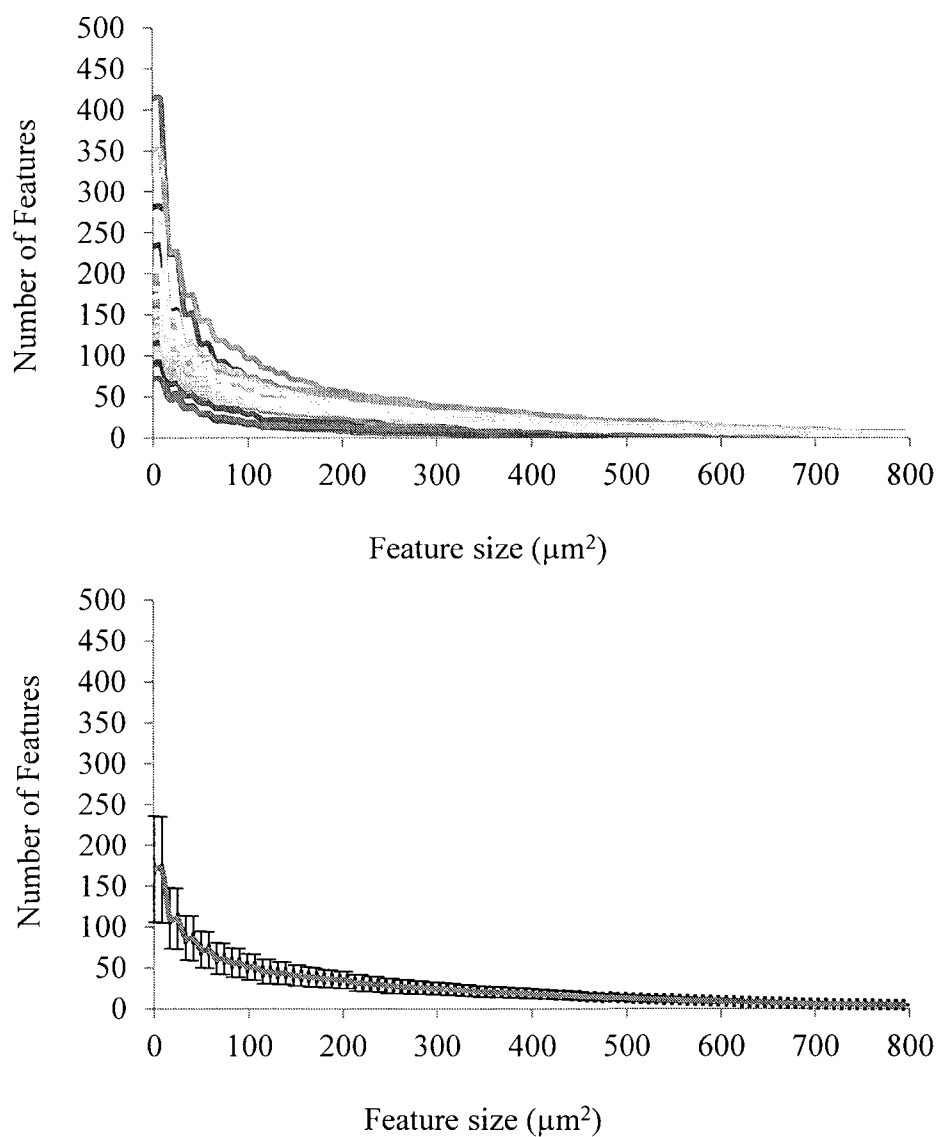


Figure 54 Feature size vs. number of features at that size for dLbL-collagen surfaces exposed to PRP+ADP at low shear rate. Top: Curves for each image. Bottom: Mean of all images with standard deviation.

### 3.9 Statistical Comparisons

#### 3.9.1 Statistical Comparison of Platelet Coverage Confirmation

Figure 55 displays the average peak values for a glass slide that was exposed to PRP and for LbL slides that were not exposed to PRP. The average peak height for the PRP plain glass slide was statistically higher than the averages for the samples that were

unexposed to PRP. This result suggests that surfaces unexposed to PRP LbL do not have peak heights equivalent to or great than PRP exposed surfaces. The \* in Figure 55 represents the statistical insignificance of PRP plain glass slide bar compared to the other bars. Table 5 lists the t-test p-values that were used to determine whether the AFM-derived peak heights for a glass slide exposed to PRP were significantly larger than those for LbL slides that were not exposed to PRP. In all cases, the p-values are  $\leq 0.05$ .

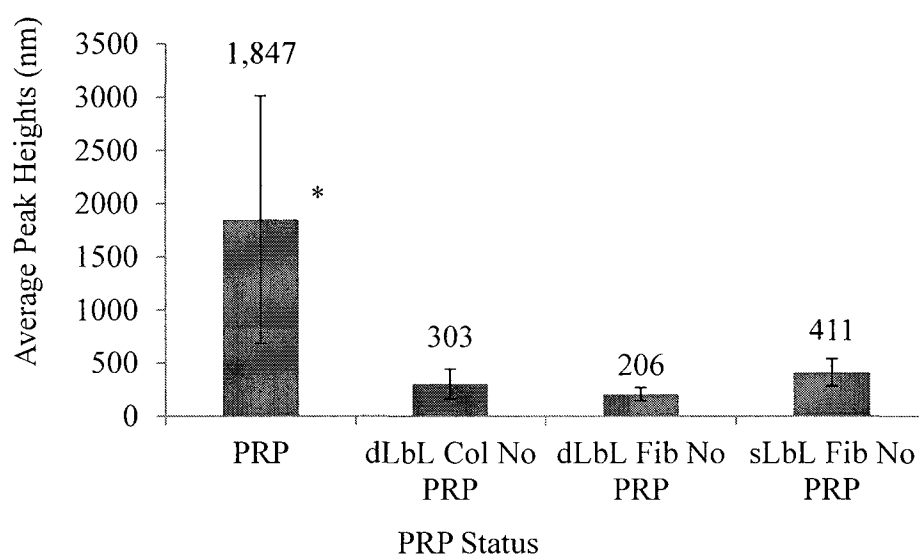


Figure 55 Average peak heights and standard deviations from AFM scans of glass slides exposed to PRP and surfaces that were not exposed to PRP

Table 5 AFM peak height t-Test p-values (2-tail) for statistical comparisons between a glass slide exposed to PRP and unexposed LbL surfaces

Surface Type	t-Test: P (2 tail)
dLbL Fibrinogen	0.035
sLbL Fibrinogen	0.049
dLbL Collagen	0.042

### 3.9.2 Statistical Comparison of LbL Surfaces

Table 6 lists the t-test two tail p-values and mean percent coverage from fluorescence microscopy of the different protein-coatings. Under high shear conditions, adhesion on dLbL-fibrinogen was significantly different from adhesion on sLbL-fibrinogen, both with and without added L-A. The two surfaces were also statistically different under no shear with added L-A.

Table 6 Comparison of fluorescence-derived percent surface coverage between sLbL-fibrinogen and dLbL-fibrinogen surfaces

Chemical	Shear Condition	Surface	Mean % Coverage	t-Test: P (2 tail)
None	Static	sLbL	5.515	0.093
		dLbL	0.410	
	Low	sLbL	0.388	0.211
		dLbL	0.448	
	Medium	sLbL	0.513	0.748
		dLbL	0.559	
	High	sLbL	3.392	0.003
		dLbL	0.782	
20 $\mu$ M L-A	Static	sLbL	3.195	4.92E-09
		dLbL	0.395	
	Low	sLbL	0.428	0.754
		dLbL	0.431	
	Medium	sLbL	0.999	0.135
		dLbL	0.435	
	High	sLbL	1.196	0.044
		dLbL	0.581	

Figure 56 compares AFM-derived peak heights for the different LbL-generated surfaces with no exposure to PRP. On average, peak heights are largest for dLbL-fibrinogen, smaller for dLbL-collagen, and smallest for sLbL-fibrinogen. This graph indicates that although dLbL-fibrinogen maintains an overall smoother surface as evident



in previous AFM dLbL-fibrinogen figures, the randomly selected scan areas corroborate higher peak heights than sLbL-fibrinogen surface.

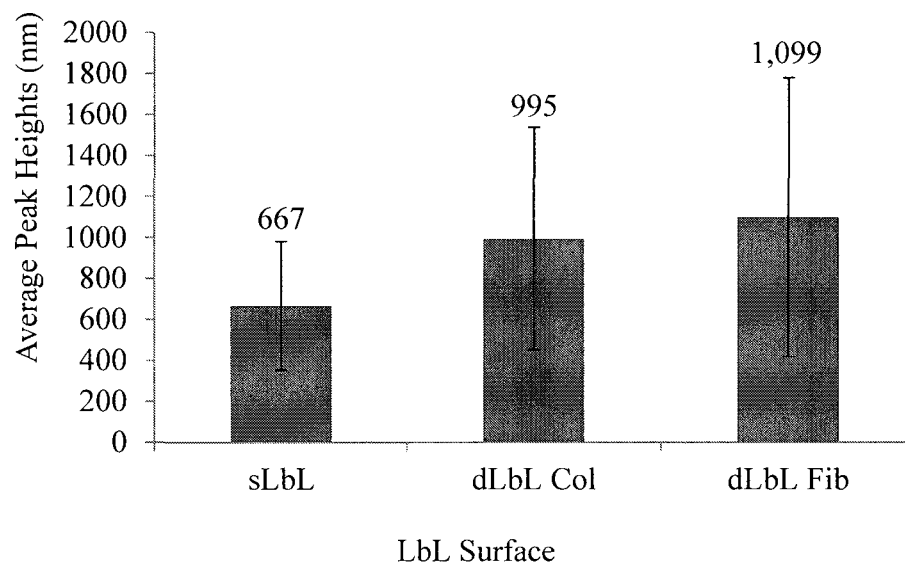


Figure 56 Peak heights, with standard deviations, from AFM scans of LbL-generated surfaces, not exposed to PRP.

AFM peak heights for all sLbL-fibrinogen scans were compared to all dLbL-fibrinogen scans and to all dLbL-collagen scans with t-tests (Table 7). Both comparisons indicated statistical significance.

Table 7 t-Test two tail P-values using AFM to obtain peak heights of LbL technique interests

Surface Type	t-Test: P (2 tail)
sLbL Fib vs. dLbL Fib	0.002
sLbL Fib vs. dLbL Col	0.013

### 3.9.3 Statistical Comparison of Biointerface Substrates

Table 8 presents p-values for t-tests that compared mean coverage percentages between dLbL-fibrinogen and dLbL-collagen surfaces that were exposed to PRP and

stained with AO. For plain PRP, the difference in percent coverage for fibrinogen and collagen was significant only under static conditions. With 20  $\mu$ M added L-A, adhesion on the two surfaces was different only under dynamic conditions. For PRP+ADP, the difference in percent area coverage on the two surfaces was significant only under the medium shear conditions.

Table 8 Statistical tests to compared percent surface coverage between dLbL-fibrinogen and dLbL-collagen from fluorescent microscopy

Chemical	Shear Condition	Surface	Mean % Coverage	t-Test: P (2-tail)
None	Static	Fibrinogen	0.469	2.28E-12
		Collagen	0.276	
	Low	Fibrinogen	0.448	0.095
		Collagen	0.526	
	Medium	Fibrinogen	0.559	0.934
		Collagen	0.564	
	High	Fibrinogen	0.782	0.793
		Collagen	0.799	
20 $\mu$ M ADP	Static	Fibrinogen	0.429	0.343
		Collagen	0.396	
	Low	Fibrinogen	0.368	3.04E-07
		Collagen	0.600	
	Medium	Fibrinogen	0.450	0.002
		Collagen	0.656	
	High	Fibrinogen	0.614	0.0002
		Collagen	1.074	
20 $\mu$ M L-A	Static	Fibrinogen	0.395	0.140
		Collagen	0.442	
	Low	Fibrinogen	0.431	0.077
		Collagen	0.375	
	Medium	Fibrinogen	0.435	0.028
		Collagen	0.371	
	High	Fibrinogen	0.581	0.052
		Collagen	0.483	

Figure 57 compares the average peak heights averaged over all fibrinogen experiments and all collagen experiments. The error bars represent standard deviations. A

t-test comparison (Table 9) indicates no statistical difference between the means. This information suggests that peak heights show no real variation among scan sets. Therefore, the data provided on fibrinogen and collagen prove to only differ with ADP under dynamic conditions while plain PRP and L-A suggest no difference between biointerfaces.

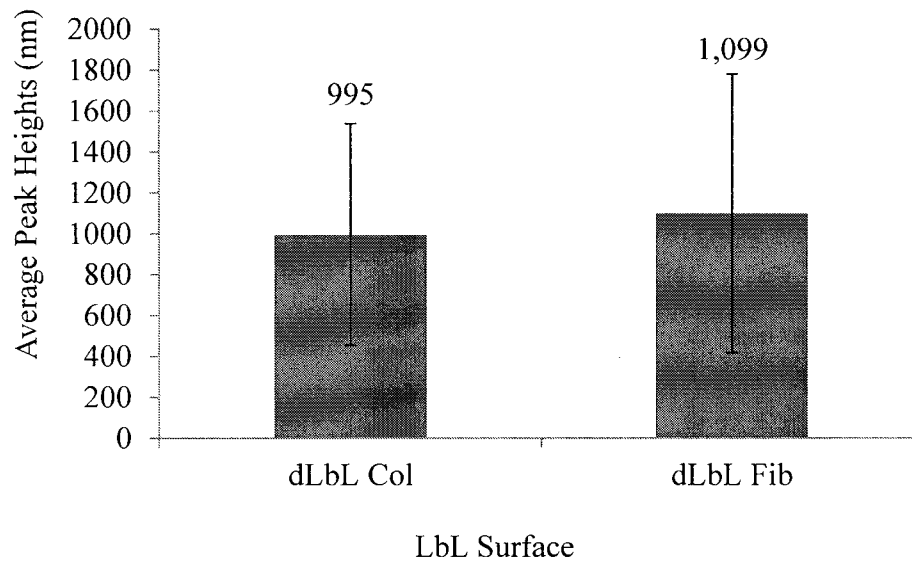


Figure 57 Average peak heights of biointerface interests with standard deviation error bars

Table 9 P-values using AFM to obtain peak heights of biointerface interests

Biointerface	t-Test: P (2 tail)
dLbL Fib vs. dLbL Col	0.35

### 3.9.4 Statistical Comparison of Shear Stress

#### 3.9.4.1 Fluorescence Microscopy Statistics

Table 10 shows the results of t-test comparisons of the percent surface coverage on dLbL-fibrinogen at no shear rates to coverage at low, medium and high shear rates, as

determined from fluorescent microscopy. The static coverage was always significantly different from the dynamic coverage. From plain PRP and added L-NMMA, no shear was significantly different from medium shear. With added L-A, no shear was significantly different from low shear. These values highlight the differences seen in Figure 20 in that high shear regions have more platelet adhesions than the static condition. The mean coverage percentages across all shear regions typically demonstrate an increasing gradient of percentages as the shear rates increase.

Table 10 Fluorescence microscopy used to obtain statistical analysis of shear region interests from dLbL-fibrinogen

Chemical	Shear Condition	Mean % Coverage		t-Test: P (2-tail)
		Static	Dynamic	
None	Static vs. Low	0.469	0.448	0.307
	Static vs. Medium		0.559	0.001
	Static vs. High		0.782	5.93E-10
20 $\mu$ M ADP	Static vs. Low	0.429	0.368	0.010
	Static vs. Medium		0.450	0.444
	Static vs. High		0.614	1.62E-06
20 $\mu$ M L-A	Static vs. Low	0.340	0.431	0.143
	Static vs. Medium		0.435	0.152
	Static vs. High		0.581	2.1E-07
20 $\mu$ M L- NMMA	Static vs. Low	0.447	0.436	0.654
	Static vs. Medium		0.515	0.016
	Static vs. High		0.850	4.61E-07

Table 11 shows the results of t-test comparisons of the percent surface coverage on dLbL-collagen at no shear rates to coverage at low, medium and high shear rates, as determined from fluorescent microscopy. Both, plain PRP and PRP+ADP demonstrate statistical differences between the no shear condition and all three other conditions. For L-A, statistical significance was found only between no shear and medium shear. The

lack of significance with L-A may be caused by the smaller amount of surface coverage, which suggests, in turn, a smaller difference between the different cases.

Table 11 Fluorescence microscopy used to obtain statistical analysis of shear region interests from dLbL-collagen

Chemical	Shear Condition	Mean % Coverage		t-Test: P (2-tail)
		Static	Dynamic	
None	Static vs. Low	0.276	0.526	2.40E-06
	Static vs. Medium		0.564	3.36E-05
	Static vs. High		0.799	4.11E-14
20 $\mu$ M ADP	Static vs. Low	0.400	0.600	3.86E-05
	Static vs. Medium		0.656	0.0001
	Static vs. High		1.074	4.16E-07
20 $\mu$ M L-A	Static vs. Low	0.442	0.375	0.074
	Static vs. Medium		0.371	0.032
	Static vs. High		0.482	0.389

#### 3.9.4.2 AFM Statistics

Figure 58 shows AFM-derived peak heights for dLbL-fibrinogen and dLbL-collagen, exposed to plain PRP at no shear, low shear and high shear conditions. For fibrinogen peak heights were larger in the high shear region than in the other two regions. For collagen, peak heights increased monotonically with shear rate. If larger AFM peak heights can be associated with adhesion, then the reduced peak heights on fibrinogen at higher shear rates are consistent with a study that finds an reduced ability of fibrinogen, compared to von Willebrand factor, to hold platelet aggregations under in high shear stress [69].

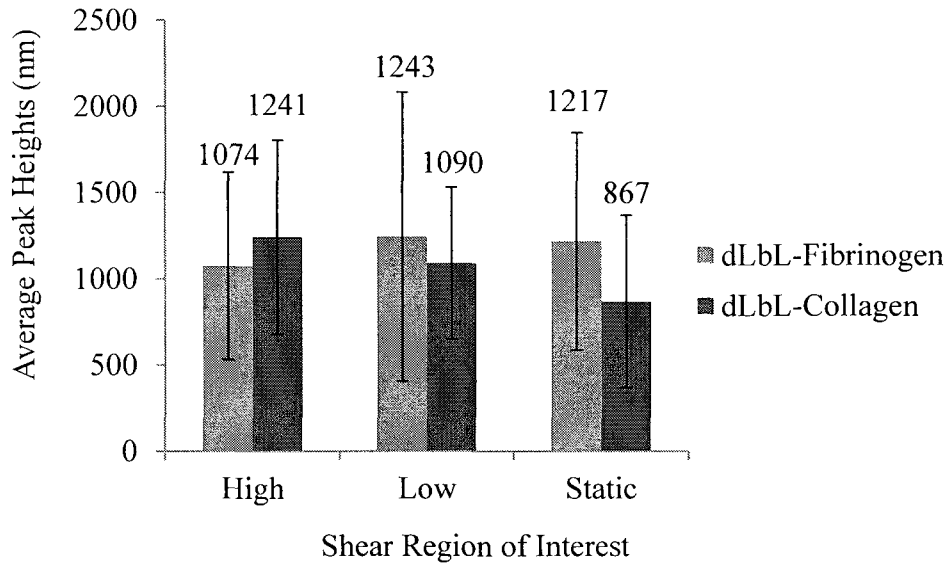


Figure 58 AFM-derived peak heights for dLbL-fibrinogen and dLbL-collagen surfaces that have been exposed to plain PRP. Error bars represent standard deviation.

Table 12 lists the p-values for comparison of peak heights in different shear regions for the dLbL-fibrinogen and dLbL-collagen surfaces. All p-values are greater than 0.05, indicating that there is no statistically significant difference in peak heights from one shear region to the other on both surfaces.

Table 12 P-values for comparisons of AFM-derived peak heights within different shear regions

Surfaces	LbL with Biointerface	t-Test: P(2-tail)
dLbL Fibrinogen	Static vs. High	0.415
	Low vs. High	0.433
dLbL Collagen	Static vs. High	0.074
	Low vs. High	0.422

### 3.9.5 Statistical Comparison of Chemicals

Table 13 shows the ANOVA-derived p-values for the variability in percent surface coverage on fibrinogen caused by each of the variables. The PRP experiments

were repeated on multiple days to produce different experimental sessions. For plain PRP, all shear regions exhibited significance. One contribution to the large significance is the larger number of experiments performed with plain PRP, which is three times the number for any of the chemical additive cases. When experiments are examined for plain PRP on a single day, the p-values tend to show a significance difference between the low and medium shear stress regions. For example, these p-values from the 5/17/2010 session 6 were 0.014 for the low shear rate area and 0.012 for the medium shear rate area. Therefore, the larger p-values obtained for the cases with chemical additives may not represent a substantial difference in the character of the probability distributions as much as a difference in the number of experiments performed. The high shear regions with added ADP, L-A and L-NMMA contributed strongly to the variability ( $p = 5.8 \times 10^{-6}$ ,  $7.7 \times 10^{-7}$ , and  $3.1 \times 10^{-9}$ , respectively). Low shear contributed to variability for the cases with L-A and L-NMMA, and no shear contributed to variability for the cases with ADP and L-NMMA.

Table 13 P-values from ANOVA analysis of surface coverage of dLbL-fibrinogen, as derived from fluorescence microscopy

Chemical	Shear Condition	Mean % Coverage	ANOVA: (P-value)
None	Static	0.468	5.12E-07
	Low	0.448	7.53E-11
	Medium	0.560	6.86E-06
	High	0.783	7.13E-29
20 $\mu$ M ADP	Static	0.429	0.011
	Low	0.368	0.065
	Medium	0.450	0.501
	High	0.614	5.76E-06
20 $\mu$ M L-A	Static	0.395	0.060
	Low	0.431	0.001
	Medium	0.434	0.525
	High	0.571	7.73E-07
20 $\mu$ M L-NMMA	Static	0.448	1.52E-07
	Low	0.434	0.001
	Medium	0.515	0.261
	High	0.850	3.06E-09

Table 14 shows p-values for t-tests in which the percent surface coverage on dLbL-fibrinogen, as obtained from fluorescence microscopy, is compared between the no-chemical-additive case and the other chemical additive cases. Adhesion for PRP+ADP was significantly different from adhesion for plain PRP for all shear regions, but not for the static case. Adhesion for PRP+L-A was significantly different from adhesion for plain PRP for all cases except low shear. Adhesion for PRP+L-NMMA was not significantly different from adhesion on plain PRP.



Table 14 Comparison of percent surface coverage on dLbL-fibrinogen, as determined from fluorescence microscopy, for different chemical additives to coverage with plain PRP

Chemical Comparison	Shear Condition	Mean % Coverage		t-Test: P(2-tail)
		None	Additive	
None vs. 20 $\mu$ M ADP	Static	0.469	0.429	0.113
	Low	0.448	0.368	0.001
	Medium	0.559	0.450	0.0002
	High	0.782	0.614	0.003
None vs. 20 $\mu$ M L-A	Static	0.469	0.395	0.001
	Low	0.448	0.431	0.438
	Medium	0.559	0.497	7.51E-05
	High	0.782	0.581	0.0003
None vs. 20 $\mu$ M L-NMMA	Static	0.469	0.447	0.328
	Low	0.448	0.436	0.604
	Medium	0.559	0.515	0.170
	High	0.782	0.850	0.437

Table 15 shows p-values for t-tests in which the percent surface coverage on dLbL0collagen, as obtained from fluorescence microscopy, is compared between the no-chemical-additive case and the other chemical additive cases. Adhesion for PRP+ADP was significantly different from adhesion for plain PRP for no shear and high shear. Adhesion for PRP+L-A was significantly different from adhesion for plain PRP for all shear cases. The p-value for PRP+L-A in the high shear region indicates that L-A strongly affects percent surface coverage. The mean percent coverage generally increases with rate.

Table 15 Fluorescence microscopy used to obtain statistical analysis of chemical additive interests for dLbL-collagen

Chemical Comparison	Shear Condition	Mean % Coverage		t-Test: P(2-tail)
		None	Additive	
None vs. 20 $\mu$ M ADP	Static	0.276	0.396	0.0007
	Low	0.526	0.600	0.202
	Medium	0.564	0.656	0.276
	High	0.799	1.074	0.027
None vs. 20 $\mu$ M L-A	Static	0.276	0.442	1.65E-06
	Low	0.526	0.375	0.004
	Medium	0.564	0.371	0.004
	High	0.799	0.483	2.21E-06

Figure 59 shows peak heights obtained from the AFM scans on dLbL-fibrinogen and dLbL-collagen from different chemical additives. For fibrinogen, plain PRP led to the lowest peak heights, followed by PRP+L-A, PRP+L-NMMA, and then PRP+ADP. Although, L-A's peak heights are above plain PRP values, these numbers are low compared to the other chemicals. This information suggests that platelet-derived NO maintains a low overall peak height. The bottom graph's AFM scans for dLbL-collagen produce similar results to dLbL-fibrinogen. However, dLbL-collagen's L-A peak heights remain lower than plain PRP. ADP produced the highest peaks though all only slightly greater than one another. For collagen, PRP+L-A led to the lowest peak heights, followed by plain PRP and then PRP+ADP. This information implies that the ADP and L-NMMA produce more platelet adhesions along the surface and/or modify the general surface morphology. This result is consistent with the role of ADP as a platelet activator and the role of L-NMMA as an inhibitor of NO production.

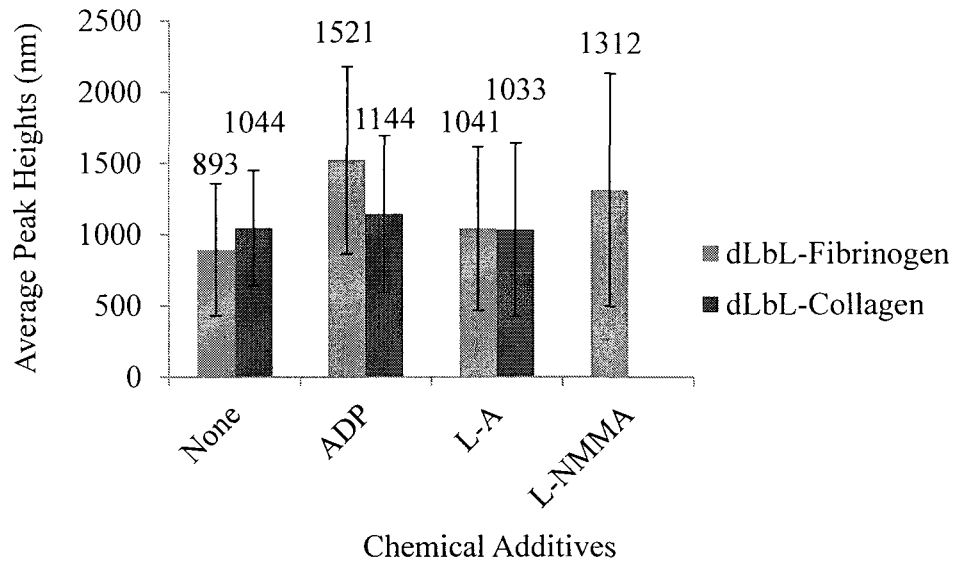


Figure 59 dLbL-fibrinogen and dLbL-collagen surfaces using AFM to obtain average peak heights of chemical additive interests with standard deviation error bars.

Table 16 lists p-values for t-tests performed to compare the adhesion of PRP+Additives to PRP alone. Only PRP+ADP led to significantly different peak heights than plain PRP alone.

Table 16 P-values using AFM to obtain peak heights of chemical additive interests using dLbL-fibrinogen and dLbL-collagen surfaces

Surface	Additives	t-Test: P (2 tail)
dLbL Fibrinogen	ADP	0.003
	L-A	0.402
	L-NMMA	0.087
dLbL Collagen	ADP	0.577
	L-A	0.956

## CHAPTER 4

### DISCUSSION

#### 4.1 Evaluation and Optimization of Experimental Conditions

##### 4.1.1 Overview

To characterize the platelet concentrations in the PRP samples, platelet counts were attempted, first with a hemocytometer, and then with a Bioanalyzer<sup>®</sup>. The platelets were too small to be seen in the hemocytometer. The Bioanalyzer<sup>®</sup> provided consistent platelet counts, but they were an order of magnitude lower than would generally be expected from PRP extracted from bovine blood. The company that makes this instrument confirmed that it does perform cytometry, but they stated that the device has not been tested for counting platelets. Thus, whereas the device may verify consistent platelet counts from experiment to experiment, it may not provide accurate counts.

In some of our early experiments, the behavior of the whole blood varied strongly from one experiment to the next. In some cases the blood had completely clotted by the time it was transported to the laboratory, while in other cases the blood did not appear to clot at all, even after several days in the laboratory. It was suspected that slight variations in the sodium citrate concentration might strongly affect the blood's behavior. Therefore, a series of tests was performed to determine the extent to which the sodium citrate concentration in the whole blood affected coagulation. In the first test, ten blood samples were collected, one with no citrate, three with the usual 9:1 ratio, three with 10% less

sodium citrate, and three with 10% more sodium citrate. For each concentration of citrate, each of the three mixing methods was applied, no mixing, normal mixing, and strong mixing. The behavior was similar for all cases, except the no-citrate case, which clotted completely. Therefore, a second test was performed with -33% and -66% below the normal 9:1 ratio with the same mixing techniques. In turn, we also added the chemical additives to whole blood sample in 100  $\mu\text{L}$  increments as time progressed. No difference could be found between the behavior of samples with different citrate concentrations. Some of the effects of the added chemicals may have been caused by an increase in the dilution as the chemical was added. Overall, these tests suggest that moderate changes in the citrate ratio would not dramatically affect the clotting of blood.

The tests on PRP extraction indicated that more consistent results could be obtained if the temperature, time and duration of centrifugation were all increased. In addition, the use of a larger number of smaller centrifuge tubes increased the amount of blood that could be processed in one centrifugation and therefore decreased the amount of time PRP sat unused while all of the citrated whole blood tubes were centrifuged.

#### 4.1.2 Limitations

The Bioanalyzer<sup>®</sup> could be used only to compare platelet counts from one experimental session to another, not as an absolute measure of platelet counts. The tests on PRP separation demonstrated that PRP tended to become cloudy and difficult to separate as a cow's pregnancy stage developed toward full maturation.

#### 4.1.3 New Questions

While the different citrate concentrations did not cause obvious changes in the clotting of the whole blood, it may still affect the amount of adhesion on biointerfaces.

Such an effect can be tested directly through the methods described in the dissertation. The more interesting issue relates to the difficulty of extracting PRP from a cow during the late stages of pregnancy. The mechanism for this problem is unknown, nor is the extent to which it affects other properties of the platelets.

#### **4.2 PRP Experimentation Overview**

On fibrinogen, at high shear, PRP+L-A reduced percent surface coverage and PRP+L-NMMA increased percent surface coverage, as expected. However, surface coverage increased with PRP+ADP, in contrast to the expected activation effect of ADP. The effect of L-A agrees with the results of Eshaq [13], while the ADP results contrast with that work. It is possible that ADP causes platelet aggregation and either prevents platelet receptors from binding with fibrinogen or generates larger thrombi that tend to be sheared off of the surfaces as a result of larger hemodynamic forces caused by the larger size. The effect of ADP may be much different at the larger shear stresses in Eshaq's work. The minimal effect of L-A under static condition agrees with Frilot's work, although his studies were on collagen rather than fibrinogen.

The dLbL-collagen substrate provided slightly different results from the dLbL-fibrinogen surface when performed under dynamic conditions. As with fibrinogen, dLbL-collagen surfaces imaged in the high shear regions displayed the expected average surface coverage percentage results. Addition of ADP increased the surface coverage, while addition of L-A decreased it, as expected. The results substantiate Eshaq's work with chemical additives when performed under dynamic conditions. For static conditions, dLbL-collagen results for PRP+L-A were larger than those of the dLbL-fibrinogen result. However, the average surface coverage percentages between plain PRP, PRP+ADP and

PRP+L-A were only slightly difference from one another. The insensitivity to added L-A agrees with Frilot results on collagen under static conditions.

#### 4.2.1 Limitations

The percent surface coverages differed from session to session. However, results from most sessions were consistent. Some variability may be caused by differences in the blood itself, including changes that occur near the end of a cow's pregnancy. The day-to-day variability emphasizes the need to perform control experiments on each collected blood sample.

Two other limitations arise in this work. First, far fewer experiments were performed on the collagen interface than on the fibrinogen interface, so less information was obtained about adhesion on collagen than of fibrinogen. Secondly, although the use of a swirled Petri dish simplified the experimentation in comparison to the use of a microfluidic device, the shear rates generated were time-dependent and much lower than were used by Eshaq [13]. It will be useful reexamine the results of the present experiments in that device to obtain large and more consistent shear rates.

#### 4.2.2 New Questions

Of particular interest are the results obtained with added ADP on fibrinogen. These tests need to be repeated at the low shears used here. If they are repeatable, further experiments can be performed to understand the mechanism through which ADP could reduce adhesion.

### 4.3 Platelet Coverage Confirmation

#### 4.3.1 Overview

Platelet adhesions were visually confirmed on all plain glass slides exposed to PRP by comparing the images to similar previous published works. The AFM peak heights for plain slides exposed to PRP were significantly higher than those for LbL surfaces not exposed to PRP. In addition, AFM peak heights were higher for all layered slides exposed to PRP than for layered slides not exposed to PRP. These results indicate that the exposure of slides, whether unlayered or layered, to PRP allowed platelets to adhere to the surfaces.

FE-SEM images of sLbL-fibrinogen, dLbL-fibrinogen and dLbL-collagen surfaces exposed to PRP showed evidence of platelet adhesions. These adhesions were similar to features recorded by Zilla et al. [67], Tsai et al. [64] and Fritz et al. [66]. Moreover, the LbL surfaces not exposed to PRP did not display similar structures.

#### 4.3.2 Limitations

The AFM and FE-SEM studies were limited in that the regions that could be scanned were small. AFM images, for example, were confined to a 40  $\mu\text{m}$  by 40  $\mu\text{m}$  region, and it was not possible to confirm prior to a scan that the region being imaged would include platelet adhesions. In addition, the number of AFM scans that could be examined per sample was limited. With more time, a larger sampling of peak heights might have provided a more accurate representation of the surface. The AFM was also limited in that it could not scan surfaces that were too smooth or too rough for the cantilever tip. This inability affected the smooth dLbL-collagen surfaces more frequently than it affected the dLbL-fibrinogen surfaces. It also prevented the AFM from scanning



plain glass slides that were not exposed to PRP. With the FE-SEM images, it was possible to view larger regions of the surface and then narrow the field of view to smaller areas. However, the exposure time in small regions was limited because the scanning beam would eventually damage the adhered material. This problem arises because the surfaces were not gold-coated prior to imaging. Because the slides were dried, platelet adhesions did not appear in their hydrated state. Lastly, some images displayed a beading effect covering the surface especially in smooth areas when AO staining on LbL surfaces with and without PRP exposure. Hence, potential platelet adhesions and aggregations may have been obscured by the AO stain.

#### 4.3.3 New Questions

In the AFM and FE-SEM images, it is still not clear whether the larger features were single platelets that had spread or aggregates of platelet.

### **4.4 Layered Surfaces Exposed to PRP**

#### 4.4.1 LbL Surface Comparisons

##### 4.4.1.1 Overview

Fluorescent microscopy images of sLbL-fibrinogen in the current study resembled those in Eshaq's thesis. The shorter exposure time requirements for these surfaces, as compared to dLbL-fibrinogen surfaces, and the similarity between images taken from dLbL-fibrinogen surfaces and glass slides, after both are exposed to PRP, indicates that much of the staining on sLbL-fibrinogen surfaces does not identify platelets. Lopez demonstrated that sLbL-fibrinogen surfaced not exposed to PRP showed AO fluorescence [56]. Nonetheless, it is still possible that the adhesion of platelets to sLbL-fibrinogen surfaces is different from adhesion to dLbL surfaces. The dLbL surfaces had

an advantage in that the required exposure time for fluorescence microscopy was consistent from image to image, whereas sLbL-fibrinogen required continual adjustment from location to location. Given that the longer exposure time used in dLbL images would naturally lead to brighter images, it is certain that the darker images obtained with dLbL were not a consequence of the different exposure time.

AFM scans of the sLbL-fibrinogen and dLbL-fibrinogen surfaces exhibited, crater/mountainous characteristics topographies, but the dLbL-fibrinogen surface was less rough. Also, the dLbL-fibrinogen surfaces exhibited troughs along the surface. It is possible that the thinner layers obtained from dLbL were weaker and more susceptible to local removal during PBS rinses. The dLbL-collagen surfaces were smoother than the other two and did not display the same topographical features.

FE-SEM images of sLbL-fibrinogen and dLbL-fibrinogen also showed rough surfaces, with rougher surfaces for sLbL-fibrinogen than dLbL-fibrinogen. Again, dLbL-fibrinogen displayed troughs similar to those in the AFM images, while dLbL-collagen images displayed striations or collagen fibers along the PRP exposed surfaces.

sLbL-fibrinogen and dLbL-fibrinogen surfaces had significant differences in fluorescence-derived surface coverage for exposure to plain PRP at high shear and for exposure to PRP+L-A under both no shear and high shear conditions. Surprisingly, dLbL-fibrinogen surfaces displayed higher peak heights than sLbL-fibrinogen surfaces despite the greater roughness found with sLbL-fibrinogen. Therefore, we assumed that dLbL-fibrinogen retained either more platelet adhesions or larger platelet adhesions.

#### 4.4.1.2 Limitations

Measurements of peak heights with the AFM were limited to using the self-scaling of the complete image as a measure of the tallest peak. It was not possible to download the height data and examine multiple peaks in a given image. Therefore, the peak height data from the AFM is limited.

#### 4.4.1.3 New Questions

The mechanism that causes the dLbL-fibrinogen peaks to be larger than the sLbL-fibrinogen peaks remains to be investigated. Furthermore, it is not clear whether AO staining of the fibrinogen surface, without exposure to PRP, is caused by trapping of AO in pockets within the surface or binding of AO to the fibrinogen. However, if it is caused by binding it is not clear why the binding would occur for sLbL-fibrinogen and not for dLbL-fibrinogen.

### 4.4.2 Biointerface Substrate Comparisons

#### 4.4.2.1 Overview

Fibrinogen surfaces exposed to PRP+ADP produced much lower surface coverage percentages than collagen surfaces exposed to PRP+ADP. PRP+ADP did not increase percent surface coverage on dLbL-fibrinogen, but did increase it on dLbL-collagen. PRP+L-A decreased percent surface coverage for both dLbL-fibrinogen and dLbL-collagen for all shear stress regions of interest. Surface coverage of plain PRP under no shear conditions was significantly different between dLbL-fibrinogen and dLbL-collagen. Both PRP+ ADP and PRP+ L-A surface coverage percentages were statistically significant between dLbL-fibrinogen and dLbL-collagen. For the AFM samples, fibrinogen and collagen peak heights were similar.

#### 4.4.2.2 Limitations

The AFM was not able to scan the collagen surface when it was too smooth. Therefore, only regions in which the collagen had some roughness, or in which other material was superimposed on the collagen, could be imaged. Several dLbL-collagen scans often had to be executed for a given surface. This problem may alter the statistics of the collected peak height data.

#### 4.4.2.3 New Questions

Because no fluorescent images were taken from sLbL-collagen after exposure to PBS-only and staining with AO, it is unknown whether the collagen would be subject to the same staining problem as fibrinogen. This question is important for the interpretation of Frilot's work, which used AO staining on a collagen surface. However, the process used by Frilot to produce the surface differed from the LbL process used in the current studies. Also, the source of collagen was liquid formulation, whereas the current studies used a powdered form.

### 4.4.3 Dynamic vs. Static Conditions

#### 4.4.3.1 Overview

Fluorescent images of dLbL-fibrinogen substrates for all chemical additives and the plain PRP samples in the high shear area revealed a platelet elongation or platelet rolling effect. The effect was strongest for dLbL-fibrinogen exposed to plain PRP. This effect was also observed on dLbL-collagen when it was exposed to PRP+L-A and to plain PRP, although it is possible that the presence of collagen fibers may have contributed to the elongated features in the images.

The dLbL-collagen and dLbL-fibrinogen surfaces behaved similarly when exposed to PRP, with different additives, under no shear and low shear conditions. The high shear conditions always led to the greatest amount of percent surface coverage in any group. For dLbL-fibrinogen, differences among no shear, low shear and medium shear cases were weak. For dLbL-collagen, there was a more monotonic increase in adhesion with shear. The exception is PRP+ L-A, for which adhesion showed little dependence on shear.

AFM scans of dLbL-fibrinogen substrates exposed to PRP+ ADP revealed a streaking effect for no shear, low shear and high shear conditions. It also showed the platelet rolling effect at high shear when exposed PRP+ L-A. For dLbL-collagen substrates the streaking effect was seen with PRP+ADP exposure. The mechanism for the streaking is still unknown, but it is clear that shear is not a necessary condition.

#### 4.4.3.2 Limitations

The ability to control shear stress was limited. Lopez's dissertation examined this issue as a source of error for dynamic conditions and suggested using a microfluidics device for controlling and regulating shear stresses [56].

#### 4.4.3.3 New Questions

The nature of the elongation effect and streaking effect is unknown. It is particularly interesting to consider sources of streaking that occur under no shear conditions.

#### 4.4.4 Chemical Additive Comparisons

##### 4.4.4.1 Overview

The plots of feature size show that the fluorescent features decrease in number with increasing size. The PRP+ADP samples tended to have larger feature sizes. The platelet adhesion size graphs for plain PRP showed a moderate curve cluster with medium size standard deviation error bars. PRP+L-A displayed a tight band with one exponential curve offset from the others with small standard deviation error bars on the mean chart. PRP+ADP displayed a large spread with larger standard deviation error bars. For AFM scans, collagen fibers and platelet adhesions were revealed along the dLbL-collagen surfaces for the plain PRP, L-A and ADP. These particles and fibers were surrounded by smooth surfaces.

The dLbL-fibrinogen surfaces exposed to plain PRP resulted in variant data. As explained in Results Section 3.9.5, triple the amount of plain PRP samples were tested as compared to the chemical additives giving much larger variations for plain PRP. Therefore, we determined another method for testing consistence between plain PRP. We analyzed a single day's plain PRP samples. The results supplied only slightly statistically insignificant p-values and compared well to the chemical additives. PRP+ADP, PRP+L-A and PRP+L-NMMA in the low and medium shear regions related very well between sessions. However, the high shear regions for these chemicals varied between days. Static conditions for plain PRP and chemical additives displayed differences between the sessions, except for PRP+L-A.

For the dLbL-fibrinogen substrate exposed to chemical additives and plain PRP executed under the dynamic conditions, PRP+ADP and PRP+L-A varied from plain

PRP's surface coverage percentages while PRP+L-NMMA displayed similar results to plain PRP. For the static condition of dLbL-fibrinogen surfaces, PRP+ADP and PRP+L-NMMA showed an indifference to plain PRP while PRP+L-A varied to plain PRP. For dLbL-collagen surfaces performed under dynamic conditions, PRP+ADP's high shear region contrasted plain PRP while PRP+L-A was indifferent to plain PRP for all shear regions. The static condition of dLbL-collagen substrates resulted in PRP+ADP and PRP+L-A distinctions from plain PRP.

For the AFM results, dLbL-fibrinogen surfaces exposed to plain PRP and chemical additives were compared to one another. Peak heights for PRP+L-A and PRP+L-NMMA were not significantly different from plain PRP, while peak heights for PRP+ADP were significantly different from those for plain PRP. On the collagen surface, no significance was found for the comparison of peak heights obtained with any of the additives to peak heights obtained with plain PRP.

#### 4.4.4.2 Limitations

Day-to-day variability in the experiments with plain PRP was high. However, single day results provided smaller variations from slide to slide, and the relationships between results for different chemical additives were consistent from one day to the next. The results on collagen under no shear also varied strongly between days.

#### 4.4.4.3 New Questions

The feature sizes should be examined to a greater extent. While there is some indication that the variability in the feature size distribution depends on the chemical additive, enough data is not yet present to determine whether the feature size tends to

increase or decrease for a given additive. Feature size should be an important indicator of the interaction among activators and inhibitors and the transport of these agents.



## CHAPTER 5

### CONCLUSIONS AND FUTURE WORK

#### 5.1 Concluding Hypotheses Assessments

Previously discussed analyses of this dissertation's experiments have supplied an assessment of the hypotheses. Based on these prior discussions, conclusions about the hypotheses and future work were considered during this section.

##### 5.1.1 Hypothesis 1

LbL surfaces that have been exposed to platelet-rich-plasma will demonstrate features that are consistent with adhered platelet aggregates and that are not present on LbL surfaces that have not been exposed to platelet-rich-plasma.

Plain glass slides exposed to PRP were compared to sLbL-fibrinogen, dLbL-fibrinogen and dLbL-collagen slides with and without PRP exposure. Through AFM and FE-SEM images, platelet adhesions were evident on PRP-exposed surfaces via visual affirmation and peak height comparisons. Slides without PRP exposure displayed no such platelet-like structures and maintained lower AFM peak heights. These results strongly indicate the presence of platelet adhesions on surfaces exposed to PRP, whereas surfaces that are not exposed to PRP do not contain platelet adhesions.

### 5.1.2 Hypothesis 2

Fluorescence Microscopy, FE-SEM and AFM images from surfaces generated by static LbL will indicate a rougher surface than those from surfaces generated by dynamic LbL.

Glass slides prepared with sLbL-fibrinogen, dLbL-fibrinogen and dLbL-collagen were compared for surface roughness. Fluorescence microscopy, AFM and FE-SEM images visually confirmed that the sLbL technique generated stronger topographical features when compared to the smoother dLbL-fibrinogen and dLbL-collagen substrates.

### 5.1.3 Hypothesis 3

Peak heights for AFM images taken from bioactive surfaces exposed to PRP will be greater when the surface is generated with dynamic LbL instead of static LbL.

sLbL-fibrinogen, dLbL-fibrinogen and dLbL-collagen surfaces exposed to PRP were scanned with an AFM. Statistical comparison of the peak heights suggested that the dLbL-fibrinogen and dLbL-collagen surfaces displayed greater peak heights, on average, than sLbL-fibrinogen surfaces.

### 5.1.4 Hypothesis 4

Fluorescence Microscopy, FE-SEM and AFM images of fibrinogen surfaces generated by dynamic LbL will indicate a rougher surface than those of collagen surfaces generated by dynamic LbL.

Glass slides prepared with sLbL-fibrinogen, dLbL-fibrinogen and dLbL-collagen techniques were generated for capturing platelet aggregates. Fluorescence microscopy images did not indicate differences between fibrinogen and collagen. However, AFM and FE-SEM images revealed differences, with fibrinogen exhibiting rougher surfaces than

collagen. Collagen displayed smooth surfaces surrounding collagen fibers, whereas fibrinogen showed topographical features. In spite of these visual differences, the statistical information from fluorescence microscopy and AFM data suggested that fibrinogen and collagen provided similar surface coverage percentages and peak heights.

#### 5.1.5 Hypothesis 5

L-A, ADP and L-NMMA will have a stronger effect on platelet adhesion at higher shear rates than at lower shear rates. Specifically, increased L-arginine will decrease platelet adhesion to a greater extent at high shear rates than at low shear rates, whereas ADP and L-NMMA will increase platelet adhesion at high shear rates than at low shear rates.

dLbL protein-coated surfaces exposed to plain PRP, PRP+ADP, PRP+L-A and PRP+L-NMMA were tested under static and dynamic conditions. Fluorescence microscopy images of the chemical additives on the fibrinogen surfaces once exposed to PRP provided shear region statistical results. These results demonstrated extreme variations of surface coverage percentages in the high shear regions whereas there were no such differences at the static and low regions. The dLbL-collagen substrate exhibited similar results to the fibrinogen with the exception of PRP+L-A displaying little variations for all shear regions and the static condition. From dLbL-fibrinogen results in the high shear regions, PRP+ADP and PRP+L-A revealed decreased platelet adhesions while PRP+L-NMMA indicated increased platelet adhesions when compared to plain PRP. The dLbL-collagen substrate imaged in the high shear region disclosed increased platelet adhesions for PRP+ADP and decreased adhesions for PRP+L-A. Therefore, dLbL-fibrinogen surfaces exposed to PRP+ADP did not perform as expected while

PRP+L-A and PRP+L-NMMA did provide the expected results. dLbL-collagen surfaces exposed to PRP+ADP and PRP+L-A performed as expected. However, these cases only hold true for the high shear region results.

Fluorescence microscopy and AFM results demonstrated a rolling effect found only in the high shear region. This effect was found in several of the dLbL-fibrinogen images and a few of the dLbL-collagen images. However, the collagen rolling effect images may simply be collagen fibers. With ADP, a streaking effect was produced across both types of biointerfaces in fluorescence microscopy images, AFM images and statistical results. In addition, AFM averages for dLbL-fibrinogen high shear region surfaces resulted in decreased peak heights compared to the static condition and low shear region.

## **5.2 Future Work**

### **5.2.1 Testing the dLbL Technique using Flow Conditions**

Experiments should be performed using a microfluidics device and microchannel silicon elastomer sheets for the dynamic condition instead of the current shaker table oscillation technique. The experimental results will determine whether a perfusion pump, microchannel Plexiglas<sup>®</sup> template, and silicon elastomer sheets provide better control of flow conditions as opposed to the shaker table method. Performing the dynamic conditions with flow instead of oscillations will allow for more control over the shear rates and provide a better analysis for higher shear stress effects on platelet adhesions contained on a dLbL surface.

### 5.2.2 ADP Streaking Effect

More experiments that evaluate the addition of ADP to PRP would clarify the streaking effect found on several ADP/PRP fluorescence microscopy, AFM and FE-SEM images. These tests would aid in understanding if ADP increases platelet adhesions through surface coverage results or simply changes the LbL surfaces generating a false positive for surface coverage percentages. To achieve these results, the researcher will use the dLbL technique, ADP, PRP and multiple imaging methods.

### 5.2.3 Platelet Rolling Effect

More studies involving the platelet rolling effect are suggested to help explain the higher shear stress results. With suggestions from Savage, platelets do not adhere well to fibrinogen surfaces when exposed to higher shear stresses [69], so a platelet rolling effect is expected on fibrinogen surfaces at high shear stresses. Additionally, tests would require the use of the dLbL-fibrinogen substrate, plain PRP, the addition of chemical additives if deemed necessary, and multiple imaging methods.

### 5.2.4 dLbL-Collagen Surface

The limited use of the collagen substrate in the present studies leads to new questions and indicates the need for further dLbL-collagen surface studies. Further investigation would determine whether collagen consistently produces the results discovered in this project. These results include similar fibrinogen surface coverage percentages and peak heights. To carry out this recommendation, the dLbL-collagen surface will need to be exposed to PRP, with and without the addition of chemical additives, and imaged by multiple techniques.

### 5.2.5 Imaging Improvement

Improvement to the previous fluorescence microscopy technique was necessary as this method provided only a partial platelet adhesion analysis. AFM and FE-SEM methods provided a more complete assessment of platelet adhesion than fluorescent microscopy alone. However, the AFM and FE-SEM images of platelet adhesion on our laboratory's LbL surfaces were still limited. An Interferometer can be used to obtain more complete information. This instrument will provide a much larger scan area than the AFM and FE-SEM and may also supply an analysis of the z-dimension of the platelet adhesion.

### 5.2.6 PRP vs. PPP

Because the platelet counts from the Agilent Bioanalyzer<sup>®</sup>'s did not agree with normal values for bovine PRP, an instrument should be used that is specifically designed to analyze PRP. An article by Woodell-May recommends using an automated hematology analyzer called the Cell-Dyn 3700 that includes a veterinary package for producing accurate platelet counts. The article also describes a method for collecting whole blood samples particularly for PRP accumulation [70]. Marx's work with PRP suggests what is and is not PRP [71]. The journal article recommends how to acquire PRP and properly centrifuge the plasma using a double spin technique. With these articles and others like them, a researcher could improve our method and determine whether similar samples using the methods described in this project are PRP or PPP. These new methods could be incorporated into our current centrifuge methods to achieve quality PRP [72].

### 5.2.7 Coagulation Control

Based on our difficulty using sodium citrate, a literature review was performed to incorporate new anticoagulation techniques using different fluids that would produce superior platelet adhesion results. The paper by Marx recommends ACD-A and CPD as alternatives to sodium citrate to best support platelet viability [71]. This project suggests incorporating these anticoagulation liquids into the current research methods.

### 5.2.8 Platelet Detection

To ensure platelet staining instead of biointerface surface staining, platelets should be stained with AO in tandem with anti-platelet antibodies conjugated with fluorochrome labels. One example of a platelet label is phycoerythrin coupled to cyanine 7 (PE-Cy 7). Such simultaneous dye and label tagging would allow the user to confirm platelet aggregations and adhesions along the LbL surfaces using fluorescence microscopy. The dye and label would also facilitate flow cytometry platelet counting methods [57]. One further confirmation of platelet adhesion detection would incorporate the use of an anti-fibrinogen ligand label with the PE-Cy 7. The fibrinogen label would be incorporated onto the surface after the last dLbL-fibrinogen generation step and before PRP surface exposure. With both the fibrinogen and platelets labeled, fluorescence imaging may provide further differentiation between the surface background and the platelet adhesions.

Further platelet detection methods may be necessary to provide a more quantitative approach to fluorescence microscopy's more qualitative method of determining surface coverage percentages. A quantitative method might determine platelet aggregations and adhesions confirmations, sizes and counts after our LbL

biointerface surfaces are exposed to PRP. One such method may involve scraping or flushing the LbL surface post-PRP exposure to release and collect any platelet adhesions. Once gathered, the adhesions could be analyzed with flow cytometry, spectroscopy and other assay methods. These results could be compared to initial PRP results before PRP/surface exposure. Therefore, one may conclude any platelet size and/or count changes. One similar work by Mattley incorporates a UV-Vis spectroscopy to quantify platelet particle size distribution and the particle number of platelet suspensions [73]. This method was used to provide a description of platelet activation processes. Mattley's work may prove useful in determining our laboratories post-PRP exposure platelet adhesion size distributions when compared to our laboratory's current platelet adhesion size graphs.



## **APPENDIX A**

### **FLUORESCENCE MICROSCOPY PROCESSING—MATLAB**

This MATLAB program was originally designed by Randa Eshaq and modified by Juan Lopez. Its use provides black and white images, a color montage of all the images and a black and white image montage. The following information is the MATLAB m file which is provided for future laboratory use:

```

%% Image processing program
%% Dr. Jones' Lab
%% Copyright (C) 2010 Juan M. Lopez
% %
% %This program is free software: you can redistribute it and/or modify
% %it under the terms of the GNU General Public License as published by
% %the Free Software Foundation, either version 3 of the License, or
% %any later version.
% %
% %This program is distributed in the hope that it will be useful,
% %but WITHOUT ANY WARRANTY; without even the implied warranty of
% %MERCHANTABILITY or FITNESS FOR A PARTICULAR PURPOSE. See the
% %GNU General Public License for more details.
% %
% %You should have received a copy of the GNU General Public License
% %along with this program. If not, see <http://www.gnu.org/licenses/>
% %
%% Original Version 8/5/2008
%% Updates:
%%3-31-2010 - Added directory handling and cycling through all the
%%file directories involved in a study
%%5-21-2010 - Added outlier processing and a new method for collecting
%%final data. - FINAL VERSION

function [l,m,n]=improcess_FINAL;
clc, clear all, close all

%%In this new section (3-31-2010), the user is asked to pick the main
%%directory from which the files will be extracted. The new format requires each
individual imaging to be placed in a subfolder within that directory, without any further
subfolders (for example, low/med/high portions of an imaging should each have their
own directory, with the
%%images within the main folder there). This makes for simpler processing of a full data
set without having to pick individual folders and having to count the files in the folder
before starting.

%%note that the images that have been converted to jpegs from the original tiff need to
be in the same main directory, the program will take care of generating a results folder on

```

its own.

```

workingFolder = uigetdir; % pick the main working folder
folderDirectory = dir(workingFolder); %list the folders in the working folder
cd(workingFolder); %change the working directory to the picked folder

%% establish the matrix to collect the areas of every result set
% don't include the thumbs.db as part of the directory tree, in case one was generated.

maxFolders = length(folderDirectory);

if strcmpi(folderDirectory(maxFolders).name, 'Thumbs.db')

    maxFolders = maxFolders-1;

else
end

collectedAreas = {};
areasNoOutliers = {};

for i = 3:1:maxFolders

    collectedAreas(1,i-1) = cellstr(folderDirectory(i).name);

end

%Write the headers in the first column
collectedAreas{1,1} = 'File Names';
collectedAreas{2,1} = 'Mean';
collectedAreas{3,1} = 'Standard Deviation';
collectedAreas{4,1} = 'Minimum Value';
collectedAreas{5,1} = 'Maximum Value';
collectedAreas{6,1} = 'Data';
areasNoOutliers = collectedAreas;

%% The main for loop, which goes through the entire directory of folders.

for folderNumber=3:1:maxFolders

%make a list of the files within the first working folder, and change
    %to the individual folders within the list with each iteration

    dirFiles =
dir(fullfile(workingFolder,folderDirectory(folderNumber).name,'Image*.jpg'));
    fileName = {dirFiles.name};

```

```

currentFolder = fullfile(workingFolder,folderDirectory(folderNumber).name);
cd(currentFolder);

%make a results directory
mkdir('Results');

%open new figures and reset the PercentArea Matrices
figure(1);
figure(2);
figure(3);
PercentArea = [];

% added an indexing variable
index = 1;

%% The nested for loop which processes through all the files in a given folder

for x=1:1:length(fileName);

%Clear the variables and the figure windows. Saves time on re-opening
    %figure windows.
    clear all;
    figure(1); clf;

% Resize the image, show the image, and save it as a "mini-"
    I = [];
    J = [];
    I = imread(char(fileName(x)));
    J = imresize(I,[480,604]);
    saveName=fullfile(currentFolder,'Results',strcat(strcat('mini-
Image',num2str(x)),'.jpg'));
    imwrite(J,saveName);

% The portion that changes the image to black and white
    BW1=J;
    %figure, imshow(BW1)
    background=imopen(BW1,strel('disk',70,4));
    %figure (1);
    %figure,imshow(background)
    S=imsubtract(BW1,background);
    %figure,imshow(S)
    [l,m,n]=size(S);
    W=zeros(l,m,n);
    r=S(1:l,1:m,1);
    g=S(1:l,1:m,2);
    b=S(1:l,1:m,3);

```

```

for i=1:l
    for j=1:m
        if r(i,j)<55
            W(i,j,1)=0;
        else
            W(i,j,1)=255;
        end
        if g(i,j)<80
            W(i,j,2)=0;
        else
            W(i,j,2)=255;
        end
        if (b(i,j)<72)
            W(i,j,3)=0;
        else
            W(i,j,3)=255;
        end
    end
end
%figure, imshow(uint8(W))
g=rgb2gray(uint8(W));
MF=medfilt2(g);

% added the automatic figure save command:
saveName=fullfile(currentFolder,'Results',strcat(strcat('mini-
Image',num2str(x)),'_gray.jpg'));
imwrite(MF,saveName,'jpg');

% This does the thresholding
figure(1); imshow(MF);

% Replaced that obsolete command
impixelinfo
T=roicolor(g,76,255);
figure(1); clf;
saveName=fullfile(currentFolder,'Results',strcat(strcat('mini-
Image',num2str(x)),'_BnW.jpg'));
imwrite(T,saveName,'jpg');

% Now, the black and white area can be calculated
u=bwarea(T);
z=l*m;
p=(u/z)*100;
% Changed this so the indexing is correct, the area is stored in
PercentArea(index)=p;
% increase the index

```

```

    index = index +1;

end

%% Do the post-processing
% Save the resulting variable as an excel file, with the transposed
% variable
% Transpose
Area = PercentArea.';

% Save
xlswrite(strcat('PercentArea','.xls'),Area);
%% A for loop to save the percent area to a composite file
%calculate the means, standard deviation, min/max
tempMean = mean(Area);
tempStdDev = std(Area);
tempMin = min(Area);
tempMax = max(Area);
collectedAreas{2, folderNumber-1} = tempMean;
collectedAreas{3, folderNumber-1} = tempStdDev;
collectedAreas{4, folderNumber-1} = tempMin;
collectedAreas{5, folderNumber-1} = tempMax;

%Write the original data file
for i = 1:length(Area)
collectedAreas(i+5, folderNumber-1) = cellstr(num2str(Area(i)));

end

%write the no-outliers data file, and calculate the mean, stddev, min,
%and max...
indexOutlier = 1; %set an indexing variable
tempNoOutlier = [];

for j = 1:length(Area)

    if abs(Area(j)-tempMean)>3*tempStdDev
        areasNoOutliers(j+5, folderNumber-1) = cellstr(num2str(NaN('double')));
    else

        areasNoOutliers(j+5, folderNumber-1) = cellstr(num2str(Area(j)));
        tempNoOutlier(indexOutlier) = Area(j);
        indexOutlier = indexOutlier+1;

    end

end

```

```

end

%calculate the means, standard deviation, min/max
tempMean = mean(tempNoOutlier);
tempStdDev = std(tempNoOutlier);
tempMin = min(tempNoOutlier);
tempMax = max(tempNoOutlier);
areasNoOutliers{2, folderNumber-1} = tempMean;
areasNoOutliers{3, folderNumber-1} = tempStdDev;
areasNoOutliers{4, folderNumber-1} = tempMin;
areasNoOutliers{5, folderNumber-1} = tempMax;

%% Create the montages
% Get the image file names and creat the montages
% Get the file names for all files of the type Image*.jpg, i.e.
% Image001.jpg.
dirOutput1 = dir(fullfile(currentFolder, 'Image*.jpg'));
fileNames1 = {dirOutput1.name};
% Get the file names for all files of the type mini-Image*_BnW.jpg, i.e. mini-
Image001_BnW.jpg.
dirOutput2 = dir(fullfile(currentFolder, 'Results', 'mini-Image*_BnW.jpg'));
fileNames2 = {dirOutput2.name};
figure(2); clf;
figure(3); clf;
%Create the individual Montages, and saves the images
figure(2)
montage(fileNames1);
saveas(2, 'MontageColor.jpg');
cd('Results');
figure(3)
montage(fileNames2);
cd(currentFolder);
saveas(3, 'MontageBnW.jpg');
cd(workingFolder);
save('processedData.mat'); %saves the current variables and results to an archive .mat
file

end

%% Save the collected areas:
cd(workingFolder);

% Save the collected percent areas.
xlswrite(strcat('CollectedPercentArea', '.xls'), collectedAreas);
xlswrite(strcat('CollectedNoOutlier', '.xls'), areasNoOutliers);

```

## **APPENDIX B**

### **PARTICLE SIZE COMPARISON – MATLAB**



This MATLAB program was designed by Juan Lopez and used with his permission so as to provide particle size comparisons based on pixel size and the number of particles at those particular pixel sizes. This data was collected from fluorescence microscopy images taken by myself and Juan Lopez. Below is the MATLAB m file information for this program:

```

%% Centroids particle size program
%% Dr. Jones' Lab
%% Copyright (C) 2010 Juan M. Lopez
% %
% %This program is free software: you can redistribute it and/or modify
% %it under the terms of the GNU General Public License as published by
% %the Free Software Foundation, either version 3 of the License, or
% %any later version.
% %
% %This program is distributed in the hope that it will be useful,
% %but WITHOUT ANY WARRANTY; without even the implied warranty of
% %MERCHANTABILITY or FITNESS FOR A PARTICULAR PURPOSE. See the
% %GNU General Public License for more details.
% %
% %You should have received a copy of the GNU General Public License
% %along with this program. If not, see <http://www.gnu.org/licenses/>
% %
%% Original Version - 6-23-2010

%% This portion does the setup for the main processing loop
clear all;
close all;
clc;

workingFolder = uigetdir; % pick the main working folder

particleTrackFolder = uigetdir('C:\Users\Nacho\Documents\MATLAB\Particle
Tracking','Pick the folder containing the particle tracking m-files'); % need to identify the
folder containing the particle tracking information.

folderDirectory = dir(workingFolder); %list the folders in the working folder

cd(workingFolder);

addpath(particleTrackFolder); %includes the folder in which particle tracking software
resides.Don't include the thumbs.db as part of the directory tree, in case one was

```

generated.

```

maxFolders = length(folderDirectory);
if strcmpi(folderDirectory(maxFolders).name, 'Thumbs.db')
    maxFolders = maxFolders-1;

else
end

% generate a list of all the folders
folders = {};

for i = 3:1:maxFolders
    folders(1,i-2) = cellstr(folderDirectory(i).name);
end

%% The loop that processes each of the results folders.
numberFolders = length(folders); %the total number of folders to be looked at
for folderNum = 1:1:numberFolders

    %switch to the next sub-folder in the main folder
    if folderDirectory(folderNum+2).isdir == 1 % only process data in a folder.
        cd(workingFolder);
        currentFolder = folders(folderNum);
        currentWorkingFolder = char(strcat(workingFolder,'\',currentFolder, '\Results'));
        cd(currentWorkingFolder);

        % clears the variables for the next time around
        particles = struct([]);
        results = struct([]);
        imageResultsTemp = [];
        plottableDataCentroids = [];
        legendValues = [];
        means = [];
        stdDev = [];
        excelMeans = [];
        excelData = [];
        close all;

        % get the index of images
        imagesDirectory = struct([]); % clears the structure
        imagesDirectory = dir(currentWorkingFolder); %list the folders in the working
        folder

        % Count the number of items to be used in calculating the images

```

```

maxImages = length(imagesDirectory);

if strcmpi(imagesDirectory(maxImages).name, 'Thumbs.db')
    maxImages = maxImages-1;

else
end

% generate a list of all the images in the folder
images = {};
for i = 3:1:maxImages
    images(1,i-1) = cellstr(imagesDirectory(i).name);
end

numberOfImages = length(images);
counter = 1;

for imageNumber = 2:1:numberOfImages
    if isempty(strfind(char(images(imageNumber)), 'BnW'))
        %checks to see whether the image name is a black and white result
    else

imageTemp = imread(char(images(imageNumber))); %read in the image
imageTempBnW = roicolor(imageTemp, 250,255); %threshold the image

        if counter > 1
            %clear the temporary structures
            clear particles;
            clear imageResultsTemp;
        else
            end

        for sz = 2:1:100

particles(sz-1).peaks = pkfnd(imageTempBnW,0.5,sz); %find the estimated peaks for a
presumed particle size
particles(sz-1).centroids = cntrd(imageTempBnW,particles(sz-1).peaks,sz); %calculate
the centroids from the peaks

            if or(isempty(particles(sz-1).peaks),isempty(particles(sz-1).centroids)) %if
there were no particles or centroids found

                imageResultsTemp(sz-1,1) = sz; %size threshold value
                imageResultsTemp(sz-1,2) = 0; %number of peaks found
                imageResultsTemp(sz-1,3) = 0; %number of centroids estimated
                imageResultsTemp(sz-1,4) = 0; %maximum radius of gyration of centroid
            end
        end
    end
end

```

```

imageResultsTemp(sz-1,5) = 0; %minimum radius of gyration of centroid
imageResultsTemp(sz-1,6) = 0; %average radius of gyration of centroid
imageResultsTemp(sz-1,7) = 0; %stdDev of radius of gyration of centroid

    else %if there were particles and centroids

imageResultsTemp(sz-1,1) = sz; %size threshold value imageResultsTemp(sz-1,2) =
length(particles(sz-1).peaks); %number of peaks found
imageResultsTemp(sz-1,3) = length(particles(sz-1).centroids); %number of centroids
estimated
imageResultsTemp(sz-1,4) = max(particles(sz-1).centroids(:,4)); %maximum radius of
gyration of centroid
imageResultsTemp(sz-1,5) = min(particles(sz-1).centroids(:,4)); %minimum radius of
gyration of centroid
imageResultsTemp(sz-1,6) = mean(particles(sz-1).centroids(:,4)); %average radius of
gyration of centroid
imageResultsTemp(sz-1,7) = std(particles(sz-1).centroids(:,4)); %stdDev of radius of
gyration of centroid

    end

    end

    results(counter).particles = particles;
    results(counter).imageData = imageResultsTemp;
    results(counter).name = images(imageNumber);
    counter = counter+1;

    end

    end

% Generate plottable data from the results
%generate the results for all the individual results on a single plot
numberResults = length(results);

    for resultsNum = 1:1:numberResults
plottableDataCentroids(:,resultsNum)=results(resultsNum).imageData(:,3);
    legendValues(resultsNum) = resultsNum;

    end

% generate the results for a mean+standard deviation on a single plot
lengthData = length(plottableDataCentroids);

    for j = 1:1:lengthData

```

```

    means(j) = mean(plottableDataCentroids(j,:));
    stdDev(j) = std(plottableDataCentroids(j,:));
end

for k = 1:length(legendValues)
    excelData(:,k) = [legendValues(k);plottableDataCentroids(:,k)];
    excelMeans(:,k) = [legendValues(k);mean(k);std(k)];

end

xlswrite('plottableData.xls',excelData,'Sheet1');
xlswrite('plottableData.xls',excelMeans,'Sheet2');
save('centroidsData');
figure(1);
plot(plottableDataCentroids);
title(strcat(folders(folderNum),'-Individual Image Centroid Sizes Vs. Number at a
Size'));
xlabel('Centroid Size calculation threshold, in pixels');
ylabel('Number of centroids calculated in the image at that size initial estimate');
xlim([0 100]);
ylim([0 1000]);
saveas(1, 'IndividualImageCentroids.jpg','jpg');
saveas(1, 'IndividualImageCentroids.fig','fig');
figure(2);
errorbar(means,stdDev);
title(strcat(folders(folderNum),'-Overall Mean/StdDev Centroid Size Vs. Number at
a Size'));
xlabel('Centroid Size calculation threshold, in pixels');
ylabel('Number of centroids calculated in the image at that size initial estimate');
xlim([0 100]);
ylim([0 1000]);
legend(char(folders(folderNum)));
saveas(2, 'MeanImageCentroids.jpg','jpg');
saveas(2, 'MeanImageCentroids.fig','fig');
else end
end

```

## **APPENDIX C**

### **MONTAGE PICTURES PROGRAM – MATLAB**

This MATLAB program was designed by Juan Lopez and Melanie G. Watson. This program provides image montages to collectively view AFM and FE-SEM images within designated groups. These montages are provided in the Appendix compact disc. This data was collected from AFM and FE-SEM images. Below is the MATLAB m file information for this program:

```

%% Image montage program
%% AFM results
%% Dr. Jones' Lab
%% Copyright (C) 2010 Juan M. Lopez, Melanie G. Watson
% %This program is free software: you can redistribute it and/or modify
% %it under the terms of the GNU General Public License as published by
% %the Free Software Foundation, either version 3 of the License, or
% %any later version.
% %
% %This program is distributed in the hope that it will be useful,
% %but WITHOUT ANY WARRANTY; without even the implied warranty of
% %MERCHANTABILITY or FITNESS FOR A PARTICULAR PURPOSE. See the
% %GNU General Public License for more details.
% %
% %You should have received a copy of the GNU General Public License
% %along with this program. If not, see <http://www.gnu.org/licenses/>
% %
%% Versions
%% 1 - 7/28/2010 Initial version - collected folder information, processed individual
montages
%% FINAL - 7/28/2010 FINAL version, worked as written
%% Begin Program
% Note, the original bmp format pictures need to be converted to jpg, more compressed
formats using a converter such as IrfanView. Pick the main working folder via the GUI
workingFolder = uigetdir;

% list the folders in the working folder
folderDirectory = dir(workingFolder);

% change the working directory to the picked folder
cd(workingFolder);

% don't include the thumbs.db as part of the directory tree, in case one was generated.

maxFolders = length(folderDirectory);
if strcmpi(folderDirectory(maxFolders).name, 'Thumbs.db')

```

```

    maxFolders = maxFolders-1;
else
end
%% Main Program Loop
% Start from folder 3 because the first two folders are always the "." and the ".."
previous folder items.
for folderNumber=3:1:maxFolders
    %make a list of the files within the first working folder, and change to the individual
    folders within the list with each iteration
    dirFiles =
dir(fullfile(workingFolder, folderDirectory(folderNumber).name, 'Image*.jpg'));
    fileName = {dirFiles.name};
    %Change the current working folder to the current folder in the folder iterations.
    currentFolder = fullfile(workingFolder, folderDirectory(folderNumber).name);
    cd(currentFolder)
    %make a results directory inside the current folder.
    mkdir('Results');
% Get the file names for all files of the type Image*.jpg, i.e.
% Image001.jpg.
    dirOutput1 = dir(fullfile(currentFolder, 'Image*.jpg'));
    fileNames1 = {dirOutput1.name};
    %Open a new figure
    figure(1);
    % Create a montage of all the figures
    montage(fileNames1);
    title(char(folderDirectory(folderNumber).name));
    %Change to the results folder
    cd('Results');
%save the figure with handle #1 to a filename generated by the folder %name
    saveName = char(strcat(folderDirectory(folderNumber).name, '-Montage.jpg'));
    saveas(1, saveName);
    % Clear the variables and close the image
    clear fileName;
    close all;
end
%% End Program

```



**APPENDIX D**

**BOVINE BLOOD JOURNAL**

Table D1 Bovine Blood Collection Journal

Date	Time of Day	Cow Number	Notes about Cow	Amount Drawn
3/11/09	14:30	39	Ornery cow	50 mL
3/16/09	14:10	698	Good cow/older	50 mL
7/01/09	14:08	55	Good cow	2 x 50 mL
7/14/09	14:09	770	No problems	50 mL
7/27/09	13:45	43	Small but healthy	50 mL
7/29/09	13:55	770	Good cow	50 mL
9/18/09	14:00	855	Kicked a bit	50 mL
9/21/09	13:55	854	Good cow	50 mL
10/14/09	14:07	Jersey 2	Good cow	50 mL
10/16/09	13:55	Jersey 2	Too young, kicks	50 mL
10/21/09	13:30	Jersey 840	Older, gentle	50 mL
10/23/09	13:30	Jersey 840	Older, gentle	50 mL
10/26/09	13:30	Jersey 840	Older, gentle	50 mL
12/17/09	13:30	Jersey 840	Older, gentle	2 x 50 mL
1/23/10	13:30	Jersey 840	Older, gentle	2 x 50 mL
2/18/10	13:30	Jersey 840	Older, gentle	4 x 50 mL
2/19/10	13:30	Jersey 840	Older, gentle	175 mL
3/16/10	13:30	Jersey 840	Older, gentle	50 mL
3/17/10	13:30	Jersey 840	Older, gentle	2 x 50 mL
3/19/10	13:30	Jersey 840	Older, gentle	2 x 50 mL
3/24/10	13:30	Jersey 840	Older, gentle	2 x 50 mL
3/31/10	13:30	Jersey 840	Older, gentle	2 x 50 mL
4/02/10	13:30	Jersey 41	Older, gentle	2 x 50 mL
5/17/10	13:30	Jersey 41	Older, gentle	2 x 50 mL
5/20/10	13:30	Jersey 41	Older, gentle	2 x 50 mL
6/4/10	13:30	Jersey 41	Older, gentle	2 x 50 mL
6/21/10	13:30	Jersey 41	Older, gentle	2 x 50 mL
6/28/10	13:30	Jersey 41	Older, gentle	Multiple tubes
6/30/10	13:30	Jersey 41	Older, gentle	Multiple tubes

**APPENDIX E**

**IACUC (ANIMAL CARE COMMITTEE) FORM**

INSTITUTIONAL ANIMAL CARE AND USE COMMITTEE  
Louisiana Tech University

10 April 2006

Dr. Steven Jones  
Biomedical Engineering  
Louisiana Tech University  
Campus Box # 58

Dear Dr. Jones:

The Institutional Animal Care and Use Committee (IACUC) met earlier today and approved your protocols entitled: (1) *Microdevice to Study Effects on Platelets* (2) *Nitric Oxide Transport as a Mechanism for Control of Thrombosis*

You had been approved with a limit of 50 blood samples for each year over the five year period. Please remember that you are required to keep adequate and accurate records of all procedures, results, and the number of animals used in this protocol for three years after termination of the project. These records must be available for review by the IACUC or state and federal animal use agencies. Each year in October you will be required to complete a summary of animals used for the United States Agricultural Agency (USDA). Note that failure to follow this protocol as approved may result in the termination of research. If you have any questions please call me at r via e-mail at [jgspauld@latech.edu](mailto:jgspauld@latech.edu).

Sincerely,



James G. Spaulding, Chair  
Louisiana Tech University IACUC

## REFERENCES

- [1] P. M. Mannucci and S. Gorini, Eds., *Advances in Experimental Medicine and Biology: Platelet Function and Thrombosis: A Review of Methods*. New York City, New York , USA: Plenum Press, 1972, vol. 34.
- [2] S. Sherry et al., Eds., *Thrombosis*. Washington, D. C.: National Academy of Science, 1969.
- [3] M. T. Hinds, Y. J. Park, D. P. Giddens, and B. R. Aleviadou, "Local Hemodynamics Affect Monocytic Cell Adhesion to a Three-Dimensional Flow Model Coated with E-selectin," *Journal of Biomechanics*, vol. 34, pp. 95-103, 2001.
- [4] S. A. Jones and A. Fronek, "Analysis of Break Frequencies Downstream of a Constriction in a Cylindrical Tube," *Journal of Biomechanics*, vol. 20, no. 3, pp. 319-327, 1986.
- [5] M. A. Berny et al., "Rational Design of an Ex Vivo Model of Thrombosis," *Cellular and Molecular Bioengineering*, vol. 3, no. 2, pp. 187-189, June 2010.
- [6] S. A. Jones and A. Fronek, "Effects of Vibration on Steady Flow Downstream of a Stenosis," *Journal of Biomechanics*, vol. 21, no. 11, pp. 903-914, 1988.
- [7] W. Paulson and S. Jones, "Hemodynamics of the Hemodialysis Access: Implications of Clinical Management," *Hemodialysis Vascular Access and Peritoneal Dialysis Access*, vol. 142, pp. 238-253, 2004.
- [8] B. Alberts et al., *Molecular Biology of The Cell*, 5th ed. New York: Garland Science, Taylor & Francis Group, LLC, 2008.
- [9] J.E. Freedman et al., "Nitric Oxide Released from Activated Platelets Inhibits Platelet Recruitment," *Journal of Clinical Investigation*, vol. 100, pp. 350-356, 1997.
- [10] J. S. Beckman and W. H. Koppenol, "Nitric Oxide, Superoxide, and Peroxynitrite: the Good, the Bad, and the Ugly," *The American Physiological Society: Invited Review*, pp. C1424-C1437, 1996.

- [11] C. Nathan and Q. W. Xie, "Nitric Oxide Synthases: Roles, Tolls, and Controls," *Cell*, vol. 78, pp. 915-918, September 1994.
- [12] W. R. Platt, *Color Atlas and Textbook of Hematology*, 2nd ed. Philadelphia: J. B. Lippincott Company, 1979.
- [13] R. Eshaq, *The Effect of the Local Concentrations of Nitric Oxide and ADP on Platelet Adhesion and Thrombus Formation*, Master of Science in Engineering Thesis Ed. Ruston, Louisiana, US: Louisiana Tech University, 2006.
- [14] G. R. Sambrano, E. J. Weiss, Y. W. Zheng, W. Huang, and S. R. Coughlin, "Role of Thrombin Signalling in Platelets in Haemostasis and Thrombosis," *Nature*, vol. 413, pp. 74-78, September 2001.
- [15] A.C. Guyton and J.E. Hall, *Text Book of Medical Physiology*, 11th ed. US: W.B. Saunders Company, 2000.
- [16] N. Duraiswamy, B. Jayachandran, J. Byrne, J. E. Moore, and R. T. Schoepfoerster, "Spatial Distribution of Platelet Deposition in Stented Arterial Models Under Physiologic Flow," *Annals of Biomedical Engineering*, vol. 33, no. 12, pp. 1767-1777, 2005.
- [17] J. Jesty, W. Yin, P. Perrotta, and D. Bluestein, "Platelet Activation in a Circulating Flow Loop: Combined Effects of Shear Stress and Exposure Time," *Platelets*, vol. 14, pp. 143-149, 2003.
- [18] B. Fisslthaler, S. Dimmeler, C. Hermann, R. Busse, and I. Fleming, "Phosphorylation and Activation of the Endothelial Nitric Oxide Synthase by Fluid Shear Stress," *Acta Physiologica Scandinavica*, vol. 168, pp. 81-88, 2000.
- [19] L. F. Brass et al., "Agonist Receptors and G Proteins as Mediators of Platelet Activation," *Mechanisms of Platelet Activation and Control*, pp. 17-33, 1993.
- [20] D. A. Hammer and D. A. Lauffenburger, "A Dynamical Model for Receptor-Mediated Cell Adhesion to Surfaces," *Biophysical Society Journal*, vol. 52, pp. 475-487, September 1987.
- [21] Z. M. Ruggeri, J. A. Dent, and E. Saldívar, "Contribution of Distinct Adhesive Interactions to Platelet Aggregation in Flowing Blood," *The American Society of Hematology: Hemostasis, Thrombosis, and Vascular Biology*, vol. 94, no. 1, pp. 172-178, 1999.
- [22] S. Dimmeler et al., "Activation of Nitric Oxide Synthase in Endothelial Cells by Akt-dependent Phosphorylation," *Nature*, vol. 399, pp. 601-605, June 1999.

- [23] R. K. Davda, L. J. Chandler, and N. L. Guzman, "Protein Kinase C Modulates Receptor-Independent Activation of Endothelial Nitric Oxide Synthase," *European Journal of Pharmacology - Molecular Pharmacology Section*, vol. 266, pp. 237-244, 1994.
- [24] R. G. Knowles, "Nitric Oxide Release Accounts for the Biological Activity of Endothelium-Derived Relaxing Factor," *Nature*, vol. 327, pp. 524-526, 1987.
- [25] Y. L. Chen and J. L. Mehta, "Further Evidence of the Presence of Constitutive and Inducible Nitric Oxide Synthase Isoforms in Human Platelets," *Journal of Cardiovascular Pharmacology*, vol. 27, no. 1, pp. 154-158, 1996.
- [26] J. D. Laskin and D. L. Laskin, *Cellular and Molecular Biology of Nitric Oxide*, Dekker Inc., Ed., 1999.
- [27] V. Randiamboavonjy, "Endothelial Nitric Oxide Synthase (eNOS) in Platelets: How Is It Regulated and What Is It Doing There?," *Pharmacological Reports*, vol. 57, pp. 59-65, 2005.
- [28] I. Fleming, "AMP-Activated Protein Kinase (AMPK) Regulates the Insulin-Induced Activation of the Nitric Oxide Synthase in Human Platelets," *Thrombosis Hemostasis*, vol. 90, pp. 863-871, 2003.
- [29] L. Queen, "Beta2 - Adrenoceptors Activate Nitric Oxide Synthase in Human Platelets," *Circulation Research*, vol. 87, pp. 39-44, 2005.
- [30] I. Fleming, "The Physiology of Nitric Oxide: Control and Consequences," *Current Medicinal Chemistry Anti-Inflammatory & Anti-Allergy Agents*, vol. 3, pp. 189-205, 2004.
- [31] D. Alonso, "Nitric Oxide, Platelet Function, Myocardial Infarction and Reperfusion Therapies," *Heart Failure Review*, vol. 8, pp. 47-54, 2003.
- [32] S. L. Elfering, T. M. Sarkela, and C. Giulivi, "Biochemistry of Mitochondrial Nitric-Oxide Synthase," *The Journal of Biological Chemistry*, vol. 277, no. 41, pp. 38079-38086, October 2002.
- [33] M. G. Vila-Petroff, A. Younes, J. Egan, E. G. Lakatta, and S. J. Sollott, "Activation of Distinct cAMP-Dependent and cGMP-Dependent Pathways by Nitric Oxide in Cardiac Myocytes," *Journal of the American Heart Association: Circulation Research*, vol. 84, pp. 1020-1031, 1999.

- [34] I. Fleming, "Molecular Mechanisms Involved in the Regulation of the Endothelial Nitric Oxide Synthase," *American Journal of Physiology - Regulatory, Integrative and Comperative Physiology*, vol. 284, pp. R1-R12, 2003.
- [35] C. Nathan and Q. Xie, "Regulation of Biosynthesis of Nitric Oxide," *The Journal of Biological Chemistry*, vol. 269, no. 19, pp. 13725-13728, May 1994.
- [36] D. I. Simon et al., "Antiplatelet Properties of Protein S-Nitrosothiols Derived from Nitric Oxide and Endothelium-Derived Relaxing Factor," *Journal of The American Heart Association: Arteriosclerosis, Thrombosis, and Vascular Biology*, vol. 13, pp. 791-799, 1993.
- [37] A. J. Gowt et al., "Basal and Stimulated Protein S-Nitrosylation in Multiple Cell Types and Tissues," *The Journal of Biological Chemistry*, vol. 277, no. 12, pp. 9637-9640, March 2002.
- [38] K. Varahramyan and Y. Lvov, "Nanomanufacturing by Layer-by-Layer Assembly," Ruston, Lousiana, US: Louisiana Tech University, 2006
- [39] A. Hua, M. Fang, S. A. Jones, and Y. M. Lvov, "Electrostatic Layer-by-Layer Nanoassembly on Biological Microtemplates: Platelets," *American Chemical Society*, pp. 1-5, December 2001, Published on Web.
- [40] A. Hua, S. A. Jones, and Y. M. Lvov, "Biomedical Applications of Electrostatic Layer-by-Layer Nano-Assembly of Polymers, Enzymes, and Nanoparticles," *Cell Biochemistry and Biophysics*, vol. 39, pp. 23-43, 2003.
- [41] M. Turgeon, Ed., *Clinical Hematology Theory and Procedures*, 4th ed. Baltimore: Lippincott Williams & Wilkins, 2005.
- [42] D. M. Harmening, Ed., *Clinical Hematology and Fundamentals of Hemostasis*, 4th ed. Philadelphia: F. A. Davis Company, 1997.
- [43] A. Ramamurthi and R. S. Lewis, "Influence of Agonist, Shear Rate, and Perfusion Time on Nitric Oxide Inhibition of Platelet Deposition," *Annals of Biomedical Engineering*, vol. 28, pp. 174-181, 2000.
- [44] M. I. Furman, D. Grigoryev, P. F. Bray, K. R. Dise, and P. J. Goldschmidt-Clermont, "Platelet Tyrosine Kinases and Fibrinogen Receptor Activation," *Journal of the American Heart Association: Circulation Research*, vol. 75, pp. 172-180, 1994.
- [45] B. Lim, E.H. Lee, M. Sotomayor, and K. Schulten, "Molecular Basis of Fibrin Clot Elasticity," *Structure*, vol. 16, pp. 449-459, 2008.



- [46] R. Donadelli, J. N. Orje, C. Capoferri, G. Remuzzie, and Z. M. Ruggeri, "Size Regulation of Von Willebrand Factor-Mediated Platelet Thrombi by ADAMTS13 in Flowing Blood," *Blood Journal*, vol. 107, pp. 1943-1950, 2006.
- [47] P. R. Siljander et al., "Platelet Receptor Interplay Regulates Collagen-Induced Thrombus Formation in Flowing Human Blood," *Blood Journal*, vol. 103, pp. 1333-1341, 2004.
- [48] R. H Williams and M. U. Nollert, "Platelet-Derived NO Slows Thrombus Growth on a Collagen Type III Surface," *Thrombosis Journal*, vol. 2, no. 11, pp. 1-11, November 2004.
- [49] W.M. Becker, L.J. Kleinsmith, J. Hardin, and G.P. Bertoni, *The World of the Cell*, 7th ed.: Pearson Benjamin Cummings, 2009.
- [50] G. Anfossi et al., "Adenosine Increases Human Platelet Levels of cGMP Through Nitric Oxide Possible Role in its Antiaggregating Effect," *Thrombosis Research*, vol. 105, pp. 71-78, 2002.
- [51] L. Y. Chen, "Evidence for the Presence of L-Arginine Nitric Oxide Pathway in Human Red Blood Cells: Relevance in the Effects of Red Blood Cells on Platelet Function," *Journal of Cardiovascular Pharmacology*, vol. 32, pp. 57-61, 1998.
- [52] D. A. Fryburg, "NG-Monomethyl-L-arginine Inhibits the Blood Flow but Not the Insulin-like Response of Forearm Muscle to IGF-I: Possible Role of Nitric Oxide in Muscle Protein Synthesis," *Journal Clinical Investigation*, vol. 97, no. 5, pp. 1319-1328, March 1996.
- [53] C. Frilot, *Role of Nitric Oxide as a Modulator of Platelet Dense Granule Release*, Doctor of Philosophy Dissertation ed. Ruston, Louisiana, US: Louisiana Tech University, 2001.
- [54] D. M. Wootton and D. Ku, "Fluid Mechanics of Vascular Systems, Diseases and Thrombosis," *Annals of Biomedical Engineering*, vol. 1, pp. 299-329, 1999.
- [55] K. Vyavahare, *Computational Modeling of Nitric Oxide Transport in a Channel*, Master of Science in Engineering Thesis ed. Ruston, Louisiana, US: Louisiana Tech University, 2006.
- [56] J. M. Lopez, *An Improved Layer-by-Layer Technique to Generate Biointerfaces for Platelet Adhesion Studies: Dynamic LbL*. Ruston, Louisiana, USA: Louisiana Tech University, 2010.

- [57] R. Mylvaganam and R.D. Paul, "Method for a Rapid Antibody-Based Analysis of Platelet Populations," 12/260,734, October 29, 2008.
- [58] M. Di Ventra, S. Evoy, and J. R. Heflin, Eds., *Introduction to Nanoscale Science and Technology*. New York, New York, USA: Springer, 2004.
- [59] R. L. Scheaffer and J. T. McClave, *Probability and Statistics for Engineers*. US: Duxbury Press, 1995.
- [60] O. W. Schalm, *Veterinary Hematology*, 2nd ed. Philadelphia, Pennsylvania, USA: Lea & Febiger, 1965.
- [61] A. Rzany, G. Bayer, A. Bolz, and M. Schaldach, "Molecular Imaging of Fibrinogen by Scanning Probe Microscopy for Studying Contact Activation," in *19th International Conference*, Chicago, IL, 1997, pp. 2589-2591.
- [62] J. D. Mendelsohn et al., "Fabrication of Microporous Thin Films from Polyelectrolyte Multilayers," *Langmuir*, vol. 16, pp. 5017-5023, 2000.
- [63] M. Radmacher, M. Fritz, C. M. Kacher, J. P. Cleveland, and P. K. Hansma, "Measuring the Viscoelastic Properties of Human Platelets with the Atomic Force Microscope," *Biophysiology Journal*, vol. 70, pp. 556-567, 1996.
- [64] P. Zilla et al., "Scanning Electron Microscopy of Circulating Platelets Reveals New Aspects of Platelet Alteration During Cardiopulmonary Bypass Operations," *Texas Health Institute Journal*, vol. 14, pp. 13-21, 1987.
- [65] C. Minelli, A. Kikuta, N. Tsud, M. D. Ball, and A. Yamamoto, "A Micro-fluidic Study of Whole Blood Behavior on PMMA Topographical Nanostructures," *Journal of Nanobiotechnology*, vol. 6, no. 3, 2008.
- [66] F. K. Tsai, J. L. Lauer, and J. L. Shohet, "Aggregation of Blood Components on a Surface in a Microfluidics Environment," *Journal of Applied Physics*, vol. 99, pp. 024701-1:024701-7, 2006.
- [67] M. Fritz, M. Radmacher, and H. E. Gaub, "Granula Motion and Membrane Spreading During Activation of Human Platelets Imaged by Atomic Force Microscopy," *Biophysiological Journal*, vol. 66, pp. 1328-1334, May 1994.
- [68] A. R. L. Gear, "Platelet Adhesion, Shape Change, and Aggregation: Rapid Initiation and Signal Transduction Events," *Canadian Journal of Physiological Pharmacology*, vol. 72, pp. 285-294, 1993.

- [69] B. Savage, E. Saldivar, and Z. M. Ruggeri, "Initiation of Platelet Adhesion by Arrest onto Fibrinogen or Translocation on von Willebrand Factor," *Cell*, vol. 84, pp. 289-297, January 1996.
- [70] J. E. Woodell-May, D. N. Ridderman, M. J. Swift, and J. Higgins, "Producing Accurate Platelet Counts for Platelet Rich Plasma: Validation of a Hematology Analyzer and Preparation Techniques for Counting," *Journal of Craniofacial Surgery*, pp. 1-10, January 2005.
- [71] R. E. Marx, "Platelet-Rich Plasma (PRP): What is PRP and What Is Not PRP?," *Implant Dentistry*, vol. 10, no. 4, pp. 225-228, 2001.
- [72] H Mani, B Luxembourg, C Klaffling, M Erbe, and E Lindhoff-Last, "Use of Native or Platelet Count Adjusted Platelet Rich Plasma for Platelet Aggregation Measurements," *Journal of Clinical Pathology*, vol. 58, no. 7, pp. 47-50, 2005.
- [73] Y. Mattley, G. LeParc, R. Potter, and L. Garcia-Rubio, "Light Scattering and Absorption Model for the Quantitative Interpretation of Human Blood Platelet Spectral Data," *Photochemistry and Photobiology*, vol. 71, no. 5, pp. 610-619, May 2000.